Developing 3D Cell Cultures for Synthetic Bone Models

By Laurence Hill

A thesis submitted to The University of Birmingham for the degree of

DOCTOR OF PHILOSOPHY

School of Chemical Engineering

College of Engineering and Physical Sciences

The University of Birmingham

November 2022

Abstract

Bone is a difficult tissue type to investigate with much of the primary investigations performed in animals. While this can improve our understanding of the basic mechanisms of the tissue, the pace of research can be slow and have poor clinical translation from benchtop to clinic. Therefore, there is a need for an intermediate step, a synthetic tissue model that accurately recapitulates the biology of bone. This can be used as a substitute for animals in primary and investigatory research without the cost and ethical concerns associated with animal models. This thesis focused on the development of such models. A composite bioink formulation of alginate, collagen and hydroxyapatite was developed. A key feature of this bioink was fibrillar collagen formed within the alginate and in the presence of the hydroxyapatite mineral. To achieve the fibrillar collagen, low concentrations of alginate had to be used within the bioink that meant the printed constructs could not self-support. A suspended printing technique was incorporated and facilitated the 3D printing of the constructs, due to the low structural stability of the bioink, the constructs could not be removed from the bath. A novel *in situ* hybrid crosslinking 3D printing mechanism was developed to semi crosslink the constructs which allowed them to be retrieved. This mechanism was compatible with cell incorporation and fibril collagen formation.

Acknowledgments

I would like to take this opportunity to thank my supervisors Dr David Bassett and Dr Amy Naylor who were continually optimistic and supportive throughout my project, pushing me to improve at every opportunity. Your knowledge, patience, and endless time for me is appreciated beyond words, I know that with your guidance I have become a better scientist and for that I thank you both.

I would also like to thank Prof Liam Grover for your help and support as well as the members of the HTI. I would like to particularly thank Dr Erik Hughes who provided both technical and personal advice and helping me along my research career.

Special mention to members of the Naylor group Dr Georgiana Neag, Dr Jonathan Lewis, Dr Kieran Patrick and Melissa Finlay who not only provided great company throughout but constructive discussions about both work and personal life, you made this research project an enjoyable experience and were a source of ideas and knowledge.

I would also like to thank my family for being ever supportive and to those that inspire us but aren't here to see where our passions lead us.

Table of Contents

1 Introduction 1
1.1 Structure of bone 2
1.2 Bone Research 4
1.3 Tissue Engineered 3D Models 5
1.4 Approach Taken in this Study 10
1.5 Aims and Hypotheses 12
2 Materials and Methods 13
2.1 Cell encapsulation 14
2.1.1 Gel Preparation 14
2.1.2 Encapsulation 14
2.1.3 Dose Response 14
2.1.4 Mechanical testing 15
2.1.5 Statistical analyses 15
2.1.6 Scanning Electron Microscopy 15
2.1.7 Post Chelation Proliferation 15
2.1.8 Proliferation and Viability 16
2.1.9 Cell Attachment 16
2.1.10 Cell Type Used 16
2.2 Bioink- continuing development 17
2.2.1 Competitive Ligand Exchange (CLEX) 17
2.2.2 CLEX Bioink 17
2.2.3 Suspended Layer Additive Manufacture (SLAM) 17
2.2.4 Construct pH Optimisation 18
2.2.5 Fluorescent Collagen Staining 18
2.2.6 Alginate Concentration Optimisation 19
2.2.7 Collagen Concentration Optimisation 19
2.3 CLEX Collagen Interpenetrating (IPN) Mineral 20
2.4 Osteoblast maturation in vitro 21
2.4.1 Differentiation Media 21
2.4.2 RNA Extraction and Quantification. 21
2.4.3 cDNA Conversion 22
2.4.4 RT-qPCR 22
2.4.5 RNA Extraction for qPCR/Expression Profile for cells in Constructs 23
2.5 3D printing 24

2.6 X-ray Fluorescence (XRF) and Mineralisation of Constructs 25
3 Development of Methods For The Effective Encapsulation and Retrieval of Cells in Alginate Microbeads 27
3.1 Preface 28
3.2 Abstract 31
3.3.1 Aims and Hypotheses 33
3.4 Methods 33
3.5 Results 34
3.6 Discussion 45
3.7 Supplementary information 49
4 Formulation Development of Hybrid Bioinks Using Internal Gelation Strategies 50
4.1 Introduction 51
4.1.2 Aims and Hypotheses 59
4.2 Results 60
4.2.1 CLEX 60
4.2.1.1 initial Limits and compatibility concentrations 61
4.2.2.1 pH 64
4.3 Discussion 77
5 Optimising cell differentiation for 3D bioprinted culture 82
5.1 Introduction 83
5.1.1 Biology of Bone 83
5.1.2 Genes of interest 85
5.1.3 Aims and Hypothesis 87
5.2 Results 88
5.2.1 Optimising differentiation media for ink 88
5.2.2 Cell differentiation within constructs 95
5.3 Discussion 104
5.3.1 Limitations of mineralization work 105
5.3.2 3D constructs 106
5.3.4 3D culture limitations 107
6 Optimization of Collagen and Hydroxyapatite Incorporation and 3D Printing Conditions 108
6.1 Introduction 109
6.1.1 3D Printing 109
6.1.2 Bioink Properties 110
6.1.3 Collagen and Hydroxyapatite 111
6.1.2 Aims and Hypotheses 113

6.2 Results 114
6.2.1 Printing resolution 114
6.2.2 alginate concentration limits 121
6.2.3 collagen concentration limits 128
6.2.4 Calcium phosphate biomimetic tubes incorporation 132
6.3 Discussion 138
6.3.1 Printing resolution 138
6.3.2 Collagen incorporation into the bioink 139
6.4 Conclusion 142
7.Summary 144
8 References 147

Table of Figures

Figure 1.1.1 Schematic hierarchical layout of bone tissue from nano to micro scale……3

Figure 1.3.1 A schematic diagram of diffusion zones in a 3D spheroid……7

Figure 1.4.1 Possible stackable chip culture chamber for bone models……11

Figure 3.1.1 Fluorescently labelled collagen within alginate crosslinked with 25 mM calcium chloride and uncross linked alginate……28

Figure 3.1.2 Images of cells in either 10 or 20% FCS with either 1.5 or 3 mL EDTA versus EDTA alone after 8 days in culture with 1 wash and media change……29

Figure 3.1.3 Cultured MC3T3 cells post release from alginate beads……30

Figure 3.5.1 Overview of the development process for encapsulating cells in alginate microbeads (AMBs)……34

Figure 3.5.2 Metabolic activity measured by reduction of Resazurin……35

Figure 3.5.3. Effect of long-term 3D encapsulation culture on cells encapsulated in 2% alginate αMEM microbeads. ……37

Figure3.5.4. Effect of long-term culture on cells encapsulated in 1% alginate αMEM microbeads on proliferation potential post chelation……39

Figure 3.5.5**.** Fluorescent imaging showing cell attachment to alginate microbeads, as observed by Calcein AM (green) staining……40

Figure 3.5.6. Effect of long-term culture on cells encapsulated in 2% alginate αMEM microbeads on proliferation potential post chelation and cultured in supplemented media……42

Figure3.5.7 Effect of long-term culture on cells encapsulated in 1% alginate αMEM microbeads on proliferation potential post chelation and cultured in supplemented media……43

Supplementary Figure S3.7.1. SEM micrograph of a cell monolayer (false coloured gold) forming an interconnecting network between two 2% alginate beads cultured in supplemented media (x300 magnification)……49

Supplementary Figure S3.7.2. A. Compression stress strain curves of solid alginate cylinders made with either 1 or 2% alginate and complete cell culture media. B. Elastic modulus of the alginate cylinders……49

Figure 4.1.1 Results by year for 3D Printing Tissue Engineering in NCBI Pubmed search……51

Figure 4.1.2 SLAM printing schematic……55

Figure 4.1.3. A schematic diagram of the modified CLEX SLAM gelling systems. CLEX alginate bioink is extruded into CLEX agarose SLAM to facilitate *in situ* crosslinking……56

Figure 4.1.4 A schematic diagram of Alginate cross linking and the production steps for sodium alginate……57

Figure 4.2.1 Cell compatibility with initial CLEX SLAM conditions……61

Figure 4.2.2 Increasing the incubation time of the bioink to improve construct retrieval……62

Figure 4.2.3 Metabolic activity of 3D constructs crosslinked with CLEX of different final zinc concentrations……63

Figure 4.2.4 SLAM Agarose bath starting pH with CLEX B components buffered to pH 7.40……..65

Figure 4.2.5 Final pH of co-incubation of bioink and SLAM agarose bath when CLEX components of bioink and bath are buffered at pH 7.40……66

Figure 4.2.6 SLAM Agarose Bath Starting pH with CLEX components buffered to pH 7.0……68

Figure 4.2.7 Final pH of co-incubation of Bioink and SLAM Agarose bath when CLEX components of bioink and bath are buffered at pH 7.0……69

Figure 4.2.8 Increasing Calcium Concentration in the CLEX SLAM system……70

Figure 4.2.9 Effects of lowering SLAM CLEX B final zinc concentration to 10mM……71

Figure 4.2.10 pH after incubation of CLEX SLAM + Bioink when only CLEX B components are lowered to pH 6.8……72

Figure 4.2.11 Effects of differentiation media and proliferation media and lowering final zinc concentration in the SLAM bioink system……73

Figure 4.2.12 Reformulating CLEX SLAM from Glycine to Diglycine……74

Figure 4.2.13 Effect of the crosslinking cation concentration on pH……..75

Figure 5.2.1. A panel view of cell mineralisation at 7-day intervals over 28 days……..89

Figure 5.2.2. Image J analysis of the alizarin red coverage with each media formulation……90

Figure 5.2.3. Alizarin red extractions from the well plates of the cells treated with the 3 media formulations and control……91

Figure 5.2.4. Real-time RT-PCR analysis of the expression of pre-osteoblast genes, normalised to housekeeping gene and expressed as relative fold change in gene expression (2^{-DDCt})……92

Figure 5.2.5 Real-time RT-PCR analysis of the expression osteoblast genes normalised to housekeeping gene and expressed as relative fold change in gene expression (2^{-DDCt})……93

Figure 5.2.6. Real-time RT-PCR analysis of the expression of late osteoblast genes, normalised to housekeeping gene and expressed as relative fold change in gene expression (2^{-DDCt})……94

Figure 5.2.7 Real-time RT-PCR analysis of the expression pre osteoblast genes expressed as relative gene expression compared to B2M housekeeper (2^{-DCt})……95

Figure 5.2.8. Real-time RT-PCR analysis of the expression osteoblast genes expressed as relative gene expression compared to B2M housekeeper (2^{-DCt})……..96

Figure 5.2.9 Real-time RT-PCR analysis of the expression of late osteoblast genes, expressed as relative gene expression compared to B2M housekeeper(2^{-DCt})……97

Figure 5.2.10 RT-qPCR analysis of the pre osteoblast gene expression, shown as relative fold change in gene expression of cells in 3D culture with 2 different osteogenic conditions compared to proliferation media(2^{-DDCt})……98

Figure 5.2.11 RT-qPCR analysis of the osteoblast gene expression, shown as relative fold change in gene expression of cells in 3D culture with 2 different osteogenic conditions compared to proliferation media (2^{-DDCt})……99

Figure 5.2.12 RT-qPCR analysis of late osteoblast gene expression, shown as relative fold change in gene expression of cells in 3D culture with 2 different osteogenic conditions compared to proliferation media (2^{-DDCt})……100

Figure 5.2.13 RT-qPCR analysis of the relative expression of early osteoblast genes expressed as relative fold change in gene expression of cells cultured with osteogenic in 3D compared to 2D (2^{-DDCt})……101

Figure 5.2.14 RT-qPCR analysis of the osteoblast gene expression, shown as relative fold change in gene expression of cells cultured with osteogenic in 3D compared to 2D……102

Figure 5.2.15 RT-qPCR analysis of late osteoblast genes expression, shown as relative fold change in gene expression of cells cultured with osteogenic in 3D compared to 2D……103

Figure 6.2.1 A schematic CAD layout of the printed cylinder design……115

Figure 6.2.2 Bioink extrusion conditions calibration……116

Figure 6.2.3 0.6% alginate filament extruded through a 22G needle at varying pressures……117

Figure 6.2.4 0.6% alginate filament extruded through a 22G needle at varying nozzle movement speeds at 5 kPa extrusion pressure……118

Figure 6.2.5 Bioink made with working concentrations of Collagen, Biomimetic tubes, CLEX, and alginate were printed using a 22 G needle……119

Figure 6.2.6 Filament diameter for working bioink composition using a 20G needle……..120

Figure 6.2.7 Polarised light microscope of collagen within an 0.6% alginate construct……..124

Figure 6.2.8 Effects of alginate concentration from 0.6% to 1.6% on collagen fibril formation……125

Figure 6.2.9 Mechanical analysis of alginate CLEX bioinks without collagen……127

Figure 6.2.10 Collagen behaviour within bioink at increasing concentrations……129

Figure 6.2.11 Maximum permissible collagen concentration within the bioink as formulated……131

Figure 6.2.12 Calcium phosphate tubes integration into bioink……133

Figure 6.2.13 An intact calcium phosphate tube integrated into the fibril collagen network……134

Figure 6.2.14 Calcium phosphate tube integrated into the fibril collagen network with fragments.135

Figure 6.2.15 Calcium Phosphate tubes with MC3T3-E1 cells attached labelled with phalloidin…..136

Figure 6.2.16 Live cell image of 3D printed CLEX SLAM bioink containing cells……137

Table of Tables

Table 2.2 List of all primer probes used and their associated gene code……23

Table 4.2.1. Different formulations and ratio of gelling conditions used for Figure 4.2.13……..76

Table 6.2.1 Formulations of bioinks used to determine collagen fibril formation within alginate concentrations ranging from 0.4% to 1.6%.....122

Table 6.2.2 An overview of the collagen fibril formation and gel state after crosslinking using the CLEX SLAM system……123

Abbreviations

αMEM – Minimum Essential Medium

2D – Two dimensional

3D – Three dimensional

ALPL – Alkaline phosphatase

AMB – Alginate microbead

B2M – Beta-2 microglobulin

BGLAP – Bone gamma-carboxyglutamate protein

CAD – Computer-aided design

Calcein-AM – Calcein acetoxymethylester

CAT – Computed axial tomography

cDNA – Complementary DNA

CLEX – Competitive ligand exchange

CLEX A – Competitive ligand exchange containing calcium and EDTA

CLEX B – Competitive ligand exchange containing zinc and glycine

COL1A1 – Collagen type I alpha I DI H_2O

DNA – Deoxyribonucleic acid

ECM – Extracellular matrix

EDDA -Ethylenediamine-N,N'-diacetic acid

EDTA – Ethylenediaminetetraacetic acid

FCS – Foetal calf serum

FGF-2 – Fibroblast growth factor

FRESH – Freeform reversible embedding of suspended hydrogels

GelMA – Gelatin methacryloyl

GPS – L-Glutamine penicillin streptomycin

HA – Hydroxyapatite

HEPES – 4-(2-hydroxyethyl)-1-piperazineethanesulfonic acid

HMP – Hexametaphosphate

IPN – Interpenetrating network

LAB – Laser assisted 3D bioprinting

MHC – Major histocompatibility complex

MMP – Matrix metalloproteinase

MOPS – 3-(N-morpholino)propanesulfonic acid

MRI – Magnetic resonance imaging

MSX2 – Msh Homeobox 2

PBS – Phosphate buffered saline

PDPN – Podoplanin

PFA – Paraformaldehyde

PPi – Sodium pyrophosphate

RFU – Relative fluorescent units

RGD – Arginine-glycine-aspartic acid

Rn18s – 18S ribosomal RNA

RNA – Ribonucleic acid

RT-qPCR – Quantitative reverse transcription polymerase chain reaction

RUNX2 – Runt-related transcription factor 2

SEM – Scanning electron microscope

SLAM – Suspended layer additive manufacture

STL – Stereolithography (Standard Tessellation Language)

TC – Tissue culture

UV – Ultraviolet l

XRF – X-ray fluorescence

1 Introduction

1.1 Structure of bone

Skeletal bone is a vital organ system which facilitates movement, protection of vital organs, regulated ionic homeostasis, and in the long bones houses haemopoietic progenitors vital for blood and immune cell production.

Superficially, bone appears to be a simple organ providing mechanical stiffness and support to the human body and acting as an anchor point for muscles and tendons to attach to, in reality it is a far more complex system which is still not fully understood [1]. Bone tissue is a complex dynamic multicellular organ undergoing continuous remodelling throughout adult life, this in itself is a marvel with very few other tissues regenerating themselves over and over [2]. This is because bone is slightly different to the soft tissues mostly found in the body. Bone can be thought of as being comprised of two major components that symbiotically work together: the physical component and the cellular component. The physical component of bone tissue is comprised of a highly mineralised hierarchical structure that is mechanically very strong due to the high mineral content and tough due to the large protein network intertwined with the mineral [3]. This physical component acts as cell culture scaffold for bone cells to attach to, modify and ultimately become encased in. The cellular component of bone is made up of three main cell populations: osteocytes, osteoclasts, osteoblasts, which are discussed further in chapter 5. Briefly, osteoblasts and osteoclasts work in conjunction at the bone surface, continually remodelling bone through formation and absorption respectively. This process is largely orchestrated by osteocytes, which are embedded within the bone tissue, and act as mechanical sensors to direct the bone remodelling process [4].

As shown in Figure 1.1.1 bone is a highly organised hierarchical structure with features spanning the nano- to milli-metre scales. The fundamental units are collagen type 1 fibrils which are mineralised

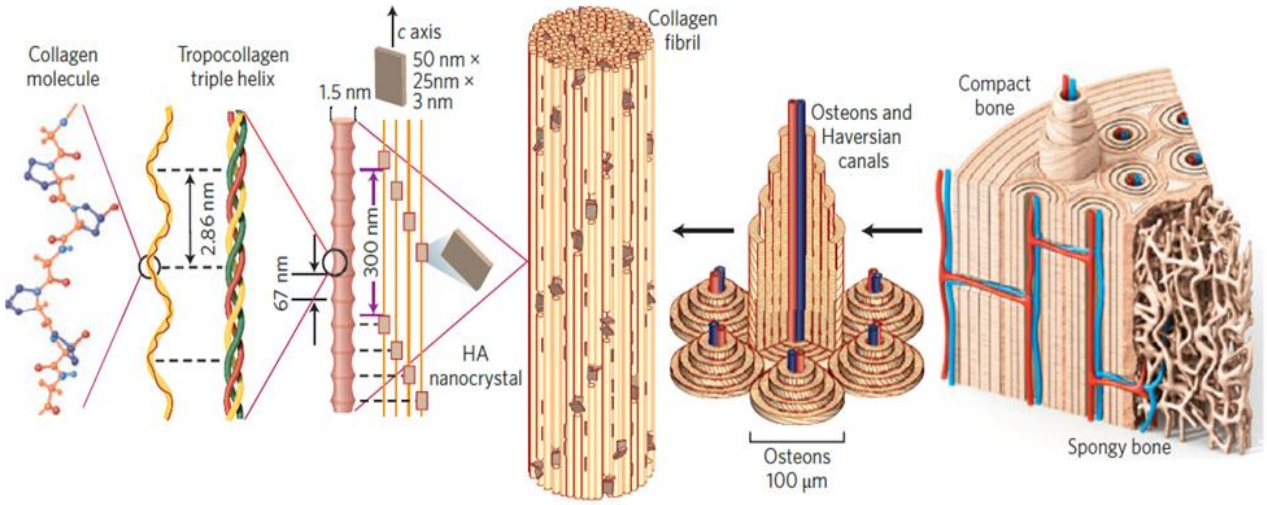

Figure 1.1.1 Schematic hierarchical layout of bone tissue from nano to micro scale.

The organised structure of collagen is innate from the nano scale with tropocollagen molecules combining into a triple helix. The triple helix is combined with hydroxyapatite nanocrystals with are arranged into a repeating orientation to build up into mineralised collagen fibrils. These form into either 100 µm struts for trabecular spongy bone or arrange further into osteons which contain haversian canals containing blood vessels [4].

with nanocrystals of hydroxyapatite (HA - $Ca_5(PO_4)_3OH$) which often appears as calcium deficient and carbonate substituted forms. The mineralised fibrils align into cylindrical lamella that are about 3-7 µm wide[5]. These fibrils vertically and horizontally crosslink in a 45° manner creating a porous honeycomb like structure. In cortical bone, which is the dense periphery found predominantly in load bearing bones. Stacks of 3-8 lamella concentrically wrap around a Haversian canal that contains the necessary blood vessels and nerves within its lumen to facilitate bone homeostasis. The Haversian canals stack into a long interconnected cluster running parallel to the bone axis, this cluster is called an osteon [6]. The complex hierarchical architecture of bone is in part where the innate strength of bone is derived from. This exquisite architecture from the nano- to milli-scale is an essential feature of healthy bone tissue and the faithful replication of it through purely synthetic means has to date eluded researchers.

In trabecular (sometimes called cancellous or spongy) bone, layers of lamella sporadically organise into bone packets along cement lines which form the rods and plates of trabecular bone, often

aligning to best withstand the mechanical load which is placed on the axis of the bone [7]. These bone packets are approximately 50 µm in diameter and 1 mm in length, the cavities created by the innate structure of trabecular bone provide host to bone marrow, adipose and immature bone cells [5].

Since it is not possible to faithfully recreate "living" bone via synthetic, i.e. tissue engineered, means, and fully synthetic "non-living" biomaterials fall short in terms of clinical performance, the current gold standard approach for the surgical replacement or repair of bone tissue is autologous grafting. Autologous grafts provide a perfect genetic match and often good clinical outcomes, however the amount of healthy bone that can be harvested is severely limited [8]. Furthermore, the harvesting procedure represents substantial risk in terms of infection and necrosis of the surgical site along with increase expense and surgical time to carry out the operation. The shortcomings of current "living" tissue engineered synthetic bone tissue also impact contemporary bone research, and due to the lack of suitable models primary osteo research is performed in either *in vivo* or *ex vivo* models which represent substantial inadequacies in the translation pathway. This in part due to the cost of procuring, housing and licences involved with animal research and the ethical concerns of performing basic science investigations *in vivo*, which does not always translate through to human physiology and the limited supply of *ex vivo* human tissue samples [9, 10].

1.2 Bone Research

To better understand the biological role of bone in osteoporosis, bone cancer, osteonecrosis, trauma, infection, reconstruction and healing a detailed appreciation of the biological processes of bone are the key to this.

Bone is a difficult tissue to grow either *in vitro* or *ex vivo* due to the terminal differentiation of osteocytes which inhibits their proliferation in culture. Osteocytes are also mechanically sensitive and require physical stimulus for optimal culture [11,12]. Due to the nature of bone tissue, mature osteocytes are incased within bone matrix which fundamentally changes their diffusion characteristics and adherence. In contrast 2D tissue culture (TC), the process of culturing mammalian cells in a control way within a laboratory setting uses polystyrene plastic conditions that; typically have high nutrient gradients, low physical adhesive points and diffusion is uninhibited. An alternative is to culture primary osteocytes on collagen gels, this method is often used to selectively screen osteocytes from primary cultures [13]. This technique, though more "biomimetic" or representative of the *in vivo* condition than TC polystyrene, still lacks the mineral content, 3D architecture and biomechanics of native bone tissue. Isolated primary cells can be cultured within a calcium phosphate matrix to replicate the lacunae of bone, however the major limiting issue with this is the initial differentiation of isolated primary osteocytes before incorporation within the model.

Notwithstanding these limitations, long term culture suggests that within the right environment cells are able regain their osteocyte phenotype [14].

Due to these limitations bone related research typically uses *in vivo* or modified *ex vivo* conditions. A widely used model for bone loss and osteoporosis is the ovariectomy animal model. This is performed in murine, rattus, ovine and primates; the ovaries are removed and the animal exhibits a post-menopausal osteoporosis phenotype [15]. This technique has some substantial limitations and is ethically dubious to perform and as such is tightly regulated in the developed world. The approach requires many animals to undergo invasive surgery, the stress of which can influence bone turn over, though this is usually controlled for by performing a sham surgery. However, this may not be an appropriate control as sham operated animals have been described as having no observed differences from unmanipulated animals [16]. The justification of needs when using animal models needs to be considered due to the ethical concerns and the dim public view of animal research.

An attractive alternative to animal studies are *ex vivo* or sometimes referred to as humanized 3D *in vitro* systems, where decellularized cadaver or surgical waste bone tissue is cultured with cells of interest, this is partially applicable to invasive mechanisms such as metastatic cancers [17]. While they are useful for providing the native tissue required for bone, they are limited by difficulty in sourcing whole healthy tissue, variability between samples and patient unknowns. While providing the ideal culture system for seeded bone cells, it lacks innate interactions of bone so with dynamic diseases such as osteoporosis and rickets many of the integral molecular and cellular processes are absent, thus fundamentally limiting the use of these models [18].

1.3 Tissue Engineered 3D Models

Tissue engineering is the application of biology, material sciences and engineering to create an artificial tissue that mimics a desired physiological environment, tissue or even a whole organ [19]. Interest and research into tissue engineering has grown significantly in the past 20 years. The applications of this emerging area of science are widespread, but two main aspects are a common theme within the research; to produce an implantable tissue construct to replace damaged or diseased tissue, or to provide a model for healthy or disease-state tissues to accelerate therapeutic interventions or the translational pathway, this thesis focuses on the latter application.

Traditional cell culture relies on a 2D monolayers of cells, which is not an accurate reflection of the *in vivo* environment. Cells in 2D present with a flat polar morphology which lack cell-cell and cell matrix interactions, as well as nutrient gradients [20]. The variation in biochemical and/or physiological

properties that define each environment is lacking, this can mislead the data as it is not representative of the corresponding *in vivo* tissue. In turn this can slow the development of therapeutics and understanding of diseases [21]. Conventional 2D cell culture uses glass or polystyrene culture flasks, the bottom of the flask can either be tissue culture treated or non-TC treated. In its simplest form TC treatment involves applying a negative charge to the bottom of the flask which electrostatically attracts the cells and allows them to attach. Polystyrene is a hydrophobic material, so a microwave plasma stream is passed over the top of the plastic which oxidises the plastic. Subsequently the top layer is modified to be hydrophilic and negatively charged when cells in media are added [22,23]. This technique encourages cell attachment and proliferation which can provide a reliable culture environment albeit not without its limitations – the first and foremost being that this is a simple 2D environment.

Mammalian cell cultures in 2D environments often present with morphologies and phenotypes not seen in comparable *in vivo* tissue, to the extent that explant and isolated cells can lose phenotypic markers within a few passages [24]. Cells grown in 2D will often proliferate faster and normal cells will demonstrate tumour like morphologies [25]. Cells are also more sensitive to chemotherapeutic agents than *in vivo* models [20, 26]. This difference could be down to a range of different factors, such as diffusion gradients, or that many chemotherapeutic agents work by interfering with DNA replication, therefore the increased proliferation rate can drive effects which can in turn lead to false conclusions.

To overcome these limitations, a 3D tissue engineered *in vitro* micro-environment can be used. These vary in size and complexity with the very basic being a cluster or spheroid of cells, to far more complex multicellular scaffold designs that replicate organoid structures or anatomical features [27]. Growing cells in 3D provides a culture environment comparable to an *in vivo* environment and ensures that they have no prescribed polarity and are able to maintain, or regain phenotypes, cease uncontrolled proliferation, and can become quiescent as appropriate [28].

A strong example of the benefits of growing cells in 3D is demonstrated by XAV939, this is an inhibitor of Wnt/β-catenin signalling, a well characterised pathway that is linked with proliferation and apoptosis, differentiation and development of cancers [29]. When XAV939 was administered to both 2D and 3D cultures of APC-mutant colorectal adenocarcinoma cells, the XAV939 had no effect on 2D cultures at any concentration. Whereas, the 3D cell cultures experienced a dose dependant decline in viability, with a 52% decline in survival at the maximum dose [21]. However, current 3D culture techniques still have drawbacks. The proliferation rate seen in cells grown in 3D is partly controlled through the reduced diffusion of nutrients into the 3D structures. Cells grown in clusters

or aggregates are limited to a maximum size of about 600 µm, beyond which a necrotic core forms (Figure 1.1.2) [30].

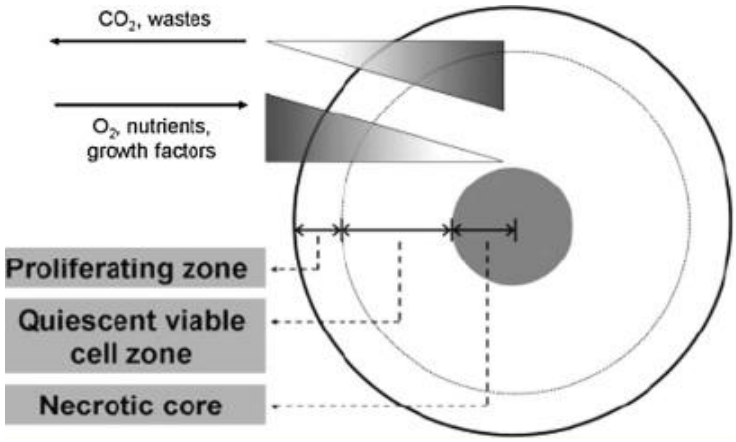

Figure 1.3.1 A schematic diagram of diffusion zones in a 3D spheroid.
The figure shows the diffusion limitation of when using 3D based models that without adequate nutrient transfer there can lead to areas deficient and impact on growth and viability of a culture system [30].

With the ever-advancing field of tissue models and engineering there is still a poor translation from the lab to clinic with many ideas falling into the so called 'valley of death'. This is where ideas and concepts have robust scientific methodologies but this poorly translates to clinic typically failing in clinical trial and is associated with the enormous cost of developing new treatments [6, 31, 32, 33]. Therefore, there is an urgent need for more representative, reliable and robust *in vitro* screening models. Although, current *in vivo* animal studies can provide robust data that is somewhat relevant to human biology, it is achieved at tremendous cost associated along with a plethora of ethical concerns, which, in turn slows down the rate of development [34]. Therefore, the development of a model that has the ease and convenience of a 2D cell culture, yet with the robustness of data produced from an *in vivo* system is of upmost importance and forms the basis for the main aims of this project.

An advantage of an engineered tissue model over traditional techniques is they can be personalised with either a patient's own cells or a genetically modified cell line. This is particularly useful when investigating congenital or rare diseases that lead to foetal death which are expensive and difficult to model *in vivo*. Early initial tissue models such as the hanging drop method have clearly

demonstrated the importance of 3D culture. The technique is simple, a suspension of cells is attached to the underside of tissue culture lids and gravity leads to the cells amassing at the bottom of the drop into spheroid clusters [35]. The cells within the spheroid cluster forms uniformed sized aggregates which have been shown to mimic early stages of embryonic development [20]. Hanging drop spheroids have also led to significant developments in tumour modelling and drug screening since *in vivo* spheroid formation is thought to be a precursor to metastasis and an intermediate step in chemoresistance. The slower growth rate and diffusional limitations of a 3D cell spheroid reduce the sensitivity to chemotherapeutic agents and better reflect an *in vivo* metastatic environment [26]. These attributes demonstrate the potential benefits even simple 3D cell cultures can have on translational research.

Due to the simplicity of the method the uses of the hanging drop method are somewhat limited. The very small volumes of media used significantly limits the number of cells that can be used within each test, additionally media changes are very difficult and long-term cultures are difficult to maintain due to evaporation during incubation [35]. This can be circumvented by culturing in round bottom non TC treated tissue culture plates but the size of the cell aggregates is limited due to nutrient transfer within the spheroid. The cell population within a spheroid can become heterogenous with the exterior cells proliferating at a greater rate than the internal cells, which may become quiescent [20]. If the size of the aggregate exceeds beyond 100-150 μm the cells will become hypoxic or even necrotic, even with the addition of a gas permeable culture chip the spheroids were limited to 600 μm [36].

The phenomenon of hypoxia, while limiting the study of normal cell-cell interactions, is very beneficial to the study of metastasis, tumorigenesis and drug resistance in cancers [37]. Human breast epithelial cells of both primary and commercial cell origin grown in 2D monolayer cell cultures develop and proliferate similarly to primary and commercial tumour cells. With all the cell types continuing to proliferate and expand indefinitely, typical of a cancer cell. In contrast, when cultured in a 3D micro environment similar to *in vivo* conditions, only the tumour cells continue to proliferate and normal cells reach confluency and arrested growth becoming senescent [38]. This dramatic difference in response to culture conditions highlights the poor translational pathway and need for culture environments to accurately represent their target tissue and state of health. In turn this approach could lead to an increased rate in the development of new therapeutic treatments.

Scaffold based 3D cell cultures have a wider scope of application than non-scaffold-based cultures due to not being limited by size to the same degree as cell aggregate cultures. 3D scaffold-based culture better reflects a normal physiological environment, therefore generating interest for

application in both tissue engineering and regenerative medicine [39]. The basic requirements of scaffold-based culture and normal 2D/3D cultures are the same, the scaffold base must be able to support or enable cellular growth and proliferation. To do this the scaffold must be stable in physiological conditions and facilitate the necessary conditions of growth, which are affected by, pH, hydration, salinity, dissolved ions, toxicity of scaffold, temperature, and available nutrients. The cells will also need to be able to attach to the scaffold if they are to become representative of the *in vivo* environment [40]. An ideal scaffold not only supports viable cell culture but actively encourages proliferation in a manner akin to the natural *in vivo* environment. This capability can even be optimised to the specific tissue needs, to the extent that implanted scaffolds can modulate regeneration in local tissue defects [6]. The incorporation of a scaffold advances a model from a basic cell culture system towards a more sophisticated tissue engineering solution. A perfect scaffold will completely mimic the Extra Cellular Matrix (ECM) of the desired tissue type and cells will be able to integrate seamlessly into the scaffold, forming adhesions to the surrounding matrix. Stable homeostasis of a tissue microenvironment is underpinned by the proper organisation and adhesion of cells involving the correct maintenance, development, survival and migration of the resident cells along with supporting appropriate cell-cell and cell-matrix communication and interactions [41]. The lack of attachment to an ECM triggers programmed cell death through apoptosis, termed anoikis [42]. To recapitulate these materials synthetically is complex and an alternative is to use pre-existing materials which can interact with cells to form a base of the scaffold. Such biomaterials are widely used in the field of tissue engineering and can greatly accelerate the pace of research.

Hydrogels are a commonly used biomaterial for tissue engineering which are comprised mostly of water (typically greater than 95%. The polymers are not typically able to dissolve in water and will swell holding the water molecules within their structure [43]. The source ranges from natural such as alginate or collagen to synthetic such as poly(vinyl alcohol) or polyethylene glycol [44]. Hydrogels that are native to human tissue such as collagen, hyaluronic acid and, fibrin are an attractive source for tissue engineering as they need little modification to maintain cell cultures [45,46]. While some cells in culture can produce these human hydrogels the quantities and rates at which they are produced is slow, therefore incorporating much of the required material within the composition of the tissue model would reduce the time scales in developing the model.

A widely used biological ECM which contains many of the structural ECM proteins and growth factors required for cell attachment and proliferation is Matrigel®. It is produced from the excretions of Englebreth-Holm-Swarm mouse sarcoma tumour, which is harvested of its contents. It is comprised of 60% laminin, 30% collagen IV and 8% entactin accompanied with an assortment of growth factors including: transforming growth factor beta, platelet derived growth factor, vascular

endothelial growth factor, nerve growth factor, fibroblast growth factor as well as DNA, RNA, fibronectin and chloroform [47].

While Matrigel® would facilitate the attachment and proliferation of osteoblasts from the cornucopia of growth factors it contains, it was excluded from the model. Due to the tumour origins of Matrigel there is large batch to batch variation which can lead to varied responses and behaviors from cells cultured on it [48]. The collagen within bone is type 1 comprised of two alpha 1 chains and one alpha 2 chain, it is a structural parallel fibril forming a tight helix [49]. Matrigel predominantly produces collagen IV is comprised from six alpha chains with form along its helix. The function of collagen IV is a membrane protein, the chain complex links linearly rather than parallel aligned leading to the protein to have kinks. Collagen IV has reduced glycine units with amino acid chains therefore it has less structural integrity as the helix is unable to tightly form as in type 1 [50]. These limitations make Matrigel unsuitable as a base for the project with the focus remaining on type 1 as found in bone.

1.4 Approach Taken in this Study

The project will use conventional 2D cell culture to proliferate an osteoblast cell line and then combine these with a sacrificial alginate collagen hybrid gel with seeded calcium phosphate mineral to further culture the cells. The initial aim is that these will form an interpenetrating network of fibril collagen within the alginate and as well as the calcium phosphate mineral, act as an anchor point for the cells to attach to within the alginate. To achieve this the cells need to adhere to the collagen and calcium phosphate within the culture material and subsequently functionalize the network by depositing osteoid, after which the supporting alginate can be removed. Therefore, leaving behind the intrinsic microstructure of bone tissue. This will then be continually cultured to develop an accurate, hierarchically structured 3D cell culture model system of bone, to improve or accelerate the translational pathway.

Two approaches will be considered to achieve this aim. The first approach will be encapsulating cells within an alginate bead scaffold where collagen will be incorporated within the bead and seeded around the bead to create a larger complex model. The collagen beads and collagen templating gel will be seeded into a novel chip like culture chamber (Figure 1.4.1). Where the can be stacked in an identical repeating manner for reproduceable and consistent culture with the potential translation to high throughput screening [51,52]. This approach uses well defined techniques of alginate cell encapsulation and bead generation [33, 53, 54,55,56]. This approach is ultimately ruled out as shown in chapter 3

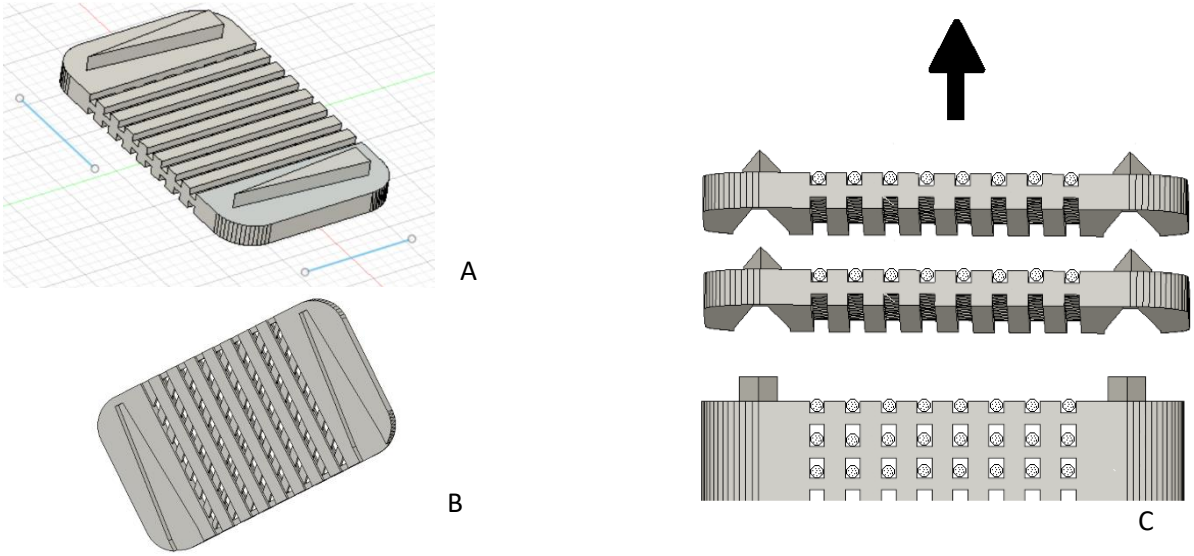

Figure 1.4.1 Possible stackable chip culture chamber for bone models.

A.) Above view of proposed culture chip showing the male part of the stacking feature. Blue scale bars 10 mm.

B.) The below view of proposed culture chip. The male triangles on top of the chip in A slot into the bottom of B allowing for the chips to be stacked. The channels within the chip allow for diffusion through the culture

C.) Stacked chips will contain cells encapsulated within alginate beads, the chips can be removed easily allowing for flexibility during culture and characterisation of the cells.

The second approach and is the main focus of the thesis is 3D bioprinting the cells within a sacrificial alginate collagen hybrid bioink with seeded calcium phosphate mineral. Where these approaches differ to many of the current approaches is to use alginate as a templating ink which allows the formation of an interpenetrating collagen network that cells can directly bind to. After which, the alginate can be removed, and the remaining cellularized collagen network can be modified further into the desired bone tissue [57,58,59,60]. This required the development of a 3D printing system that was compatible with fibril formation of collagen, calcium phosphate and integrated cells which is the focus of chapters 4, 5 and 6.

1.5 Aims and Hypotheses

The aims of this thesis are to develop a 3D bone cell culture model. This should have the ability to control spatial dimensions, size and easily reproducible. Therefore to achieve this the main objectives are:

Optimise and investigate the optimal encapsulation of bone cells within a bioink and the affect that long term culture has on the encapsulated cells.

Develop a system that can be used to control the spatial dimensions of the which is stable at physiological conditions and compatible with a collagen interpenetrating network and biomimetic hydroxyapatite incorporation.

The hypothesis is the cells will exhibit a time dependant response to time in 3D culture and that to facilitate a fibril collagen formation substantial reformulation and optimisation is required of the bioink.

2 Materials and Methods

2.1 Cell encapsulation

2.1.1 Gel Preparation

A sterile aqueous 4 wt/vol% alginate gel was prepared by exposing Sodium alginate powder (71238 Sigma, UK) to UV light (Osram Puritec HNS 15W 254nm ultraviolet lamp, UK) for 30 min before dissolving in warm (37 ^{o}C) proliferation media (Alpha Modification, Minimum Essential Medium Eagle (αMEM) (Sigma, UK), 10% Foetal calf serum (LabTech, UK) (FCS) and 1% L-glutamine 200 mM, penicillin 10,000 units, streptomycin 10 mg/mL solution (GPS) (Cat G6784 Sigma, UK)) and mixed with a magnetic stirrer for 30 min at 37 ^{o}C under aseptic conditions. The preparation was then transferred to a sterile 50 mL Falcon tube and centrifuged at 300 g for 5 min to remove any bubbles and refrigerated until use.

2.1.2 Encapsulation

MC3T3- E1 murine pre-osteoblast cells (ECACC 99072810, UK) between P16 and P20 were harvested at 80% confluency with trypsin (T4174 Sigma, UK) and seeded into αMEM alginate gel warmed to 37 ^{o}C at a density of 1x10^{6} cells per 1 ml of gel. The gel was aspirated into a 10 mL syringe using a 16 G needle and attached to the Luer lock syringe port on a Buchi 395 pro encapsulator (BUCHI Ltd, UK). The gel was extruded through a 180 µm needle at 27.5 mL/min, 2000 Hz oscillation and a 500 V electrical field and crosslinked in 100 mL 100 mM aqueous Calcium chloride (C8106 Sigma, UK) under vigorous stirring for 5 min. After incubation, the beads were washed through a 100 µm cell strainer (EASY strainer Greiner, UK) and washed with 20 mL of PBS (BR0014G Oxoid, UK) and 10 mL of proliferation media before transferring to a corning 180 mm cell culture dish and incubated in either proliferation media or supplemented media (supplemented with L-ascorbic acid (284 µM) (A5960) and β-glycerophosphate (10 mM) (G9422) – both Sigma, UK) overnight. Media was changed every 3-4 days and beads were transferred to a new cell culture dish whenever cells could be seen attached to the bottom of the culture dish.

2.1.3 Dose Response

MC3T3-E1 cells were cultured in a 48 well plate, when confluent the media was removed, the cells washed with PBS before being exposed to a concentration range of chelators from 1.56 mM to 100 mM for 30 min. The supernatant was removed, the cells washed with PBS before the media was replaced with 400 µL αMEM containing 10% Resazurin (ab129732 Abcam, UK) and incubated for 3 h in darkness. Fluorescence was recorded on a Tecan Spark plate reader (Tecan, Switzerland) at an Excitation wavelength of 550 nm and Emission wavelength of 585 nm.

2.1.4 Mechanical testing

Greiner bio-one thin cert 0.4 µm plate inserts were inserted into in a 12 well plate to which 1 and 2% alginate gels were added using a 5 mL syringe until filling the insert. One hundred mM aqueous $CaCl_2$ was added to submerge the cell inserts and left to crosslink for 48 h with $CaCl_2$ changed approx. every 16 h. The cast gel cylinders dimensions measured approx. 10 mm diameter x 15 mm height; a caliper was used for exact dimensions. A ramp compression test up to 20% strain at 0.01 mm/s was performed using a 250 g load cell attached to a Bose ElectroForce 5500 Mechanical Testing Instrument (TA Instruments, USA).

2.1.5 Statistical analyses

Statistical significance was determined by means of a two-way ANOVA with Bonferroni post-hoc test performed using GraphPad prism8.

2.1.6 Scanning Electron Microscopy

The scanning electron microscope (SEM) preparation protocol is detailed elsewhere [4]. Briefly, all cell culture media was removed, the samples were placed into a -20 ^{o}C freezer for 3 h, then transferred to a -80 ^{o}C freezer where they were stored until freeze drying for 24 h at with the condenser chamber set to -55 ^{o}C. Once lyophilised, samples were stored in a desiccator until gold splutter coating just before imaging using a TM3030 tabletop SEM (Hitachi, Japan)

2.1.7 Post Chelation Proliferation

Approximately 100 µL of alginate beads (either 1 or 2 wt/vol % containing $1x10^6$ cells per mL of gel) was transferred to a 25 mL centrifuge tube and allowed to settle before the supernatant was removed and the beads washed with 500 µL of PBS. PBS was removed before a 1.5 mL of aqueous chelator solution (either Ethylenediaminetetraacetic acid EDTA (A4892, PanReac, UK), sodium citrate (C8532 Sigma, UK), Hexametaphosphate (HMP) (S/4160/60 Fisher Chemical, UK) or Sodium Pyrophosphate (PPi) (P8010 Sigma, UK)) at a concentration of 90 mM (2% gels) or 45 mM (1% gels) at pH 7.4, supplemented with 10 % FCS (Lab Tech, UK) was added and then agitated for 5 min on a shaker plate at 200 rpm at room temperature. Samples were then mixed with a 1000 µL pipette, 3 mL of PBS was added and briefly vortexed before centrifuging at 300 g for 5 min. The supernatant was removed, and the remaining cell pellet was resuspended in 500 µL of PBS and centrifuged again at 300 g for 5 min. The supernatant was removed, and the cell pellet resuspended in 150 µL αMEM and transferred to a 1.5 mL Eppendorf, 3 tubes were used resulting in a total volume of 450 µL. A trypan blue cell count (Fast Read 102 cell counter, UK) was performed and provided total yield of cells from chelation. 10,000 cells were then transferred to a 48 well plate for proliferation analysis.

2.1.8 Proliferation and Viability

After the selected time point in 2D culture post chelation, each well had the media aspirated and washed with 200 µL PBS before being removed using 150 µL trypsin Ethylenediaminetetraacetic acid, (EDTA) (Sigma, UK) and incubated at 37 ^{o}C for 5 min. 400 µL of αMEM was added to each well, the cell suspension was then transferred to a 1.5 mL Eppendorf and centrifuged for 7.5 min at 500 g. Before the supernatant was removed and resuspended in either 50 µL or 100 µL αMEM, a 7 µL aliquot was taken for counting on a Faster cell counting chamber. The control cells (i.e. unencapsulated) were from the same stock as the encapsulated cells and cultured alongside, passaging at 80% confluency. Each week a flask of the 2D control would be dissociated with trypsin and $1x10^4$ seeded per well on the same 48 well plate. Daily counts were performed in line with the experimental samples.

Manual cell counts were performed with a (Fast Read 102 cell counter) in triplicate with and without trypan blue.

2.1.9 Cell Attachment

MC3T3-E1 cells were cultured as described above; briefly $1x10^4$ cells were seeded onto a 48 well plate to create a confluent monolayer, after which either 1 or 2 % beads containing cells encapsulated at 10^6 cells per mL of gel were deposited on top. The media was aspirated and replaced with 400 µL supplemented media. The plate was incubated at 37 ^{o}C with 5% CO_2 with media changes every 3-4 days.

After 14 days the media was removed and replaced with αMEM media containing Calcein AM ((0.4 µl per well) ThermoFisher, UK) and incubated at 37 ^{o}C, 5% CO_2 in the dark for 30 min. Images were taken with an Olympus IX81 microscope fitted with Olympus Fluoview FV1000 confocal unit and Mercury arc lamp (Olympus, UK) to record confocal and fluorescent images respectively.

2.1.10 Cell Type Used

The cell line used throughout the entirety of this research was MC3T3-E1 (ECACC 99072810, UK) it is a mouse calvaria preosteoblast, all research started from the same stock of cells and cryopreserved as appropriated to ensure continuous supply throughout. The cells were cultured with a basal media of αMEM supplemented with PS and FCS, though further media modifications were investigated in addition to this. The cells were continually cultured and used up to P20, media was changed every 2 to 3 days and passaged at 80% confluence approximately every 4 days.

2.2 Bioink- continuing development

2.2.1 Competitive Ligand Exchange (CLEX)

Stock CLEX components were made up with Part A consisting of 1 M $CaCl_2$ and 0.5 M EDTA with a buffer of either HEPES or MOPS both at 1 M in a 2:2:1 Molar ratio. Part B consisted of 1 M Zinc Acetate, 1M Glycine and 1 M buffer in a 2:4:1 Molar ratio, when formulated with 1 M Diglycine the Molar ratio was 2:2:1. All Molar ratios all were buffered using NaOH or HCl to pH 7.40. After buffering to desired pH using HCl or NaOH, αMEM (10% FCS, 1% GPS) was added until part A was at a working Ca^{2+} concentration of 240 mM and part B was at a working Zn^{2+}concentration of 120 mM ready for incorporation in the bioink and SLAM respectively.

2.2.2 CLEX Bioink

When incorporated into bioink per 1 mL: 250 µL CLEX A working concentration (240 mM $CaCl_2$) was added and mixed with 4% alginate made with complete αMEM, neutralised 3 mg/mL Rat tail collagen type 1 (A1048301, Gibco ThermoFisher, UK), and complete αMEM were added in the remaining volume depending on the desired final concentration.

For cell viability in the bioink 400 µL αMEM containing 10% Resazurin and incubated for 3h in darkness. Fluorescence was recorded on a Tecan Spark plate reader (Tecan, Switzerland) at an Excitation wavelength of 550 nm and Emission wavelength of 585 nm.

For 4.2.1 a one way ordinary ANNOVA with Dunnett's multiple comparisons test was performed in GraphPad prism 8.

For 4.2.3 a two way ANNOVA with Dunnett's multiple comparisons test was performed in GraphPad prism 8.

2.2.3 Suspended Layer Additive Manufacture (SLAM)

Agarose (BP 1356 Fisher, UK) powder was added to di H_2O at 0.6% with a stirring bar added and autoclaved @121 ^oC for 15 min, removed from the auto clave while above 50 ^oC and placed on a stirring plate and allowed to cool under sheer with a full vortex until the preparation had cooled until room temperature.

2.2.4 Construct pH Optimisation

CLEX solutions were made up to the desired concentrations and the pH was initially tested after 2 h incubation with pH testing strips (pH-indicator strips pH 6.5 - 10.0 Merck, UK) and verified with a FiveEasy Plus pH probe (Mettler Toledo, UK). The probe was calibrated with an aliquot of the same standard from the manufacturer throughout.

CLEX B was added to the SLAM component of the system and incubated at the stated temperature, the pH probe was immersed in the SLAM CLEX B solution and the readout was taken when the pH had stabilised. The bioink containing CLEX A was kept at 4 ^{o}C to ensure that the collagen did not prematurely polymerise and subsequently printed into the SLAM CLEX B and incubated for 2 h at the stated temperature. After the incubation the probe was immersed in the SLAM CLEX B + Bioink CLEX A well and the read out taken after the pH stabilised under constant stirring.

2.2.5 Fluorescent Collagen Staining

100 mg Corning rat tail Collagen type 1 was labelled using the method as described by Doyle 2018 [61]. Briefly, 15 mg of collagen was diluted to a working concentration of 3 mg /mL and polymerised at room temperature for 1hr. The polymerised collagen was either labelled with Atto-488 NHS-ester (41698-1MG-F Sigma, UK) or Atto-647N NHS-ester (18373-1MG-F Sigma, UK) with a 2 M excess. The polymerised collagen was liquefied using 500 mM acetic acid (10230753 Fischer Scientific, UK) overnight at 4 ^{o}C covered from light until all the gel had liquefied, the volume measured to determine the new concentration of the collagen solution. The labelled collagen was loaded into a dialysis chamber (Slide-A-Lyzer, 87735 Sigma, UK) and dialyzed at 4 ^{o}C in 4 L of 20 mM Acetic acid (10230753 Fischer Scientific, UK) for 4 h, the acid then changed for a further 24 h. Labelled collagen was transferred to a sterile Eppendorf and kept either at 4 ^{o}C for use within one year or indefinitely at -80 ^{o}C.

Confocal microscopy was performed using an Olympus IX81 microscope fitted with an Olympus Fluoview FV1000 confocal unit. Labelled collagen was incorporated into a working 1 mg/mL collagen solution at a 1 in 10 dilution (0.1 mg/mL) to give a clear representation of the collagen structure. 1 in 5 (0.2 mg/mL) and 1 in 15 (0.067 mg/mL) dilutions were also tested but the signal was found to be either too strong or too weak for clear fibril structures to be observed. Samples were kept hydrated in PBS and were imaged in a confocal dish (Glass Bottom Dishes, 150682 Nunc, ThermoFisher, UK) to keep the cells viable and for greater optical penetration into the sample. For optimal fibril clarity x 60 oil magnification was used for Z stacks with 4 µm slices. Images were stitched together in Imares (Version 7.2.1).

2.2.6 Alginate Concentration Optimisation

CLEX Bioink was prepared as previously described Section 2.2.2, a fixed final collagen concentration of 1 mg/mL (3 mg/mL Rat tail collagen type 1 (A1048301, Gibco, ThermoFisher, UK)) was used throughout the experimental series. Fluorescently labelled collagen was incorporated at 10% of total collagen. For each Condition 1.5 mL of bioink was made for each run. A 4% media-based alginate was prepared as previously described and used for the bioink. To vary the alginate concentration within the bioink, the media diluent volume was adjusted to maintain the same total 1.5 mL volume. All components of the bioinks were cooled on ice before use. The optimal order of mixing bioink components was found to be: (1) alginate and CLEX mixed well with (2) a pre-combined solution of collagen neutralised with 1M NaOH before finally mixing with the required media volume to achieve the desired final concentration of the bioink. A 1mL syringe was used for all mixing due to the high viscosity of the alginate at higher concentrations, and therefore minimise loss of the polymer component.

2.2.7 Collagen Concentration Optimisation

CLEX Bioink was prepared as previously described in Section 2.2.2. A fixed final alginate concentration of 0.6% was used throughout the experiment series. Fluorescently labelled collagen was incorporated at 10% of total collagen. For each Condition 1.5 mL of bioink was made for each run. By varying the media diluent of the bioink the percentage concentration of collagen was varied while maintaining a fixed concentration of alginate. Rat tail collagen (Collagen I HC, rat tail, 100 mg, Corning, UK) at a concentration of 9.1 mg/mL was incorporated into the alginate at various ratios from ranging from 1 to 6 mg/mL. Due to the fixed the concentration of the other components 6 mg/mL proved to be the maximum limit of collagen integration.

2.3 CLEX Collagen Interpenetrating (IPN) Mineral

Chemobrionic tubes were used as the mineral component of the bioink, these have been developed and characterised as previous described [62]. Briefly, agar powder (11489632, Thermo scientific, UK) was dissolved into 1 M $CaCl_2$ (C8106 Sigma, UK) at 5% w/v and autoclaved at 121 ^oC for 20 min. While still liquid 20 mL of agar $CaCl_2$ was poured into T75 cell culture flasks (Corning, UK) in an aseptic biosafety cabinet class II and set while the flasks were stood vertical with the lids on. When the Agar had set 50 mL of autoclaved 0.8 M Sodium Phosphate Dibasic (424380010, Thermo Fisher, UK) was added to each flask. The tubes were harvested when they had reached the top of the reaction solution or after 30 min which ever came first. A 10 mL stripette (Fisherbrand, UK) was used to disrupt the tubes and the contents of the flask passed through a 100 µm filter. The flask was washed with PBS which was passed through the filter until all the tubes had been collected. The tubes then were washed with complete αMEM until the colour indicated a pH range suitable for cell culture.

To label the tubes, calcein blue (M1255, Sigma, UK) was dissolved in DI H_2O at a concentration of 2 mM stock solution. A 1 mL suspension of tubes containing 20 mg tubes was placed in a 20 mL centrifuge tube. 50 µL of stock calcein solution and 3.95 mL of DI H_2O added to make a final volume of 5 mL at 20 µM calcein. The tubes were incubated overnight and rinsed with DI H_2O three times. Then resuspended in PBS without calcium.

2.4 Osteoblast maturation in vitro

2.4.1 Differentiation Media

To determine optimal osteogenic media parameters, 3 different established differentiation media protocols were tested. All were based on proliferation media αMEM (Sigma M8042), 10% Foetal calf serum (LabTech) (FCS) and 1% L-glutamine 200 mM, penicillin 10,000 units, streptomycin 10 mg/mL solution (GPS) (Sigma: Cat G6784) and supplemented as follows.

Media 1 L-ascorbic acid (284 µM) (A5960) and β-glycerophosphate (10 mM) (G9422) – both sigma, UK) [63]

Media 2 L-ascorbic acid (284 µM) (A5960) and β-glycerophosphate (2 mM) (G9422) [64]

Media 3 L-ascorbic acid (284 µM) (A5960) and β-glycerophosphate (10 mM) (G9422) and 100 nM Dexamethasone (D4902, Sigma, UK) [65]

Control – Standard proliferation αMEM media as previously described.

$5x10^4$ cells were plated on 12 well plates and allowed to proliferate to 90% confluency before media being changed to either Media 1, 2, 3 or control. At seven-day intervals cells were harvested and RNA was extracted for qPCR.

2.4.2 RNA Extraction and Quantification.

The lab bench was thoroughly cleaned down with RNase Zap and then with 70 % ethanol. A RNeasy Micro kit (50) (74004 QIAGEN, UK) was used to extract the RNA, all spins were performed at 13000 rpm (15871 g) unless otherwise stated. Cell monolayers were trypsinised for 10 min then a cell scraper was used to homogenise the monolayer and remove it from tissue plastic. Cell suspensions were then transferred to a 1.5 mL Eppendorf and spun at 500 g for 450 s to form a pellet. The supernatant was removed, and cells resuspended in 500 µL MEM for counting. 5×10^5 cells were isolated and pelleted for 2 min, the supernatant was removed and replaced with RLT buffer with 1% β-mercaptoethanol (Sigma, UK). The pellet was further broken up with a 1000 µL pipette tip until a homogeneous cell suspension was achieved, if required a 19 G needle and syringe was used. The cells were pelleted again, and 70% ethanol was added to the Eppendorf tube and the cells resuspended and transferred to a RNeasy mini spin column. The ethanol, RLT and cells were spun for 2 min the supernatant was removed. RW1 buffer added, and the cells spun again for 1 min. 80 µL of

DNase (QIAGEN, UK) was incubated at room temperature on the columns for 15 min. RW1 buffer was added again, and the columns spun for 1 min and the supernatant removed. Wash buffer RPE was added to the columns and spun for 1 min then 80% ethanol was added, the columns spun for 1 min and then the column was transferred to a new collection tube and spun for 5 min with the lids open to remove as much ethanol as possible. The columns were transferred to a 1.5 mL Eppendorf and 14 µL of RNase free water added directly onto the membrane in the column and incubated for 10 min at room temperature. The columns were spun again for 1 min and the RNA transferred back onto the membrane for a further spin for 2 min. The RNA concentration was then measured using a Nanodrop 2000 spectrophotometer (ThermoFisher, UK).

2.4.3 cDNA Conversion

A high-capacity cDNA Reverse Transcription kit (4368814, Applied Biosystems, ThermoFisher, UK) was used to convert the extracted RNA into cDNA. Briefly, 14 µL of cDNA regents mixed as per the manufacturer's instructions were combined with 500 ng of RNA in a 200 µL dome capped PCR tube (AB1770, ThermoFisher, UK), the resulting mixture was then combined with RNase free water to a total reaction volume of 28 µL in a 1:1 ratio. RNA was denatured for 5 min at 65 °C and reverse transcribed for 1 h at 50 °C then held at 4 ^{o}C before retrieval and stored at -80 ^{o}C until RT-qPCR analysis.

2.4.4 RT-qPCR

Gene expression and quantification was detected using Applied Biosystems® Taqman® Gene Expression Master Mix and FAM-conjugated Taqman® probes (Table 2.2). Quantitative polymerase chain reaction (qPCR) amplification conditions were a single 95 °C 2 min cycle followed by 40 cycles of 95 °C for 15 s and 60 °C for 1 min (Roche LC480 real-time thermal cycler (F. Hoffmann- La Roche, UK). A reaction volume of 5 µL of which 2.52 µL was Applied Biosystems® Taqman ® Gene Expression Master Mix and 0.28 µL relevant Taqman® primer in a 10:1 ratio combined with 2.3 µL cDNA as previously described in Section 2.4.3.

Table 2.1 List of all primer probes used and their associated gene code.

Primer	Code	Supplier
Msx2	Mm00442992_m1	Taqman, UK
Runx2	Mm00501584	Taqman, UK
Sp7	Mm04209856	Taqman, UK
Col1a1	Mm08801666	Taqman, UK
Alpl	Mm01187117	Taqman, UK
SPP1	Mm00436767_m1	Taqman, UK
Pdpn	Mm00494716_m1	Taqman, UK
Bglap	Mm03413826	Taqman, UK
Sparc	Mm00486332_m1	Taqman, UK
Rn18s	Mm04277571_s1	Taqman, UK
B2m	Mm00437762	Taqman, UK

The primer sequences of Taqman® probes are not published by the manufacturer. This is in part due that Taqman® does replicate DNA in the way that typical PCR does. Instead sequence specific oligonucleotides called probes bind to denatured dsDNA. The probes are not extended as with primers, instead probes bind to the target DNA region. On the 5' end of the oligonucleotide there is a fluorescent molecule which is quenched by a molecule on the 3' end. As taq polymerase extends along the denatured DNA it cleaves the probe and releases the fluorescent molecule which can be detected by the qPCR machine [66].

2.4.5 RNA Extraction for qPCR/Expression Profile for cells in Constructs

3D printed constructs were removed from culture wells with plastic tweezers and places in a 25 mL centrifuge tube, residual media was washed with 1 mL of PBS. PBS was removed before a 1.5 mL of aqueous chelator solution (sodium citrate (C8532 Sigma, UK) at a concentration of 90 mM pH 7.4, supplemented with 10 % FCS (Lab Tech,UK) was added and then agitated for 5 min on a shaker plate at 200 rpm at room temperature. Samples were then mixed with a 1000 µL pipette, 3 mL of PBS was added and briefly vortexed before centrifuging at 300 g for 5 min. The supernatant was removed, and the remaining cell, collagen and mineral pellet was resuspended in 500 µL of PBS and centrifuged again at 300 g for 5 min. The supernatant was removed and replaced with 350 µl RLT buffer with 1% β-mercaptoethanol (Sigma, UK). The sample was then treated as per RNA extraction described above.

2.5 3D printing

A RegenHU Discovery 3D bioprinter was used for all 3D printing experiments (RegenHU, Switzerland). For all bioprinting a 3 mL autoclaved syringe (7012074 Nordson EFD, UK) was used without a plunger. All constructs and print calibration files were made in RegenHU BioCAD software. A default printer movement speed of 30 mm/s was used for all prints with only the pressure and needle diameter changing.

To find suitable pressure ranges for extrusion, bioink was loaded into the printer and the extrusion pressure was set to zero. The printer was set to continuously extrude through the user interface, the pressure was manually increased until a steady flow of bioink was flowing from the needle. From this point, more refined and accurate techniques could be used to determine optimal printing pressure for each bioink condition.

For needle diameter calibration, a basic bioink maintained at 4 ^{o}C containing 0.6% alginate and fluorescein at 25 µM was used. A series of straight lines with right angle turns was printed into CLEX SLAM, incubated for 30 min at 37 ^{o}C and retrieved using 100 mM $CaCl_2$. The retrieved constructs were then imaged on a confocal dish. Multiple images were taken across the entire printed shape and the width of the filament measured using IMARES (Version 7.2.1). This was repeated using a range of 40 mm long needle gauges (20 to 27 G) and different pressures for each needle to find the optimal conditions. When the optimal extrusion conditions had been determined, the printing parameters were repeated again using bioink containing collagen, tubes and cells at working concentration and any adjustments to the pressure was made accordingly. An ordinary one-way ANNOVA with Tukey's multiple comparisons test was performed in GraphPad prism 8.

When printing experimental conditions, a cool jacket kept on ice was used keep the temperature of the bioink low to inhibit collagen polymerisation. CLEX SLAM agarose was warmed to 37 ^{o}C in a water bath before being transferred to the well plate inside the bioprinter hood, standard cell biology aseptic practices were maintained throughout the process. An autoclaved 3 mL syringe (7012074 Nordson EFD, UK) had an autoclaved metal needle attached. 2 mL of bioink was loaded into the syringe then the whole setup was loaded into a cool jacket. 3 constructs were printed sequentially in a 12 well plate and the remaining bioink was retrieved from the syringe by removing the needle and purging the syringe with constant flow. The needle was purged with sterile PBS to remove any blockages and attached to a fresh sterile 3 mL syringe and a further 2 mL of ink added for the next 3 constructs. This was repeated until the whole plate had been printed. Constructs were then transferred to an incubator at 37 ^{o}C, 5% CO_2 for 2 h to polymerise the collagen and CLEX alginate.

After incubation, plates were transferred to a biosafety class two hood and the agarose fluid gel was gently diluted off with 100 mM $CaCl_2$ to release the construct from the support bath. The partially gelled constructs were further incubated in the $CaCl_2$ to fully crosslink any remaining unpolymerized gel aiding in successful removal.

2.6 X-ray Fluorescence (XRF) and Mineralisation of Constructs

For Alizarin Red staining, 2 g Alizarin Red S (A5533, Sigma, UK) was dissolved in 100 mL DI H_2O, while shielded from the light. The pH was adjusted with ammonium hydroxide or HCl to 4.1 – 4.3, the solution was then stored in the dark until use.

At each time point, cells in 12 well plates had the media removed and were washed three times with 500 µL PBS. The PBS was aspirated and the cells air dried for 1 min then approximately 300 µl 4% PFA (HT5011-1CS, Sigma, UK) was added the well to ensure the monolayer was complete covered. The well plate was covered and gently agitated for 30 min on a shaker plate at 50 rpm at room temperature. After 30 min the PFA was aspirated and the cells were washed with 1 mL DI H_2O 4 times, 300 µl of Alizarin Red S solution was added to each well. The plates were protected from the light and gently agitated for 45 min on a shaker plate at 50 rpm at room temperature. The staining solution was carefully aspirated, and the wells washed with 1 mL DI H_2O at least 4 times or until the wash showed no more stain present. 1 mL of PBS was added to each well and the plates stored at 4 ^oC until use with the PBS topped up as required.

The stained plates were imaged on a Cytation 5 (BioTek, USA), 60 images at x 20 magnification were stitched together for each image. The red thresholding was measured with ImageJ Fiji.

Alizarin red extractions were performed in accordance with ScienCell's ARS Staining Quantification Assay (ARed-Q) protocol [67]. A two way ANNOVA a Dunnett's multiple comparisons test was was performed in GraphPad prism 8.

Monolayers of cells were cultured on T25 flasks. At the selected time point, the media was removed and the sample washed with PBS. The cells were then fixed with 4% PFA (HT5011-1CS, Sigma, UK) for 30 min. The remaining PFA was rinsed with 5 mL PBS, for two washes 5 mL of DI water was then used to rinse the samples. The flasks were then frozen at – 80 ^oC until freeze dried under vacuum at -55 ^oC overnight. The baseplate of the flask was cut out using a handheld saw (Dremel electric multitool), care was taken not to damage the monolayer of cells. The monolayer was placed into a M4 Tornado instrument Micro- X-ray fluorescence (µ-XRF) (Bruker, USA). A vacuum of 30 mbar was

pulled within the chamber. The X ray emitter was operating at 50 kV and 300 mA. The monolayers were analysed three times at 10 ms per measurement.

3 Development of Methods For The Effective Encapsulation and Retrieval of Cells in Alginate Microbeads

3.1 Preface

The initial approach of this project was to seed osteoblast cells and an interpenetrating network of collagen within sacrificial alginate. With the aims of the cells adhering to the collagen within the alginate and further functionalising the network and subsequently the alginate can be removed. To achieve this, cells were encapsulated within an alginate bead and placed in a chip like construct (Figure 1.4.1). Collagen was to be incorporated within the alginate bead and placed on top of the beads within the chip culture chamber. The hypothesis was the cells would develop within the culture chip and could easily be used for assays. This was found not to be compatible with encapsulation. Due to the dropping of beads into a crosslinking bath required for encapsulation, it was determined that the minimum concentration of $CaCl_2$ required for this was 25 mM. Due to the glycine residues on the collagen chains, fibril collagen was not able to form within the beads when cross linked under these conditions (Figure 3.1.1). This ultimately led to the change in methodologies from encapsulation to bioink formulation later investigated in chapter 4.

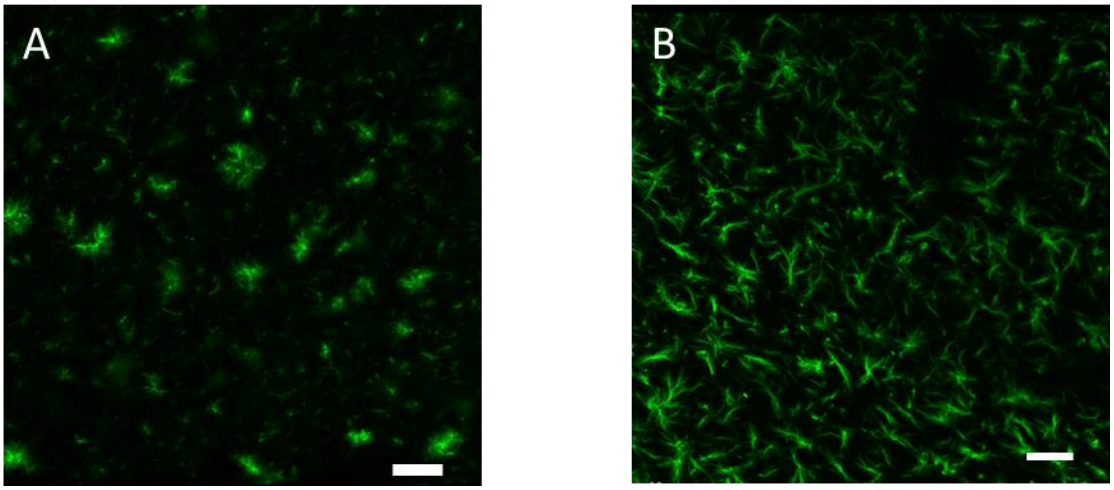

Figure 3.1.1 Fluorescently labelled collagen within alginate crosslinked with 25 mM calcium chloride and uncross linked alginate. 0.6% alginate 0.1 mg/mL rat tail collagen was used for both conditions. Scale bars 30 µm

A. Fluorescently labelled collagen within alginate crosslinked with 25 mM calcium chloride, the collagen can be seen to be clumps and undefined within the alginate.
B. Fluorescently labelled collagen within non-crosslinked alginate , the collagen forms clearly defined fibrils within the ink.

Additionally to the poor collagen structure, cell viability within the beads was not detected using alamar blue. The beads were chelated with EDTA to release the cells inside, while the cells were able to attach the 2D TC plate no metabolic activity or proliferation was measured with Resazurin reduction at 24 h, 5 or 7 days in culture. On visual inspection, cells presented with an abnormal morphology, they were rounded with very few flat cells (Figure 3.1.2).

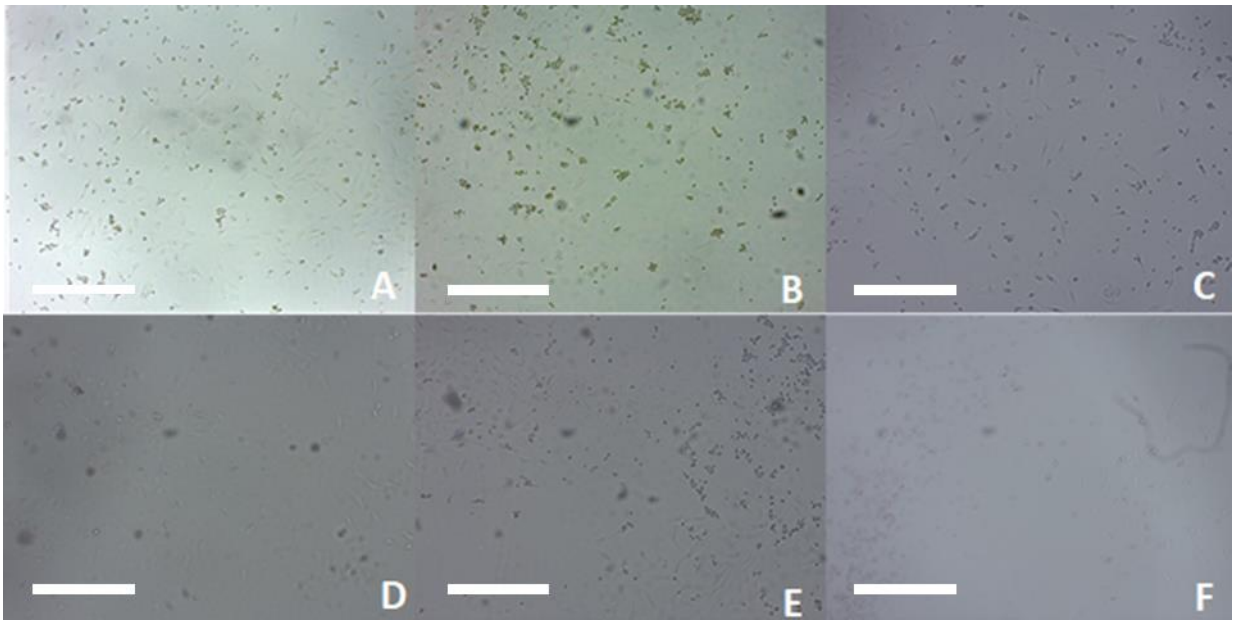

Figure 3.1.2 Images of cells in either 10 or 20% FCS with either 1.5 or 3 mL EDTA versus EDTA alone after 8 days in culture with 1 wash and media change. All images at x 4, Scale bar = 500 µm.

The top row is 1.5 mL of EDTA – A.) 10% FCS, B.) 20% FCS and C.) EDTA alone after 8 days.
The bottom row is 3mL EDTA – D.)10% FCS, E.) 20% FCS and F.) EDTA alone after 8 days

To improve the attachment and proliferation post encapsulation, reformulation of the chelating conditions was invested to ameliorate the poor cell yields. Initially tested was the addition of Foetal Calf Serum (FCS) to reduce the toxicity of the EDTA chelator. FCS is a requirement for healthy cell culture and is often used to maintain cell viability outside of culture[68]. 3 mL of 100 mM EDTA was used per condition, this was supplemented with 10 or 20% FCS, reducing the concentration to 90 mM, and bead exposure was 10 min. Next the volume of EDTA was reduced to 1.5 mL remaining at the same final concentration, again with 10 or 20% FCS. After 24 h there was no observable difference between any condition using resazurin or visual appearance. After 8 days in culture, the new methodology with 10% FCS appeared to have some colonies formed with fewer rounded cells, though, there was still no difference using resazurin which was below the threshold of detection (Figure 3.1.2). Though very slight improvements were seen, the protocol was modified to 1.5 mL of chelator supplemented with 10% FCS.

To reduce the toxicity of the chelation, the initial chelator exposure time would be tested at between 1 and 10 min. 1.5 mL of 90 mM EDTA at pH 7.4 with 10% FCS was added to 100 μl of beads at 10^6 cells/mL. The beads would be shaken at room temperature as before, and the gel beads would be well pipetted to dilute the alginate away from the cells with time being the only variable. After 24 h there were similar yields between 1 min in EDTA and 10 min, again yielding minimal viable cells and no activity measured with resazurin. Visual images show that there is a similar outcome between the two samples Figure 3.1.3.

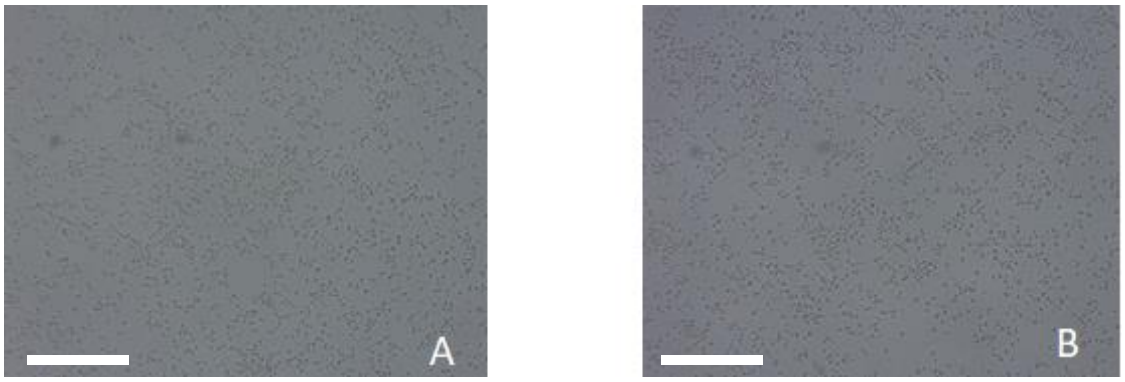

Figure 3.1.3 Cultured MC3T3 cells post release from alginate beads. The alginate beads which encapsulated the cells was exposed to EDTA for either 1 or 10 minutes. The images show little difference in cell yield or morphology. All images at x 4, Scale bar in Figure A = 500 μm. A) 1 minute exposure B.) 10 minute exposure.

With the new chelation time of 1 minute used, and the addition of 10% FCS still yielding released cells that are not viable in culture, a EDTA dose response was tested along with 3 other chelating agents. The investigation was written up into a research article shown below.

This work has been written up into a manuscript for publication, the experimental work was performed solely by L.A Hill with feedback and supervision from A. J Naylor and D.C Basset.

3.2 Abstract

Alginate encapsulation has been widely used for several decades for the storage, protection and processing of both eukaryotic and prokaryotic cells. A prevalent feature of alginate that makes it particularly useful and convenient for encapsulation, bioprocessing and biofabrication is its reversible gelation mechanism, made possible by physical junction zones with multivalent cations. This gelation process can be performed under cyto-compatible conditions to enable effective cell encapsulation, storage, distribution, and structuring.

Despite a wide body of literature describing this reversible gelation process, relatively little consideration has been given to the influence of the chelating agents (used to disrupt the hydrogel network and retrieve a cell population) on cell behaviour. In this paper, the effect of a range of commonly used chelators on the metabolism and proliferation potential of pre-encapsulated MC3T3 cells has been systematically evaluated.

A commonly used chelator, EDTA, demonstrated a strong toxic effect on the encapsulated cells whereas hexametaphosphate, citrate and pyrophosphate ions enabled timely retrieval with minimal toxicity. Furthermore, by optimising alginate content, the culture environment and chelating agent, it was possible to develop a rapid five-minute de-gelling protocol, enabling the release of cells from encapsulation with much higher levels of viability and proliferation potential than with standard protocols. This describes a quick and reliable method to release cells from alginate microbead encapsulation and addresses appropriate time limits for encapsulation to ensure maximal cell viability and proliferative capacity of the released cells.

3.3 Introduction

Cell encapsulation is a widely used technique for tissue engineering [69],[70],[51] and cell storage [71],[72],[73]. Currently there are many techniques to encapsulate cells but the reliable, simple, non-toxic release of cells for subsequent culture has not been widely reported. One of the most widely used encapsulation substrates is alginic acid (aqueously soluble salt – alginate), which is a naturally occurring biopolymer of randomly repeating mannuronic and guluronic acid residues. Primarily it is purified from marine brown algae such as *Macrocystis pyrifera, Laminaria hyperborea and Ascophyllum,* however it is also produced by certain bacteria, such as *Pseudomonas aeruginosa* [74]*.* Alginate is a highly industrially-relevant polymer, with significant use in food, medical and pharmaceutical applications [75],[76]. In the context of encapsulation of living cells, alginate has some exceptional advantages for the safe and effective protection of both eukaryotic and prokaryotic cells in terms of economics and simplicity. These advantages are particularly interesting for contemporary bioprocessing applied in 3D bioprinting [33], cryopreservation [71], tissue engineering [60], bioproduction [77], advanced drug delivery [78], microfluidics [79] and cell screening [80].

Despite a great deal of attention given to the encapsulation process, primarily in the context of gelling kinetics and emulsion formulations [54], relatively little attention has been given to the retrieval of encapsulated cells from crosslinked alginate hydrogels, particularly for recovery of viable eukaryotic cells. For example 5% peroxide has been used to degrade alginate gels [81], which is far greater than the dose required to cause intestinal inflammation[82] or significant cytotoxicity in culture[83]. Enzymatic degradation of alginate requires reaction conditions of 50 ^{o}C and pH 6.0, which are substantially outside optimal physiological conditions and are potently cytotoxic [84],[85]. Other techniques are available to dissociate alginate polymer networks for the retrieval of encapsulated cells such as acidification [81]and heating [86]. However these techniques, while effective at breaking down alginate polymers, require conditions that are not well tolerated by cells [87]. Current extraction techniques for the retrieval of live cells from crosslinked alginate hydrogels are therefore limited to chemical chelation as this is a facile technique that can be performed under physiologically compatible conditions [88],[89],[69], however the relative effect of chelators on cytotoxicity is not well documented. Here, we have explored the cytotoxicity of the more commonly used chelators and have optimised the de-gelling process, such that the cells can be safely removed from the gel within 5 minutes with low toxicity and improved recovery.

3.3.1 Aims and Hypotheses

The overall aims of this chapter are to develop the effective encapsulation and retrieval of cells in alginate microbeads. With a focus on optimising the diluent of the alginate hydrogel, the culture conditions for optimal long-term culture of cells encapsulated in alginate microbeads and an effective method for releasing viable cells for further characterization if required.

The hypothesis is that the diluent of alginate will have an effect on the encapsulated cells viability, the length of culture within the alginate will affect the cells proliferation and that the release of the cells will be vary little between each chelator.

3.4 Methods

The methods section for this manuscript can be found in Chapter 2 section 2.1.

3.5 Results

For the beads to fit within the SSL chip as previously described, a heterogeneous population with viable cells is required. Therefore initially optimal bead formation was investigated along with the alginate diluent which is most compatible with cell incorporation as shown in Figure 3.5.1.

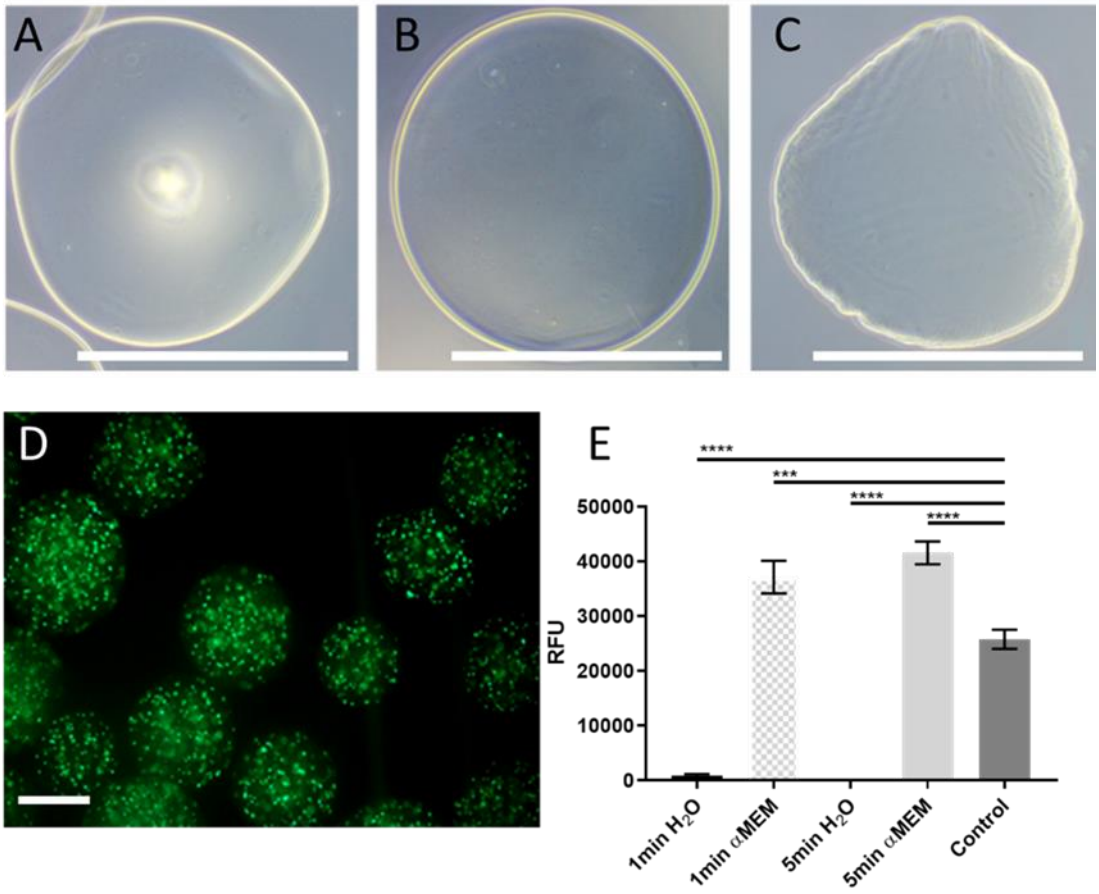

Figure 3.5.1 Overview of the development process for encapsulating cells in alginate microbeads (AMBs). **A-C)** Light micrographs of 2% w/v AMBs generated at different flow rates. **A)** 17.5 mL/min **B)** 27.5 mL/min **C)** 37.5 mL/min **D)** Confocal fluorescent light micrograph of encapsulated MC3T3-E1 cells in 2% w/v diH_2O based AMBs stained with calcein AM (green) marker of viable cells and propidium iodide (red) for dead cells. **E)** Metabolic activity of cells post-encapsulation and retrieval. Cells were encapsulated in a 2% w/v AMBs gel made with either diH_2O or with αMEM complete cell culture media (as indicated) and released using sodium citrate chelator for the indicated time and proliferated for 24h, prior to measurement of metabolic activity expressed as RFU (Relative Fluorescent Units) compared to a 2D control of the same seeding density. n=3. Error bars = +/- SD. All Scale bars 400 µm. *; P < 0.005 **; P < 0.0005 ***; P < 0.0001 ****

To achieve bead consistency, microscope images of beads formed at a range of flow rates were analysed to determine optimal flow rates during the encapsulation process. At low flow rates (<~20 mL/min), beads showed an irregular surface and a concave middle, indicated by light refracting from

the centre of the bead (Figure 3.5.1A). Optimal flow rates were achieved when the surface of the bead was smooth and regular with no discernible features (Figures 3.5.1B). At higher flow rates (>~30 mL/min), beads were produced with a wrinkled surface and distorted shape (Figure 3.5.1C). An optimal flowrate of 27.5 mL/min was determined, which was used in further cell encapsulation studies. Cells were encapsulated in 2% AMBs made with diH_2O as the aqueous phase and showed high viability (circa. 100%) immediately post encapsulation when stained with calcein AM and propidium iodide (Figure 3.5.1D). When encapsulated cells were released from water-based gels using a commonly-cited chelator (sodium citrate[90]), they initially displayed low metabolic activity. When the aqueous phase of the gel was replaced with complete αMEM there was a substantial

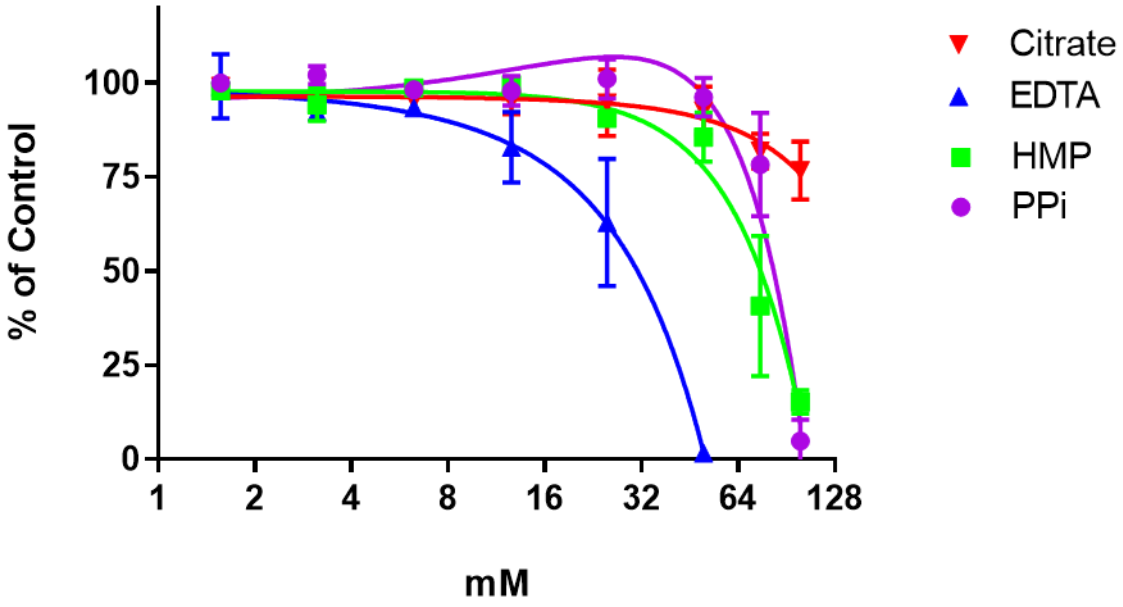

Figure 3.5.2 Metabolic activity measured by reduction of Resazurin (expressed as a percentage change from PBS-treated control) of 2D cultured cells 24 h post exposure to calcium ion chelator solutions: Citrate (red), EDTA (blue), HMP (green) and PPi (purple). Chelator concentration ranged between 1.56 and 100 mM (x axis). n = 3. Error bars +/- SD.

increase in the metabolic activity of post-encapsulated cells and in their subsequent proliferative capacity. The post-encapsulated cells continue to thrive, proliferating beyond that of the control cells maintained in 2D culture. This was the case for all conditions, irrespective of whether the cells were exposed to chelators for 1 or 5 minutes. (Figure 3.5.1E).

A dose response of chelator chemicals on cell metabolism was conducted to determine suitable concentrations of chelators for AMBs de-gelling to release encapsulated cells. A monolayer of MC3T3-E1 cultured in 48 well plates were exposed to a range of chelator concentrations between 1.56 and 100 mM for 30 minutes; their metabolic activity was recorded 24 hours post exposure and

compared to a negative control (exposure to PBS). Results are shown in Figure 2; four commonly used chelators were chosen: EDTA (blue), sodium citrate (red), hexametaphosphate (HMP) (Green) and sodium pyrophosphate (PPi) (Purple). EDTA demonstrated a clear dose response with activity steadily declining from 12 mM and reaching 0% by 50 mM. In contrast, HMP and PPi were well tolerated up to 50 mM but both resulted in a sharp decline in activity beyond 50 mM. Citrate demonstrated a minimal effect on the cellular activity at all concentrations tested, however activity was reduced at higher concentrations and was lowest at 100 mM at 76.7% of the control activity. Therefore, the order of chelator toxicity from most to least potent was determined to be EDTA > HMP ≥ PPi > Citrate when applied to 2D monolayers.

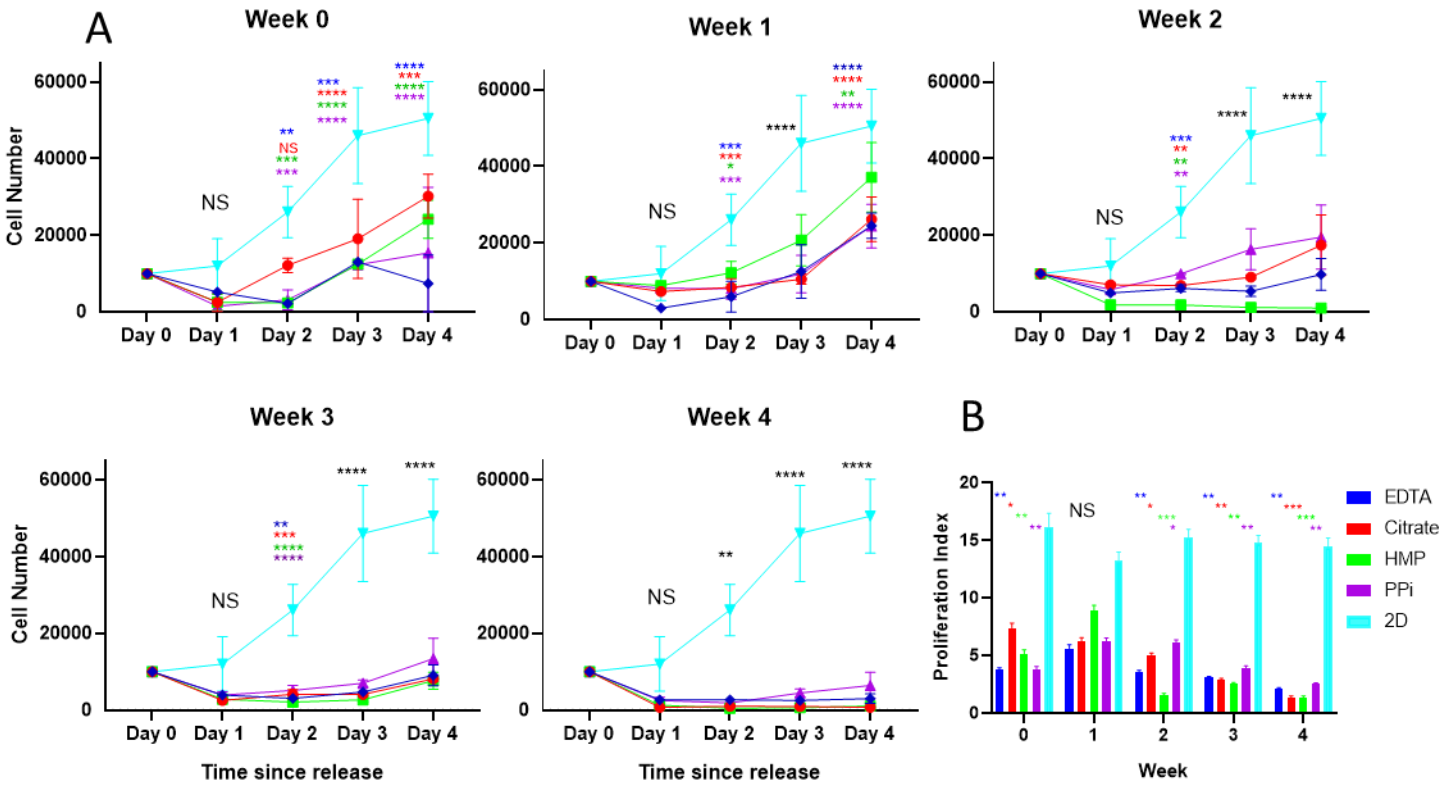

Figure 3.5.3 Effect of long-term 3D encapsulation culture on cells encapsulated in 2% alginate αMEM microbeads.

A) Cells were encapsulated and cultured for between 0-4 weeks. Each graph represents a different length of encapsulation, as indicated by the graph title. Released cells were cultured in 2D for up to 4 days (x axis). Proliferation potential post chelation was assessed, and the cell number achieved at each time point is shown post release. 2D control cells (cyan) demonstrate the baseline proliferation potential of this cell type prior to encapsulation. Error bars = +/- SD. n=3 **B)** Proliferation index of the released and expanded cells. Represents a fold increase in cells throughout the time course. Stats are compared to 2D control. n=3 Error bars = +/- SEM. $P < 0.05$ *; $P < 0.005$ **; $P < 0.0005$ ***; $P < 0.0001$ ****.

To assess the effects of encapsulation when combined with exposure to the de-gelling chelation agent, the proliferation potential of encapsulated cells after release was measured at 0, 1-, 2-, 3- and 4- weeks post-encapsulation within 2% AMBs (Figure 3.5.3) or 1% AMBs (Figure 3.5.4). The different chelators (EDTA, Citrate, HMP and PPi) were applied at a concentration of 90 mM and the proliferation of released cells was measured each day for 4 days by counting the cell numbers in culture and comparing against a conventionally cultured, unencapsulated 2D control.

Following initial release from 2% AMBs encapsulation (Figure 3.5.3), and regardless of the duration of this encapsulation, all the chelators resulted in a similar reduction in cell number of between 50 and 75%. Cells released from AMBs within 2 hours of encapsulation (week 0) with citrate or 1 week

in culture with HMP also showed an initial reduction in cell number but were still able to proliferate post chelation. Though the cells subsequently recovered, the proliferation index was still far less and significantly different than the 2D control (Figure 3.5.3 B). After one week of encapsulation in 2% AMB, cells released through exposure to citrate, EDTA or PPi all displayed decreased viability as evidenced by reduced cell number, and subsequently showed reduced proliferation index compared to 2D control cells, however this drop was not significant (Figure3.5.3 B). While HMP treatment initially resulted in released cells having the greatest proliferation of all chelators tested, at 2 weeks AMB encapsulation the total yield following release and subsequent proliferation rate were similar and significantly reduced for all the experimental conditions when compared to the 2D control group (Figure 3.5.3 B). From week 2 onwards, all the released cells showed impaired proliferation rate post chelation, regardless of the chelator chosen, however PPi-treated cells achieved a slightly higher cell number and maintained a constant proliferation index compared to the other conditions. As the duration of encapsulation increased the proliferation rate post encapsulation decreased further so that, following release after 4 weeks of encapsulation, cell proliferation was almost completely impaired, and only the PPi released cells were capable of expanding beyond their initial seeding number with a proliferation index of 1.53 +/- 0.09.

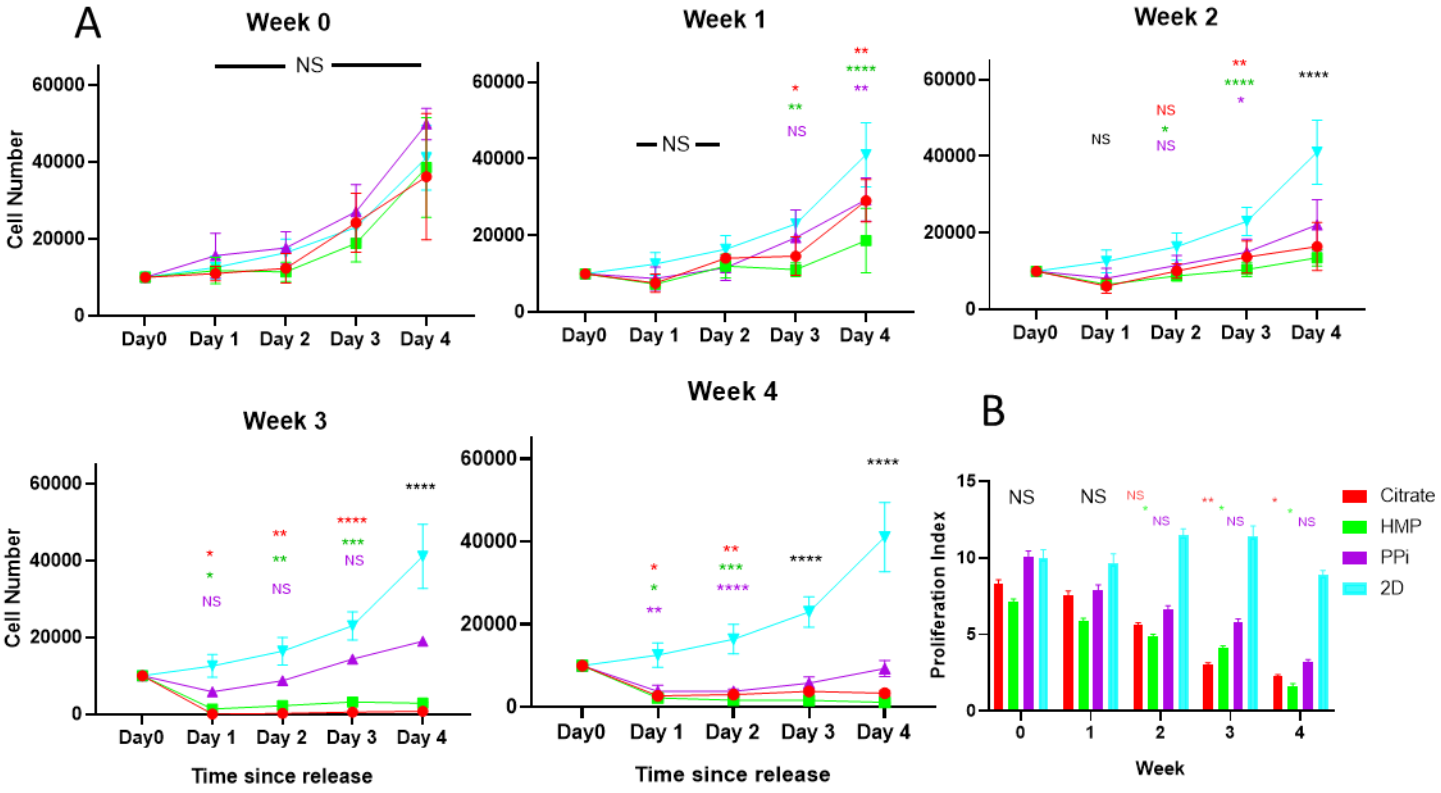

Figure3.5.4 Effect of long-term culture on cells encapsulated in 1% alginate αMEM microbeads on proliferation potential post chelation.

A) Cells were encapsulated and cultured for 0-4 weeks as indicated, then released using the indicated chelator chemical and cultured in 2D for up to 4 days. The cell number achieved at each time point is shown post release and compared to a 2D control which was never encapsulated. Error bars = +/- SD. n=3 **B)** Proliferation index of the released and expanded cells. Represents a fold increase in cells throughout the time course. Error bars = +/- SEM. $P < 0.05$ *; $P < 0.005$ **; $P < 0.0005$ ***; $P < 0.0001$ **** n=3

After observing a clear effect of encapsulation time on the proliferative potential of cells encapsulated in 2% AMBs, the alginate encapsulating gel concentration was reduced to 1% and re-evaluated. Due to the high toxicity of EDTA observed in Figure 3.5.2, this chelator was not included in subsequent cell release experiments. The concentration of the chelating agents was reduced to 45 mM, reflecting the reduction in crosslinking Ca^{2+} at the reduced alginate concentration. Similar de-gelling kinetics were achieved under these conditions (data not shown).

Cells encapsulated in 1% AMBs (Figure 3.5.3) retained a higher proliferation potential post encapsulation compared to those encapsulated in 2% alginate (Figure 3.5.4). At week 0, there was no significant difference in cell number between cells release from 1% AMBs compared to 2D controls regardless of the chelator used. Cells released from encapsulation using PPi showed equivalent proliferation rates to the control group. Cells released using citrate or HMP proliferated at a similar rate to the 2D control cells up to a week of encapsulation, as demonstrated by similar cell counts and proliferation index at each time point tested (Figure 3.5.4 A & B).

As observed with 2% AMBs, cells encapsulated for 1 week in 1% AMBs showed an initial drop in number post chelation (cf. Figures 3.5.3 & 4). However, the cell numbers for all chelators tested were quickly able to recover and proliferate with no significant difference to the control group for the first 2 days post chelation. PPi-chelated cells were the least affected and remained statistically equivalent to the 2D control until the fourth day after release. Following 3 weeks in culture, a complete cessation of proliferation was observed for HMP and citrate-treated cells. Cells released using PPi remained the only condition to continue to proliferate post release, and they did not

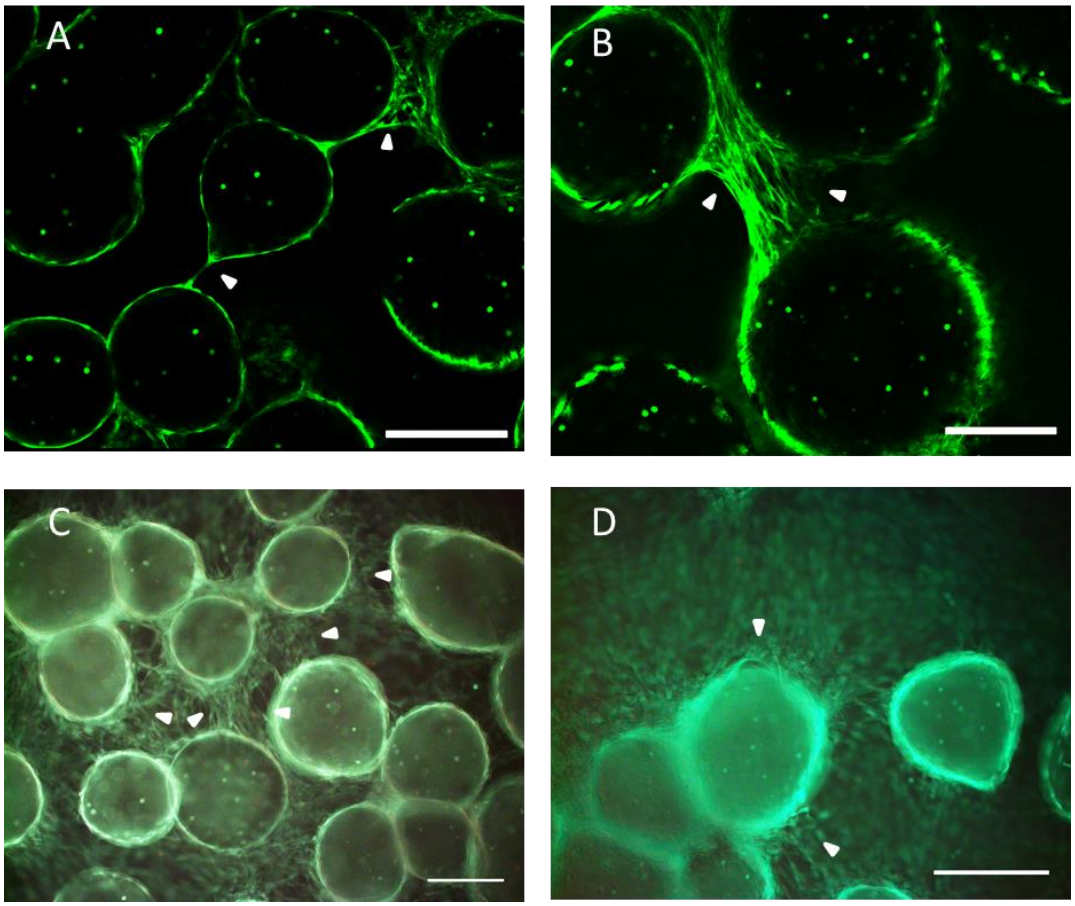

Figure 3.5.5 Fluorescent imaging showing cell attachment to alginate microbeads, as observed by Calcein AM (green) staining.

Intact microbeads containing MC3T3-E1 cells were co-cultured with a confluent monolayer of MC3T3-E1 cells in either supplemented media (**A, B, C**) or proliferation media (**D**). Cells were encapsulated in either 1% (**A & C**) or 2% (**B & D**) alginate microbeads. For the confocal images (**A & B**) the focal plane is at the widest circumference of the bead, approximately 250 – 300 µm from the TC plastic below. **C & D** are conventional wide-field fluorescent microscopy images. All scale bars 200 µm. Areas of interest mentioned in the text are highlighted with white arrows.

significantly differ from the 2D control cell count until day 4. After 4 weeks in 1% AMB encapsulation culture there was no observed proliferation post-release regardless of the ion chelator applied,

however PPi treated cells did recover slightly at day 4 and the proliferation index was never significantly different from control. This trend result was very similar to that observed previously for 2% gels but with an order of magnitude higher cell count. The effect of media supplemented with (L-ascorbic acid and β-glycerophosphate) which has been shown to stimulate differentiation of MC3T3 cells into osteoblasts[91] on cell behaviour and proliferation. Cell attachment to the microbead surface was observed to occur for both 1 and 2% AMBs in supplemented media, with very little difference noted between the two conditions (Figure 3.5.5). When cultured in supplemented media, cell attachment to the microbead surface markedly increased and the interactions between the monolayer and the beads were more apparent, with a visibly higher cell density around the beads compared to proliferation media (cf. Figure 3.5.5 C & D). For all conditions, cells formed a bridging network both between beads and between beads and the culture dish, though this was more limited when proliferation media was used compared to supplemented media (cf. Figure 3.5.5 C & D). This network provided sufficient attachment such that the culture plate could be completely inverted without displacement of the microbeads occurring.-SEM imaging of dried samples further confirmed cell attachments to the surface of the microbeads, forming bridges both between the AMBs and between the culture surface and the microbeads. These SEM images showed that the monolayer had begun to form a bridging network between the two beads which resulted in a void where the cells were previously attached (Figure S3.7.1, page 49).

Supplemented media was found to have a strong effect on the proliferation potential of the cells post encapsulation in 2% AMBs, regardless of the chelator used (Figure 3.5.6). At weeks 0 and 1 the cells followed a very similar proliferation rate to 1% AMBs cultured in regular proliferation media (Figure 3.5.4) with all chelator conditions closely following the control cells, these rates were much higher than that observed previously for 2% AMB (Figure 3.5.3) and the proliferation index was not significantly different from the control at any time point (Figure 3.5.6B). However, after 2-3 weeks, cells cultured in supplemented media maintained a strong proliferative growth phase after a short lag phase (Figure 3.5.3 & 4) compared to cells cultured in regular media which had very low rate of proliferation for both gel concentrations tested (Figure3.5.6 &7).

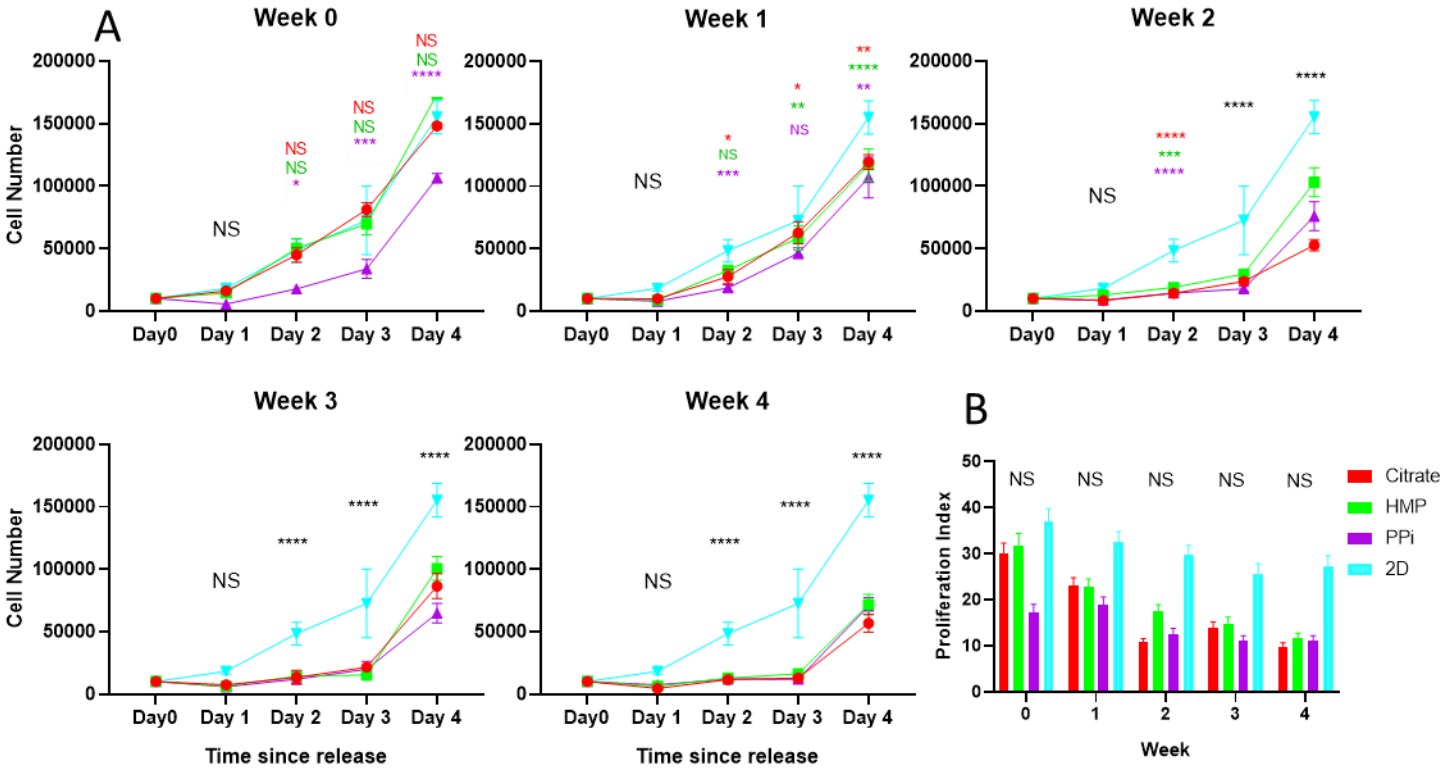

Figure 3.5.6 Effect of long-term culture on cells encapsulated in 2% alginate αMEM microbeads on proliferation potential post chelation and cultured in supplemented media.

A) Cells were encapsulated and cultured for 0-4 weeks as indicated, then released using the indicated chelator chemical and cultured in 2D for up to 4 days. The cell number achieved at each time point is shown post release and compared to a 2D control which was not encapsulated. Error bars = +/- 1SD. n=3 **B)** Proliferation index of the released and expanded cells. Represents a fold increase in cells throughout the 4 d time course. Error bars = +/- SEM. $P < 0.05$ *; $P < 0.005$ **; $P < 0.0005$ ***; $P < 0.0001$ **** n=3

Then evaluated was the proliferation of cells post encapsulation in 1% AMBs and cultured in differentiation media (Figure 3.5.7). Initially at weeks 0 and 1 the cells demonstrated a similar proliferation profile to that observed for 1% AMBs in regular proliferation media and 2% AMBs in differentiation media (cf. Figures 3.5.4 & 6) with minimal loss in cellular proliferation post chelation.

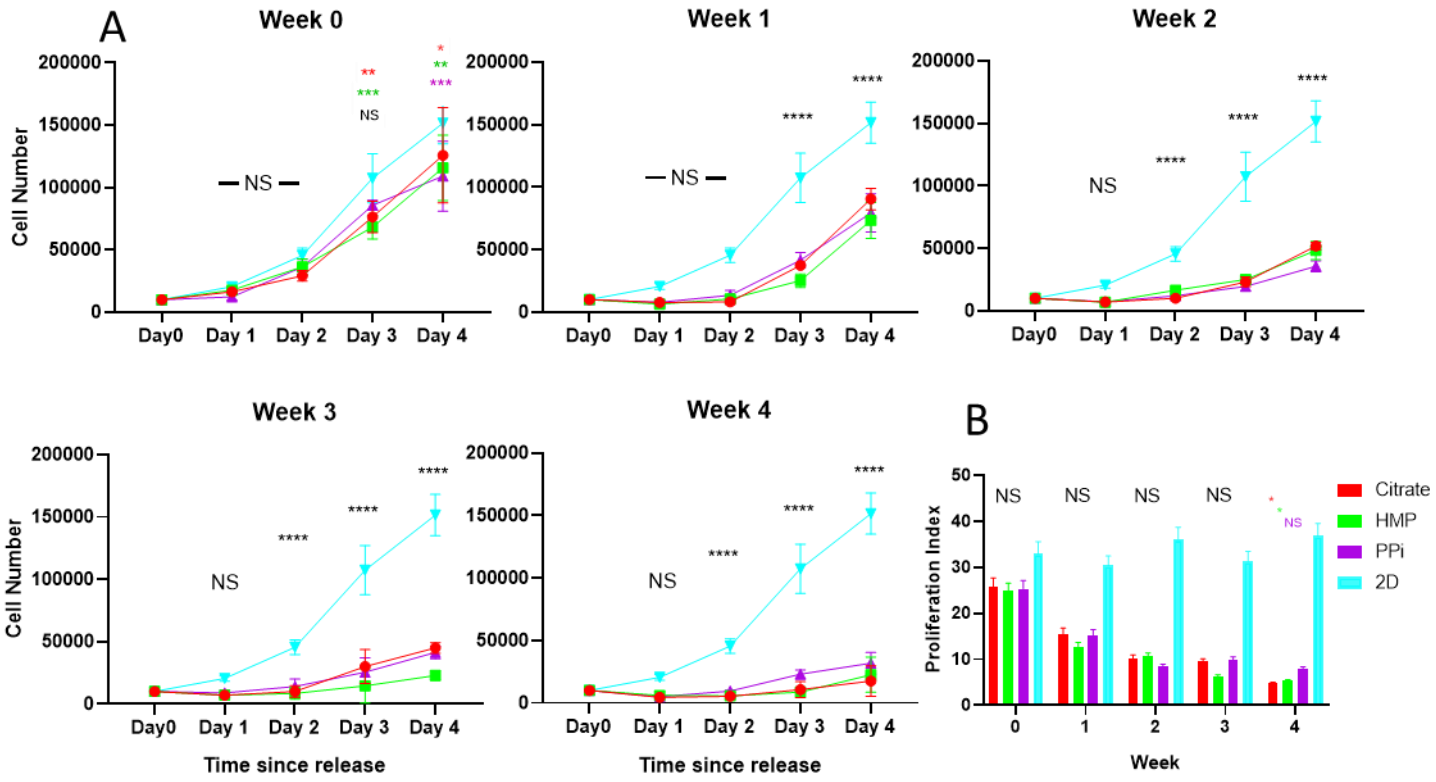

Figure3.5.7 Effect of long-term culture on cells encapsulated in 1% alginate αMEM microbeads on proliferation potential post chelation and cultured in supplemented media.

Cells were encapsulated and cultured for 0-4 weeks as indicated, then released using the indicated chelator chemical and cultured in 2D for up to 4 days. The cell number at each time point is shown post release and compared to a 2D control which was not encapsulated. *=<0.05,**=< 0.005, ***=<0.0005, ****=<0.0001 error bars = +/- 1SD. n= 3 **B)** Proliferation index of the released and expanded cells. Represents a fold increase in cells throughout the time course. Error bars = +/- SEM. n=3

Surprisingly, unlike cells cultured in proliferation media, cells cultured using differentiation media and released from 2% AMBs were inhibited less than those released from 1% AMBs (Figure 3.5.6B v Figure 3.5.7B). The 1% AMB encapsulated cells did not show the same lag phase of 24 h as observed for 2% AMB prior to proliferation, suggesting that the initial encapsulation matrix stiffness influences cells differently when cultured in standard cell culture media compared to supplemented media. Indeed, the matrix stiffness of cast bulk gel alginate cylinders made with 1 and 2% w/v alginate were significantly different with a measured elastic modulus of 11.21 +/- 1.92 and 40.52 +/- 7.4 kPa respectively (Figure S3.7.2, page 49). Both polymer concentrations demonstrated ideal elastic

behaviour and achieved a peak stress of 3.42 and 9.71 kPa respectively. The 1 and 2% alginate samples had elastic moduli of 11.21 +/- 1.92 kPa and 40.56 +/- 7.40 kPa respectively. These results suggest that alginate concentration should be carefully considered when being used for cell encapsulation for either cell storage or tissue engineering and biofabrication applications.

3.6 Discussion

The aim of this study was to find a robust and reliable way to encapsulate and release cells in an alginate hydrogel scaffold and observe the effects of long-term encapsulation and chelator chemicals on the proliferation potential of released cells.

This study demonstrates the importance of selecting the aqueous phase of alginate hydrogels and the effect it has on the viability of encapsulated cells. Cells encapsulated in non-isotonic buffered gels had minimal cellular activity when released, compared to the high viability of cells encapsulated using αMEM cell culture media as the aqueous phase as seen in Figure 3.5.1A. Literature shows that the aqueous component used for alginate hydrogels for cell encapsulation ranges from water[92], saline and buffered saline[72], to cell culture media[55]. This data suggests that great care should be taken when considering the aqueous component of alginate gels for encapsulating cells for both short and sustained culture.

In 2D cell culture, all the chelator chemicals tested (other than EDTA) were well-tolerated in the range of 1.56-100 mM (Figure 3.5.2). EDTA demonstrated a clear dose dependant response confirming the potent cytotoxicity of this molecule previously reported by others[88]. The cells were exposed for 30 minutes as this represents a realistic maximum time that encapsulated cells could be exposed to the chelators during the extraction process and far exceeds the time required for the gels to fully de-gel. For the sustained encapsulation and release experiments, the maximum applied concentration of each chelator was 90 mM as this was within tolerated ranges for most of the chelators (Figure 3.5.2). Additionally, this was to ensure a moderate excess concentration of chelator compared to Ca^{2+} within the system to ensure complete release of the encapsulated cargo. In this way, when reversing the alginate gelling to release cells from an alginate construct, the exact size and Ca^{2+} content does not need to be known to ensure adequate release, which is applicable when applying the protocol to larger and more complex constructs. Here we have shown the volume of chelator required can be approximated to cover the construct. When the concentration of the alginate was reduced to 1%, the subsequent chelator concentration was in turn reduced to 45 mM, in order to maintain a comparable ratio of chelator to Ca^{2+}.

For all gel concentrations and media conditions tested a 2D control was cultured continuously from the same starting stock of cells used for encapsulation. At the beginning of each week 1 x 10^4 cells were seeded for experimental and control conditions. The 2D control growth curve on each figure series was near identical for all weeks as the average cell number for each day was averaged. This was to provide a constant value for each week as MC3T3-E1 cells have been shown to be inconsistent in 2D culture[64]. The passage number for the 2D control never exceeded 32, this is the

upper limit for MC3T3-E1 cells to undergo supplemented differentiation[93]. From the initial release of the cells through chelation, it is possible to see a distinct difference at week 0 between 1% and 2% AMBs. The proliferation of cells released from 1% AMBs was not significantly different to the 2D control at any day and PPi released cells exceeded the control. This demonstrates that encapsulating cells in a lower alginate concentration allows cells to retain the ability to proliferate. Therefore, the cells experience a concentration and time-dependant response where reduced concentrations of alginate and time spent encapsulated increases the proliferation potential of post-encapsulated cells. We believe that this is a novel finding regarding the limitations of alginate encapsulation since previous literature has only looked at either short term storage of cells encapsulated in alginate [71,72] or long-term encapsulation without retrieval[13,94,95]. Our findings are in agreement with a recent study that suggests encapsulating cells in 3D arrests proliferation and the cell cycle while releasing the cells restarts both of these[63], however their work was performed using collagen hydrogels and up to only 10 days encapsulation, compared with 28 days in culture as investigated in this work.

The number of cells retrieved from 2% AMBs cultured in proliferation media, initially dropped from the initial seeding cell number for all weeks tested. Week 0 had the highest number of recovered cells regardless of chelator used (60% of the control cells numbers). Though this initial drop is present in all other encapsulation culture conditions it is most prominent in the non-supplemented proliferation media conditions. This suggests that culturing encapsulated cells in supplemented media may improve initial cell recovery and there is some evidence to suggest that when cells are in 3D culture supplemented media can increase proliferation[96]. A similar trend is seen in all samples for weeks 3 and 4 in both supplemented and non-supplemented media, where the cells initially remained dormant in a lag phase before beginning to proliferate by day 3 or 4.

The recovery in proliferation is more prominent following culture with supplemented media, further suggesting that the supplemented media is better for long term encapsulation and culture of the cells[96]. The effects between the chelators were less minimal with the exception of EDTA Figure 3.5.2 with PPi being slightly better tolerated, yielding a small increase in proliferation at the latter weeks (Figure 3.5.4). With 1% AMBs cultured with proliferation media, PPi released cells remained not significantly different from the control cells until 3 weeks of encapsulation. These results suggest that when culturing cells encapsulated within a non-modified alginate hydrogel, there is a limited window in which the cells maintain the ability to proliferate when released from the gel and that the encapsulation process substantially influences the behaviour of the cells. This should be taken into consideration when using alginate, and likely many other types of hydrogel, as a basis for tissue engineering scaffolds or for long term storage of encapsulated cells. Matrix stiffness alone has been previously shown to influence cell differentiation[40]. The difference between the elastic modulus of

1% and 2% alginates in combination with the supplemented media used in Figures 3.5.6 and 7 may be responsible for the increased cell survival. This finding further suggests that unmodified 2% alginate is too stiff for long term encapsulation. The stiffness may inhibit cell attachment within 2% AMBs with minimal attachment observed with proliferation media, though this was ameliorated with supplemented media (Figure 3.5.5). The supplemented media used, which is commonly applied to stimulate osteogenic differentiation, may also be influencing the cellular response.

The elastic modulus of the 2% alginate is far closer to the physiological ranges preferred by osteoblasts than 1%,[40,97]. Though for proliferation media, the lower concentration of alginate ameliorated the effects of long-term encapsulation. When the cells were incubated in supplemented media the inverse was true. Suggesting that components in the supplemented media are responsible for the increase in cell proliferation of the released 2% supplemented media cells[97].

It is commonly accepted that alginate is broadly biologically inert in its unmodified form and cells cannot bind directly to the polymer itself, therefore a large body of work has been created with the aim of modifying alginate to allow cells to attach[98,95,76]. Figure 3.5.5 and Supplementary Figure 3.7.1 demonstrate that under the right conditions, cells can bind directly to non-modified alginate hydrogels during sustained culture and additionally that supplemented media increased cell interactions with the alginate hydrogel as did reducing the alginate concentration. We propose that this increase in cell attachment is in part due to the ascorbic acid and β-glycerol phosphate supplements in the media which are commonly used to drive differentiation of osteoblast lineage cells and increase collagen and bone mineral excretion respectively[99,100]. This excretion of ECM proteins onto the surface of the alginate microbeads may provide attachment points for the cells to adhere to and increase long term viability. Further investigation into *de novo* ECM secretion and specific cell adhesion points is needed before any conclusions can be drawn about the cellular mechanics involved with this and will be the focus of future research.

The findings here demonstrate that encapsulation within unmodified alginate has a limited window of use before impacting cell proliferation potential. Supplementing the culture media with components commonly used in osteogenic differentiation media can increase the useable time for encapsulation. The mechanisms of this need to be investigated further but our observations should be taken into consideration when encapsulating cells in unmodified alginate for the purposes of tissue engineering, biofabrication and/or cell storage and serve as a general warning for the application of hydrogels in this regard. Additionally, when releasing the cells from encapsulation, careful consideration of the chelation agent should be taken depending on the length of culture; following short encapsulation times the cells are less sensitive to the chelation agents but, following

longer encapsulations, either sodium pyrophosphate or sodium citrate should be the chelator of choice to maximise cell viability and proliferation potential upon release.

3.7 Supplementary information

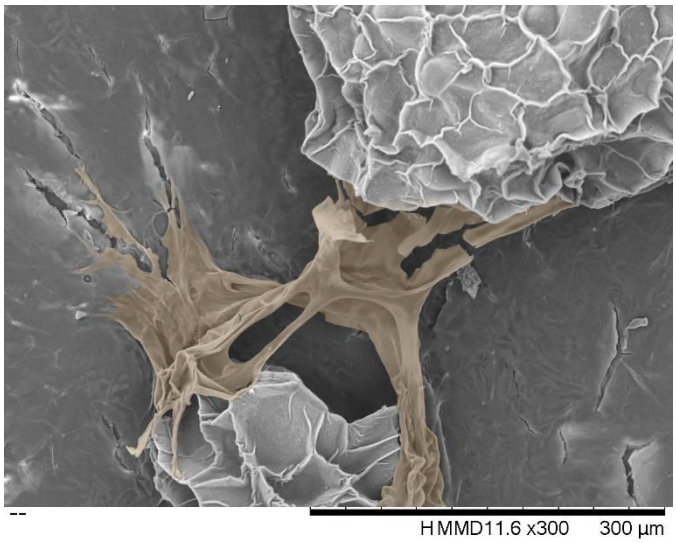

Supplementary Figure S3.7.1. SEM micrograph of a cell monolayer (false coloured gold) forming an interconnecting network between two 2% alginate beads cultured in supplemented media (x300 magnification).

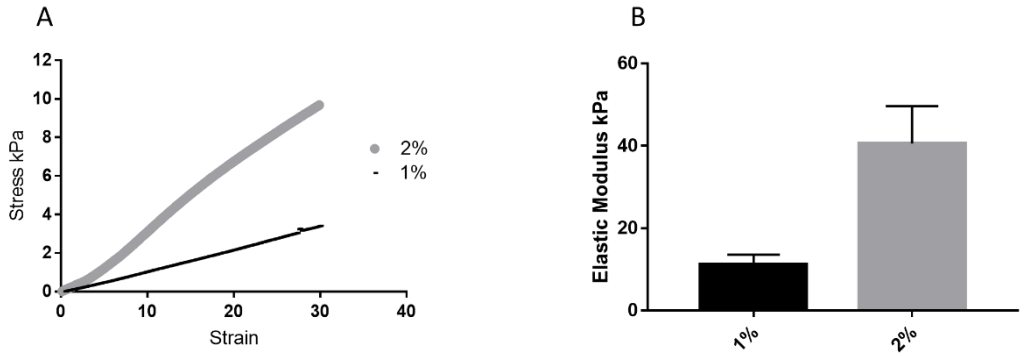

Supplementary Figure S3.7.2. A. Compression stress strain curves of solid alginate cylinders made with either 1 or 2% alginate and complete cell culture media. B. Elastic modulus of the alginate cylinders.

4 Formulation Development of Hybrid Bioinks Using Internal Gelation Strategies

4.1 Introduction

The extra cellular matrix (ECM) found in all multicellular life is a complex hierarchically structured entanglement of polymers which provide much of the intrinsic mechanical strength of biological tissues. Recapitulating this native tissue microenvironment is a complex task, which if achieved, will lead onto a multitude of advancements in important biomedical areas such as drug screening, organ replacement and regenerative medicine. The complexity of recapitulating ECM is in large part due to the specific conditions required to form the polymers in a functional state synthetically rather than being expressed directly from cells. While direct expression of ECM proteins may initially appear to be the most sensible approach to produce ECM for the purposes of tissue engineering, the rate at which it is produced is very slow. Additionally the cells typically require specific inputs that encourage ECM production and often an existing ECM, a suitable 3D environment including correct mechanical and biological cues such as cell-cell communication is required. This leads to a "chicken and egg" situation where the best way to form ECM is with an existing ECM but without ECM, ECM production is limited. While fully recapitulating native tissue is the ultimate goal, the complexity and hierarchical structures of biological tissues make the synthetic development of this challenging with current technologies. An approach to achieve this would be build a bioink or scaffold which with a sufficient but minimum number of molecular cues encourages incorporated cells to anchor and modify the existing incorporated matrix as well as depositing *de novo* ECM.

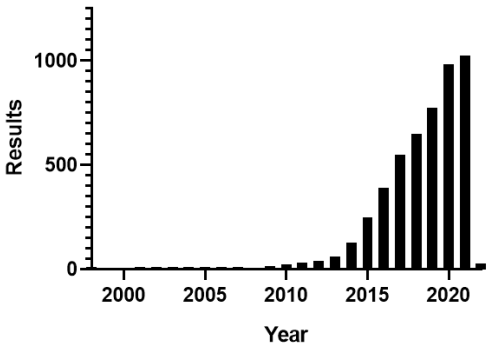

Figure 4.1.1 Results by year for 3D Printing Tissue Engineering in NCBI Pubmed search.
https://pubmed.ncbi.nlm.nih.gov/?term=3d+printing+tissue+engineering

Tissue engineering has evolved from this pioneering work and leading contemporary research uses the guiding principle of using a seeding biomimetic material as a synthetic ECM rather than waiting for cells to produce enough ECM to build complex structures. The seeding material can be: components of local microenvironment of the desired tissue type, precursor peptides which later

form into more complex structures or may be covalently bound to an inert polymer to facilitate cell adhesion, or a biomimetic/ compatible material which has the properties required for the tissue type.

Incorporating these biomaterials advances the technology by creating a number of new opportunities such as organ-on-a-chip, smart implants, and synthetic tissues. These biomaterials can also be used to speed up the translational pathway between lab and clinic by providing a better starting point for basic scientific research. Currently much of the basic science that provides the basis for clinical applications and further understanding of the cellular molecular going ons is performed with 2D tissue culture (TC) plastic. Polystyrene is predominantly used for disposable TC plastics which is inherently a hydrophobic material and therefore unsuitable for adherent cell culture. To render the TC plastic hydrophilic and negatively charged, thus enabling electrostatic attraction of cells allowing them to attach, a microwave plasma treatment is carried out to oxidise the surface [22,23]. This technique, while effective to allow adherent cells to proliferate cells can lead to cells dedifferentiating, losing phenotype and a subsequent reduction in cell specific markers[101],[63]. Thus, the cells are no longer a true representation of the tissue type the cells were sourced from, which can lead to misleading, or inaccurate results and ultimately poor clinical translation. Therefore there is a clear need for a better system to culture cells for experimental assays which more accurately represent the tissues being investigated. Currently, the gold standard for experimental investigation is using animal models. While this approach is far superior to 2D *in vitro* models at representing the true native environment found in human *in vivo* tissue, animal models can be prohibitively expensive for preliminary studies and are ethically questionable due to the large amounts of animals required for research, particularly for early-stage investigational studies where the results are less predictable. While *ex vivo* donated human tissue can solve some of these issues, it is difficult to procure reliably, may be of variable quality, often small in size and is difficult to control for age, ethnicity, gender, and location. Due to the potential infection risk from the sample typically laboratories will need to have additional precautions, storage, and staff training to handle the samples.

In 2006 Engler *et al* demonstrated the power of cellular growth matrix on controlling cell fate. Using Mesenchymal stem cells (MSC), they were able to control cell differentiation through matrix stiffness alone. Matrix with a low Youngs modulus (0.1-1 kPa) drove differentiation towards a neurogenic lineage while stiffer matrix (8-17 kPa) drove the cells towards myogenic and more rigid matrix (24-40 kPa) caused the cells to become osteogenic [40]. The influence of the growth matrix material characteristics influencing cell behaviour has been repeated may times over and built upon further

to include specific cell binding sites, which has become a foundation for tissue engineering [102,103,104,105,106].

The ground-breaking research done by Engler *et al* along with the work previously done by Langer *et al* demonstrates much of the foundation for the more recent development of larger, more complex tissue models. Such models move the field away from novel and interesting cellular behaviour and interaction studies towards fully and faithfully replicating functional tissue which can be scaled up for implantation, animal model replacement or indeed called down in size while maintaining the inherent complexity for application in advanced screening tools. To achieve this complexity in a reliable and reproducible fashion, a new approach to tissue engineering is needed, this time introducing elements from materials science and more traditional forms of engineering, making the field truly multidisciplinary. One such area of development that is showing excellent promise in this regard is additive manufacture. Additive manufacture, otherwise known as 3D printing, is a technology that allows for the repeated layer upon layer deposition of a material to build up a novel or replica model. It can be applied to materials such as plastics [107], cements [57], metals [108], water [109], and hydrogels [110]. In the past decade, an interest in 3D printing biological materials for the purposes of tissue engineering has arisen (Figure 4.1.1). Typically the main approaches to this technology are: printing biocompatible materials such as hydroxyapatite [111], titanium [59] or printing biological polymers such as fibrin [112] and collagen [113] or biomimetic polymers such as alginate [90] and nano cellulose [114].

Many of these biological polymers have the innate characteristic of shear thinning which is why they are often selected as a base for 3D printed biological materials which are referred to as bioinks.

This is when a shear force is applied to a fluid material causes its viscosity to decrease allowing extrusion through a nozzle and after go through a rapid transition to maintain shape fidelity when no shear is applied [115]. This property is highly desirable for a 3D printable material and therefore, extrusion based bioprinting is the most common 3D printing technique for bioinks due to its high cell viability, variable geometries, ease of use and low cost [116,117]. The process requires some optimisation as higher shear rates may cause the shear rate to become linearly proportional to the shear stress, indicating increased shear within the system which can induce cytotoxicity in the extruded bioink [118].

Depending on the material properties and concentrations within each bioink, different printing techniques can be used. To set the bioinks in place after printing the materials need to be able crosslink, this can be done with a variety of techniques from UV light, temperature changes, ionically and enzymatically [,77,119]. While not all bioinks are themselves able to shear thin, or the polymer

concentrations may be too low to induce this, shear thinning sacrificial supporting gels may be included to bioprint inks that lack that properties [120]

Typically, printing biomaterials uses an extrusion-based systems as other methods are limited by the viscosity of hydrogel, the available flow rates, or the cell compatibility. Extrusion based printing is still limited to higher viscosities and by the spreading of printed hydrogels, thus restricting the method to small unsupported prints and larger models requiring a rigid scaffold [27],[120]. Extrusion based bioprinters apply a force onto the bioink either pneumatically or mechanically which extrudes the bioink. The system typically uses syringes or cartridges as a vessel for the bioink and that have been preloaded with bioink and should be compatible with standard cell culture aseptic techniques. A distinct advantage of this technique is that the printing pressure, bioink vessel, needle/nozzle length and geometries can all be modified to suit the intended application and material used. The extrusion process is not affected by temperature, pH, or shear stresses within the system. However some distinct limitations with this technique exist such as low print resolution, blockage within the needle, air in the bioink which can distort the resolution, and the high shear forces generated in highly viscous bioinks can reduce cell viability [121]. Other 3D printing techniques that are used for cell laden bioinks are inkjet printers. This is where thermal, piezoelectric, or electromagnetic forces expel successive drops of bioink, this technique lacks precision, is not suitable for complex structures, requires significant optimisation and has high shear forces which can trigger apoptosis [122].

The bioink developed in this chapter has too low concentration of alginate and collagen to be able to be bioprinted as a standalone ink. the approach of this project will incorporate a recently developed technique, Suspended Layer Additive Manufacture (SLAM). SLAM enables the 3D printing of soft materials and biomaterials. It is a multicomponent system where one element is the 'ink' or material to be extruded, the second component is self-healing fluid gel matrix which supports the extruded ink, finally a crosslinker maybe added into the system after the extrusion process has finished or if a thermally crosslinked material is used then moved to an incubator (Figure 4.1.2) [120]. Because of the support gel bath, SLAM allows inks to be printed at lower pressures as there is no time limitations due to spreading [123] The limitation of SLAM as currently published is that it requires stiffer hydrogels that do not deform when a crosslinker is introduced or the bath is moved.

To further control the gelling kinetics of the alginate system during SLAM and allow for the printing of softer biomaterials, Competitive Ligand Exchange (CLEX) will be employed to facilitate *in situ* crosslinking without the need for addition components. CLEX provides controllable gelling kinetics that can limit the amount of free calcium within a gelling system [124]. This controlled chemistry has scope to increase the application and environments that divalent cation crosslinked gelling systems can be applied, through control of the concentration of free calcium ions. The typical formulation of a CLEX gelling system is a one-to-one ratio calcium chloride and EDTA and one-to-one ratio zinc ion donator and zinc chelator such as glycine or EDDA. When the two components meet, the EDTA has a higher affinity for zinc and therefore releases the calcium into the system, the zinc chelator is chosen to have a lower affinity for calcium than the alginate, thus the gel crosslinks (Figure 4.13). With the combination of these techniques and the novel approach of using alginate as a templating structure to form 3D interpenetrating networks of collagen, it is hoped a robust biologically relevant bioink for bone tissue engineering can be developed.

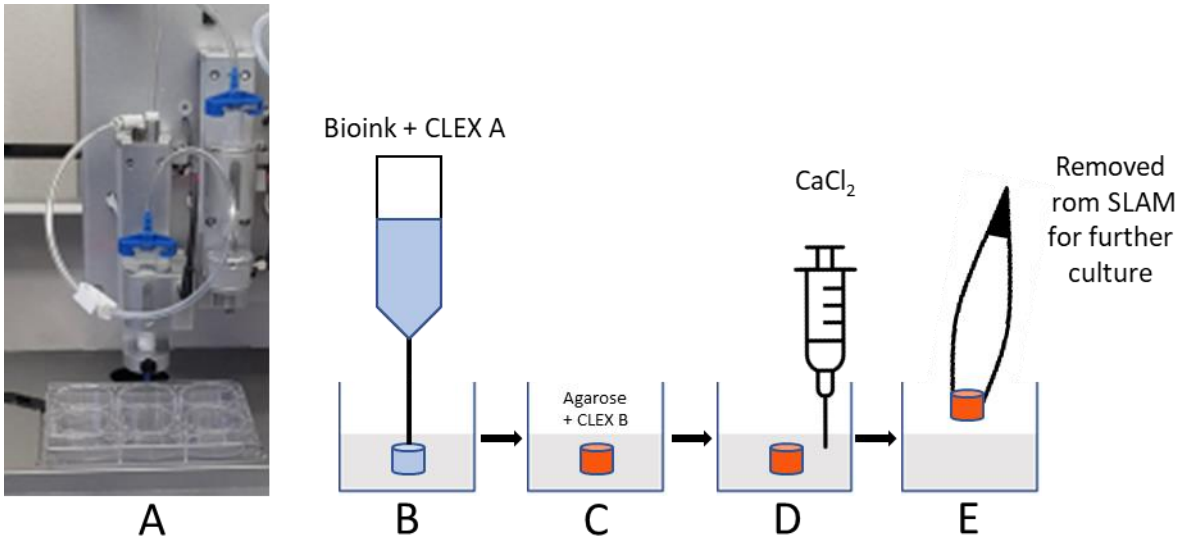

Figure 4.1.2 SLAM printing schematic
A.) A picture of the bioprinter extruding into a 6 well plate.
B.) A fluid gel bed is used to suspend the printed model.
C.) The extruded hydrogel is print is built up layer by layer then allowed to semi crosslink in the bath.
D.) After the construct has been printed, additional cross linker is added to the fluid gel bed which further crosslinks the hydrogel *in situ.*
E.) After fully crosslinking the product can be removed from the fluid gel bed by washing with PBS and cultured as required.
[120]

The templating scaffold used in this study is alginate derived from brown algae, of which 20-40% is alginate depending on the species [76]. Therefore is a is a naturally occurring hydrogel that has received a great deal interest for its useful and diverse applications, by far its main benefit in the field of tissue engineering is a proven track record of biocompatibility. The applications of alginate

are wide and vary from replacement heart valves, wound dressings, pharmacological delivery vectors to food additives and stabilisers [74,75,90,125,126,127]. Due to the intrinsic properties of alginate that are physiologically comparable to ECMs such as facilitation of nutrient and gas exchange, stability in isotonic saline and sugar solutions and comparable viscoelastic properties of soft tissue there is growing interest in the applications of alginate hydrogels for biomedical and tissue engineering [128,129].

The strength of an alginate gel comes from the proportion of G to M residues, the G units ionically bind to divalent cations such as Ca^{2+} in an 'egg box' model (Figure 4.1.4). Herein lies one of the major limitations of alginate hydrogels; as it is from a natural source the G and M residues vary massively between sub-species of algae, affecting the products and batches [76]. The variation in G residue content ranges from as low as 30% and up to 70%. The polymer chain lengths can also vary, the longer the polymer chain the stronger alginate. this variation can be reflected through the molecular weight disparity of anywhere between 32,000-400,000 g/mol [33], [76]. As previously mentioned, the

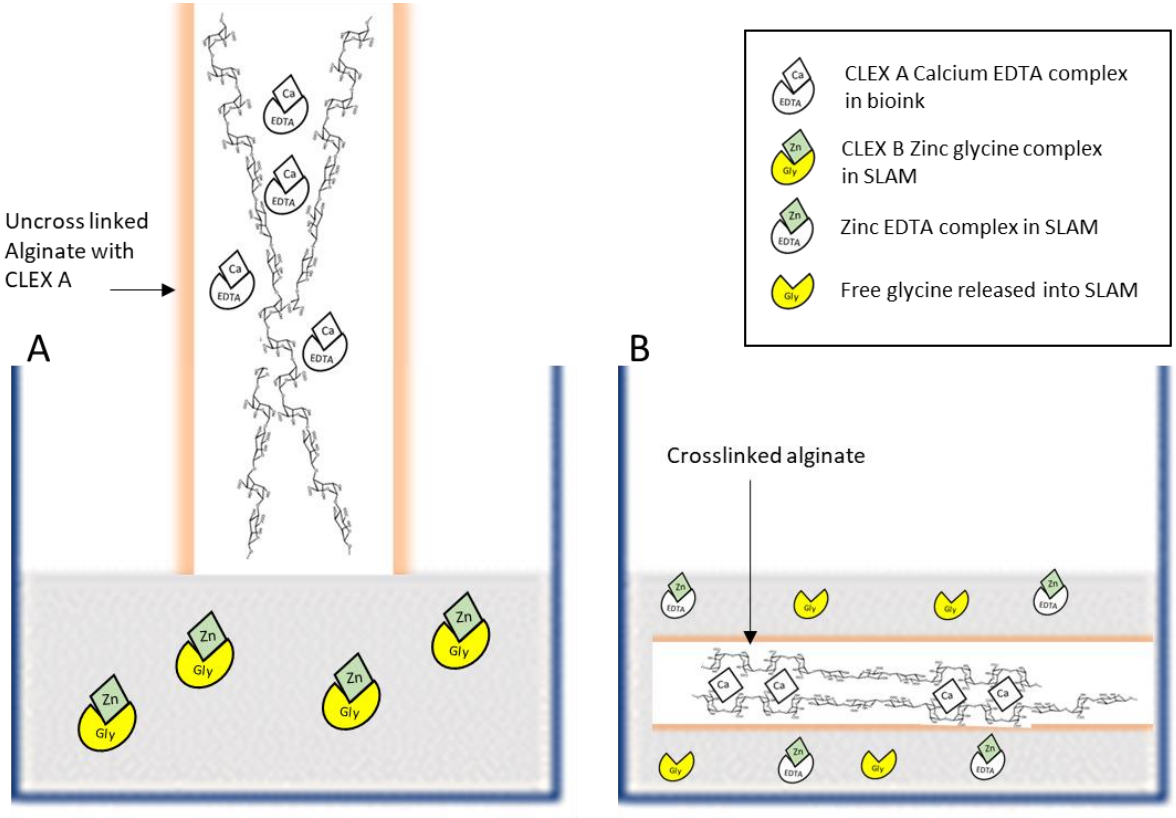

Figure 4.1.3. A schematic diagram of the modified CLEX SLAM gelling systems. CLEX alginate bioink is extruded into CLEX agarose SLAM to facilitate *in situ* crosslinking.

A. Liquid CLEX A alginate bioink extruded into SLAM CLEX B agarose bath.
B. Crosslinked CLEX A alginate bioink after CLEX interaction, ZnEDTA complexes are

work by Engler *et al* showed that different stiffnesses of a matrix substrates are preferred by different cell types, using increased alginate concentration and G ratio this can be modulated [130]. It is worth noting that increased viscosity such as with higher concentration gels and of bioinks creates strong undesirable shear forces during bioprinting extrusion, which can subsequently damage the cells and induce cell death within the bioinks[33,40,76]. While an in increased M ratio has been shown to induce immune activation and cytokine production through the NF-κB pathway [131,132].

The properties of alginate make it a great foundation for a tissue engineering scaffold, however the main limiting factor of this material is a lack of cell adhesion and therefore encapsulated cells are typically held in place unable to interact directly with their environment [76,98]. To overcome this limitation a range of techniques have been employed such as co-composition of a biologically active molecules such as fibrin, gelatin, hyaluronic acid, and hydroxyapatite [60,95,98,133,134]. Other techniques include chemically modifying the alginate and covalently binding cell adhesion molecules such as RGD to the gel [135]. RGD is a tri peptide motif that is found within the triple helix of collagen and acts as an anchor point for integrin proteins to attach the cellular extracellular matrix to the surrounding ECM [55,76]. While effective this method can be prohibitively expensive.

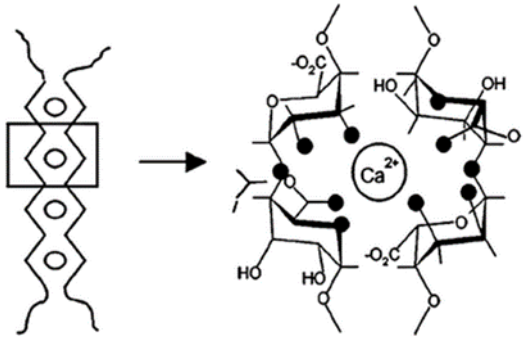

Figure 4.1.4 A schematic diagram of Alginate cross linking and the production steps for sodium alginate.
Egg box model of alginate, the G-units of alginate are ionically crosslinking around a calcium ion which intertwines the polymer strands[127].

To overcome these limitations of alginate without the need to chemically modify the alginate, a secondary polymer can be incorporated into the bioink. The secondary polymer ideally has different gelling kinetics and chemistry to the primary polymer; thus it is possible to control the gelling of the polymers independently. A polymer which facilitates cell attachment as well and having a completely different gelling kinetics to alginate is collagen.

Collagen is a key component of the ECM which acts as an anchor point for cells and provides much of the tensile strength of tissues and as much as 30% of bone is collagenous proteins [136]. There are currently 28 known types of collagen and the type predominantly found in bone is type 1. Type 1 collagen can self-form fibrils into the triple helix and the fibrils are approximately 300 nm long and 1.5 nm wide [137]. The structure of collage type 1 consists of two α1 chains and one α2 chain which when self-assembled form tropocollagen a left-handed triple helix. These tropocollagens cross link with their terminal telopeptide and build up into the collagen fibrils. The terminal telopeptides can be cleaved using acid it conditions allowing for the solubilisations and repolymerisation of collagen fibrils in solutions or bioinks [138],[49].

Current 3D scaffold models are unable to replicate the intrinsic microstructure of native collagen[139]. To imitate the characteristics of native collagen and other ECM constitutes, tissue models use collagen bound to a controllable material such as PEG, decellularized ECM, plastic or use gelatine, an irreversibly hydrolysed form of collagen [27,140,139].

Therefore using the dual polymer system, a bioink containing both alginate and collagen is used for this investigation. Alginate provides much of the desired 3D printing properties and acts as a template for collagen which provides the biological relevance. One of the key aims of this investigation is to form an interpenetrating network (IPN) of collagen fibrils within a bioprinted alginate hydrogel. This interpenetrating network provides an anchor point for incorporated osteoblasts to attach and further functionalise the network by depositing *de novo* matrix, a behaviour that MC3T3's are well characterised of [64],[91]. With the easily reversed gelling kinetics of alginate shown in chapter 3, the hypothesis is that the cells can proliferate and remodel the collagen enough that the alginate can be later removed leaving behind mineralised collagen which mimics the intrinsic microstructure of bone tissue. The bioink blend developed in this chapter enables a reliable way to 3D print biomimetic fibrillar collagen IPN. The collagen incorporation into the bioink is discussed in chapter 6, in this chapter the focus was on getting the conditions stable for both encapsulated cell culture and collagen fibril formation, both of which require a stable pH at physiological conditions which was achieved.

4.1.2 Aims and Hypotheses

The aims of this chapter are to formulate a bioink ink *in situ* crosslinking system which combines the flexibility of SLAM bioprinting and the controllable gelling ion release with CLEX. To achieve this the following were access:

1. Determine a suitable bath incubation time for construct stability and is compatible with cell culture.
2. Optimise the incubation temperate and formulate bioink to have a stable pH throughout.

The hypothesis is that cells will be sensitive to the CLEX reaction and the system may need reformulation to limit shifts in pH.

4.2 Results

4.2.1 CLEX

For all subsequent work involving the competitive ligand exchange (CLEX) reaction and suspended layer additive manufacture (SLAM)(Figure 4.1.2), 400 µl of a bioink containing CLEX A (Calcium and EDTA) was extruded into 2 mL of SLAM agarose bath containing CLEX B (Glycine and Zinc). This was due to when the A and B components were switched around there was no resolution with the inks and the entire well would set as one mass.

4.2.1.1 initial Limits and compatibility concentrations

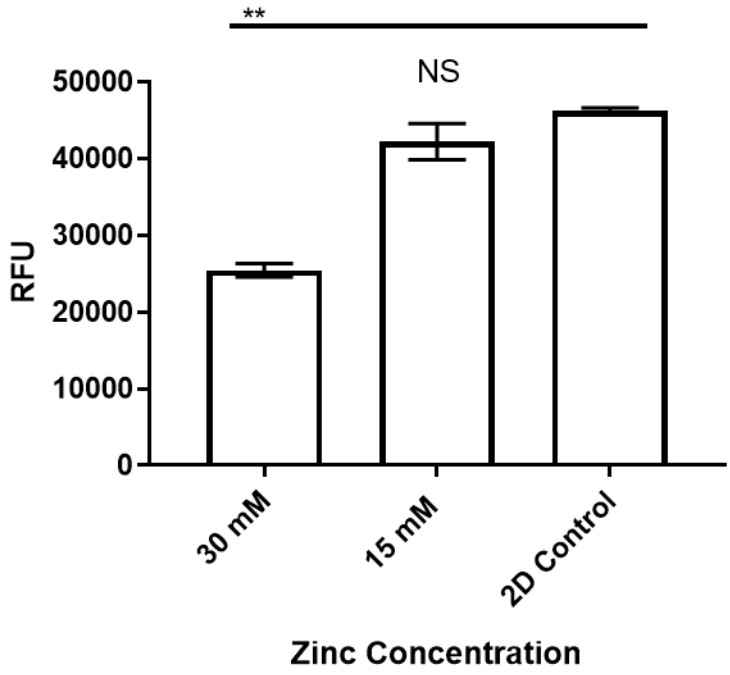

Figure 4.2.1 Cell compatibility with initial CLEX SLAM conditions.

Initial toxicity testing to determine conditions to test suitable crosslinking concentration for cell culture. Resazurin blue is used to as an indicator of cell viability to test the concentrations determined from initial CLEX SLAM gelling work are exposed to cells and their response compared to PBS control is measured. RFU (relative fluorescent units) are used to indicate cell viability, $1x10^5$ cells per condition. n=3, Errors bars +/- 1SD. *=<0.05, **=< 0.005, ***=<0.0005.

Initial optimisation work to determine suitable ranges for CLEX concentrations within bioinks. The concentrations chosen were able to crosslink the bioink within the CLEX B SLAM bath and an intact construct was retrievable from the SLAM bath. To test whether these conditions were compatible with cell encapsulation within the bioink, 0.6% w/v alginate bioinks made with CLEX A where extruded into the SLAM B bath and incubated for 60 min at 37 ^oC. While a SLAM bath with a starting concentration of 15 mM has a far greater RFU, indicating high cell viability and is not significant from the control. Constructs incubated in 15 mM were weaker than 30 mM and difficulty to remove intact.

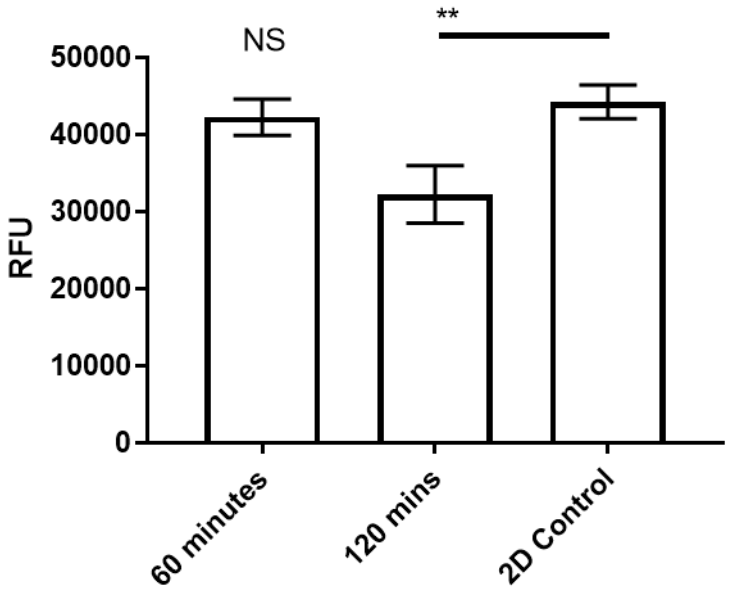

Figure 4.2.2 Increasing the incubation time of the bioink to improve construct retrieval.

With the toxicity limit determined, increases in incubation time was tested to improve the retrieval of the constructs post incubation. Using SLAM bath at a starting zinc concentration of 15 mM, the effects of increasing incubation time from 60 minutes to 120 minutes was measured using resazurin as an indicator of viability. RFU (relative fluorescent units). n=3, Errors bars +/- 1SD. *=<0.05, **=< 0.005, ***=<0.0005.

To improve the integrity of the constructs for more consistent removal from the SLAM, incubation times in the SLAM phase at a starting concentration of 15 mM zinc ions at 37 ^{o}C were increased from 60 min to 120 min. The constructs incubated for 120 min were able to be easily retrieved intact from the SLAM while the 60 min were not and often fell apart during the retrieval process. Though there was a drop in RFU indicating a lower viability of the cells when incubated for 120 min this was still greater than 30 mM (Figure 4.2.1) and is a compromise between cell retrieval and cell viability so therefore was used as the standard incubation time for CLEX SLAM bioprinting for the rest of the development.

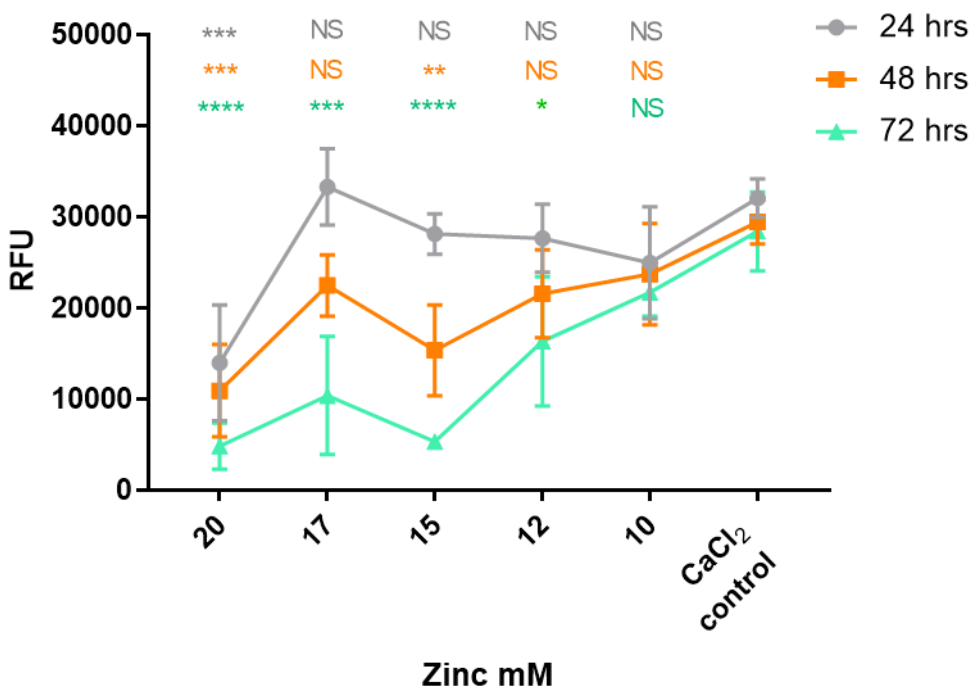

Figure 4.2.3 Metabolic activity of 3D constructs crosslinked with CLEX of different final zinc concentrations.

Constructs were incubated in concentration series of CLEX SLAM to determine how the total final zinc concentration affected the cells. Each day concentration is compared to a $CaCl_2$ control cultured for the same time period. Metabolic activity is measured using resazurin as an indicator of viability. RFU (relative fluorescent units). n=3, Errors bars +/- 1SD. *=<0.05, **=< 0.005, ***=<0.0005. NS no significant difference. When in bold indication all conditions at particular concentration.

CLEX agarose baths of varying concentrations were made. A set volume of bioink was added to each well and incubated for 2 h at 37 ^{o}C Resazurin reduction readings were taken every 24h and compared to 0.6% alginate that had been crosslinked with 100 mM calcium chloride only for each respective day. Inks crosslinked with a final zinc concentration of 10 mM showed no significant difference when compared to the $CaCl_2$ control. As the concentration of free final zinc rises the metabolic activity of the cells falls with 72 h no longer being significant for 12 mM, while 48 and 72 h are no longer significant for 15 mM.

4.2.2.1 pH

4.2.2.1.1Buffer temperature

One of the initial hurdles of using the CLEX gelling system was the rise in pH of the crosslinked bioinks after incubation. When first described CLEX used 3-(N-morpholino) propanesulfonic acid (MOPS) buffer[124], due to the intended length of the culture conditions of the bioprinted constructs this was shifted to HEPES and the rise in pH was believed to be due to the change in the buffer.

Different temperature conditions were tested to formulate the optimal conditions for the gelling system. As per previously described in section 2.2.1 page 17, CLEX components were buffered to a starting pH of 7.40. Three different starting temperatures of 4 ^{o}C, 21 ^{o}C and 37 ^{o}C were used as these are all relevant temperatures for collagen polymerisation. Similarly these temperatures were chosen as incubation temperatures to see how the buffers respond to the various change in temperature. For all conditions the bioink started at 4 ^{o}C to restrict collagen polymerisation until after printing.

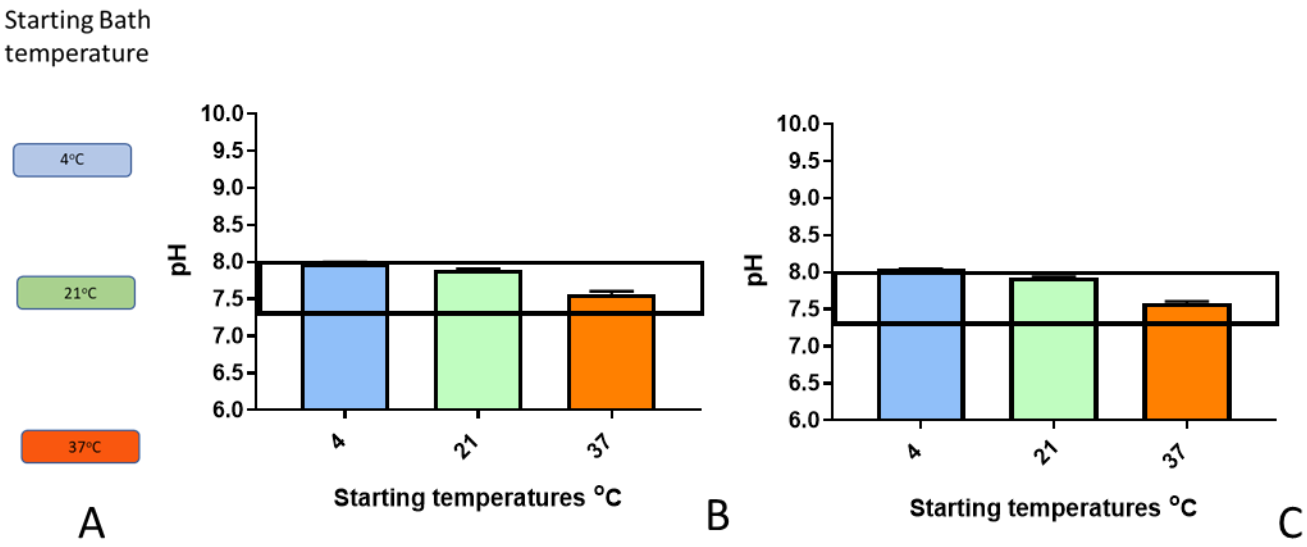

Figure 4.2.4 SLAM Agarose bath starting pH with CLEX B components buffered to pH 7.40.

CLEX SLAM was made with CLEX components buffered to pH7.4 and then incubated at either 4,21 or 37°C to measure the effect of temperature on pH. Two CLEX formulations were tested, one buffered with HEPES and one with MOPS. n=3

A. Key for the colour code for the SLAM bath starting temperatures
B. pH of the SLAM bath with CLEX components buffered to pH 7.40 with HEPES at 3 relevant temperatures for collagen polymerisation.
C. pH of the SLAM bath with CLEX components buffered to pH 7.40 with MOPS at 3 relevant temperatures for collagen polymerisation

As shown in Figure 4.2.4, the initial starting pH of the SLAM CLEX B bath is consistent between the different buffers for all temperatures. All are within the maximum pH 8 threshold target. The lowest pH and closest to the mid-range of the target zone was 37 °C, with a pH 7.57 for HEPES and 7.59 for MOPS. All conditions were made at the same time with the same formulation with only the temperature varying.

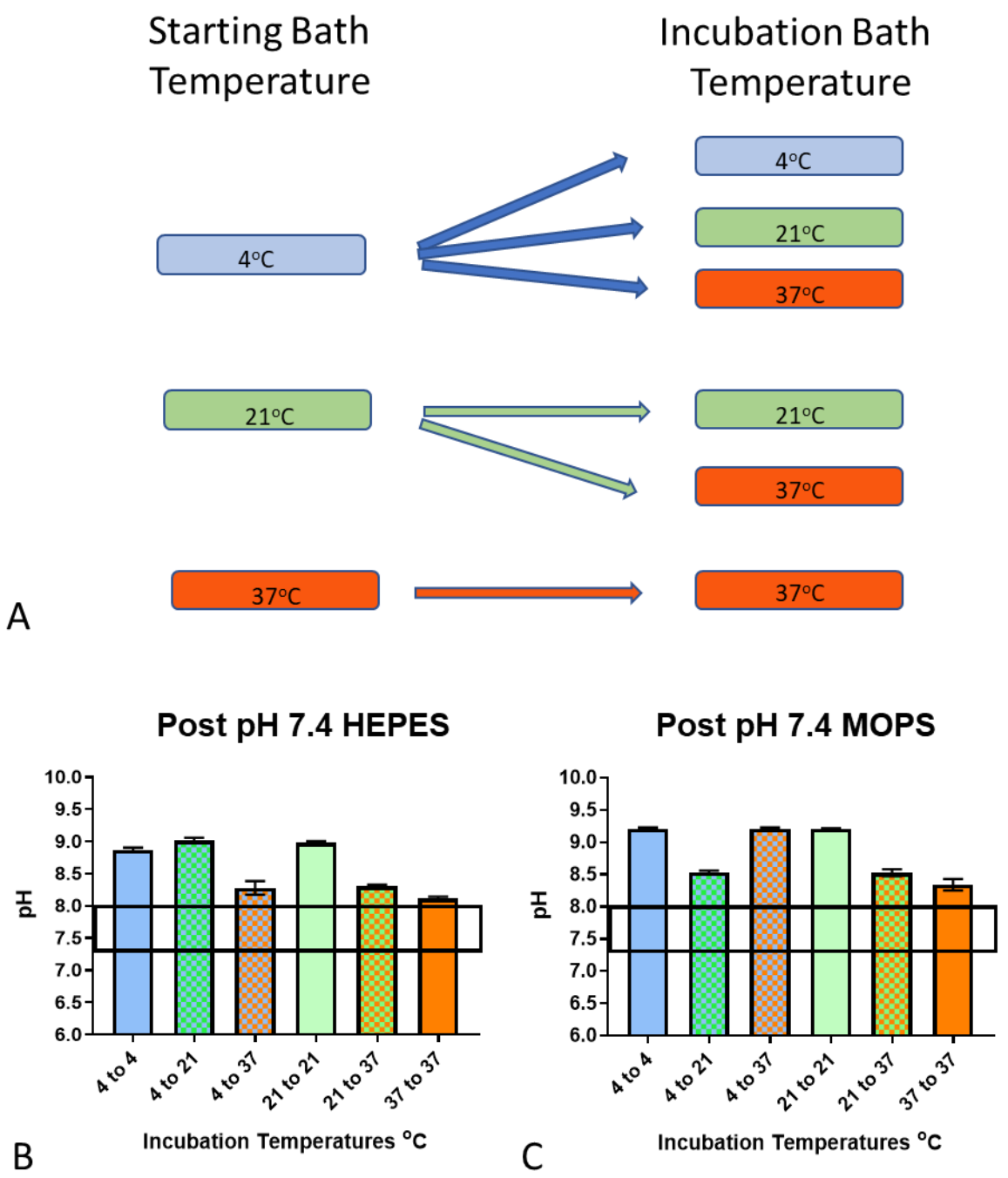

Figure 4.2.5 Final pH of co-incubation of bioink and SLAM agarose bath when CLEX components of bioink and bath are buffered at pH 7.40.

CLEX B SLAM agarose bath components were incubated initially at 4, 21 or 37°C, upon the addition of CLEX bioink the temperature was either maintained or raised to 21 or 37°C. The bioink was incubated for 2h at the stated temperature and the final pH was measured. Two CLEX formulations buffered to 7.4 were used one buffered with HEPES and one with MOPS. n=3

A. A schematic diagram of starting and final incubation temperatures for the of the SLAM for the CLEX reactions.
B. CLEX bioink incubated in CLEX SLAM and the resulting temperature dependant pH shift for HEPES based bioinks.
C. CLEX bioink incubated in CLEX SLAM and the resulting temperature dependant pH shift for HEPES based bioinks.

With Figure 4.2.4 indicating that pH of the CLEX SLAM bath is sensitive to temperature a range of starting and incubation temperatures were tested to determine the optimal starting and incubation temperatures for the CLEX reaction to occur. CLEX A bioink was added to CLEX B SLAM at the 3 starting temperatures shown in Figure 4.2.5 A and incubated for 2 h at the indicated final temperature of either 4, 21 or 37 ^{o}C Figure 4.2.5 A resulting in either a maintenance of temperature or a rise in temperature. The different buffers were investigated to ameliorate the pH shift, the bioinks were made with the same formulation and concentration of each buffer. Bioinks made with MOPS buffer had a greater rise in pH when compared to HEPES buffered bioinks at all temperature conditions. In both formulations, 37 ^{o}C to 37 ^{o}C was the optimal condition with a starting pH of 7.57 (+/- 0.03) for HEPES and 7.59 (+/- 0.02) for MOPS (Figure 4.2.4), after incubation the pH rose to 8.11 (+/- 0.03) for HEPES and 8.34 (+/- 0.07) for MOPS (Figure4.2.5 B,C). Initially indicating that HEPES is the more stable buffer at these temperatures and when shifting temperatures.

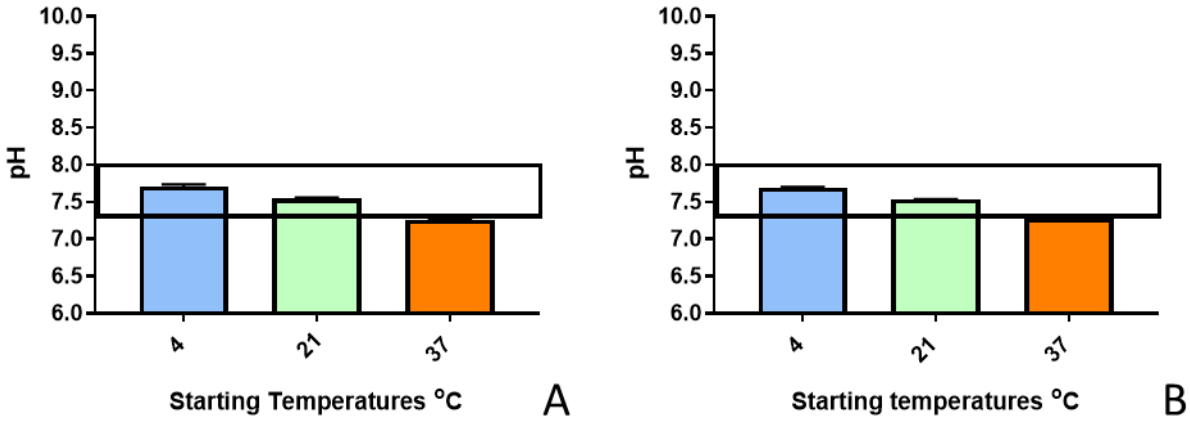

Figure 4.2.6 SLAM Agarose Bath Starting pH with CLEX components buffered to pH 7.0.

CLEX SLAM was made with CLEX components buffered to pH7.0 and then incubated at either 4,21 or 37°C to measure the effect of temperature on pH. Two CLEX formulations were tested, one buffered with HEPES and one with MOPS. n=3

A. pH of the SLAM bath with CLEX components buffered to pH 7.0 with HEPES at 3 relevant temperatures for collagen polymerisation

B. pH of the SLAM bath with CLEX components buffered to pH 7.0 with MOPS at 3 relevant temperatures for collagen polymerisation

To stabilise the pH to within the targeted range, the initial pH of the CLEX components before added to their respective constitute phases was lowered down to pH 7.0. This lowered the starting pH of the CLEX B SLAM agarose bath to be within the target pH range for all starting temperatures except for 37 °C. The HEPES buffered CLEX system had a pH of 7.26 (+/- 0.01) and the MOPS buffered CLEX system had a pH of 7.28 (+/- 0.01) both had dropped below the target of 7.4- 8.0.

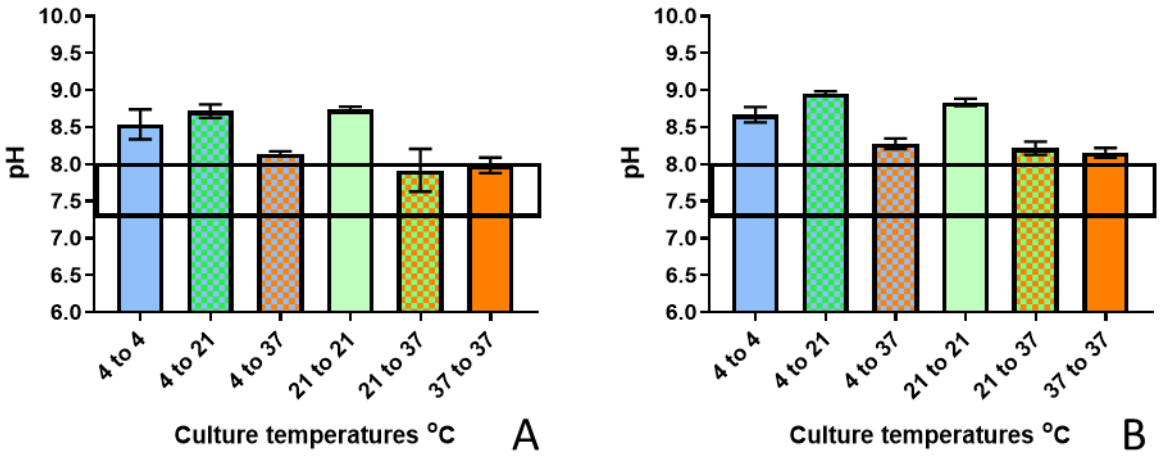

Figure 4.2.7 Final pH of co-incubation of Bioink and SLAM Agarose bath when CLEX components of bioink and bath are buffered at pH 7.0.

CLEX B SLAM agarose bath components were incubated initially at 4, 21 or 37°C, upon the addition of CLEX bioink the temperature was either maintained or raised to 21 or 37°C. The bioink was incubated for 2h at the stated temperature and the final pH was measured. Two CLEX formulations buffered to 7.0 were used, one buffered with HEPES and one with MOPS. n=3

A. CLEX bioink incubated in CLEX SLAM and the resulting temperature dependant pH shift for HEPES based bioinks.
B. CLEX bioink incubated in CLEX SLAM and the resulting temperature dependant pH shift for MOPS based bioinks.

Bioink and SLAM CLEX components buffered to pH 7.0 using the same conditions from figure (Schematic). After a 2 h incubation, the pH in all conditions rose, only the HEPES 21 °C to 37 °C and 37 °C to 37 °C conditions stayed within the target range of 7.4 to 8.0 with a pH of 7.92 (+/- 0.24) and 7.99 (+/- 0.09) respectively. Figures 4.2.5 B, C and 4.2.6, present an initial trend of a temperature dependant decline in pH. For HEPES buffered system, for any starting temperatures a final incubation at 37 °C results in the lowest pH shift. This trend is also seen in MOPS buffered system with the exception of 4 °C to 21 °C. Therefore, all continuing development of the CLEX SLAM bioink system use HEPES buffer and a 37 °C to 37 °C starting and final incubation temperature.

4.2.2.1.2 Rebalancing exchange ions

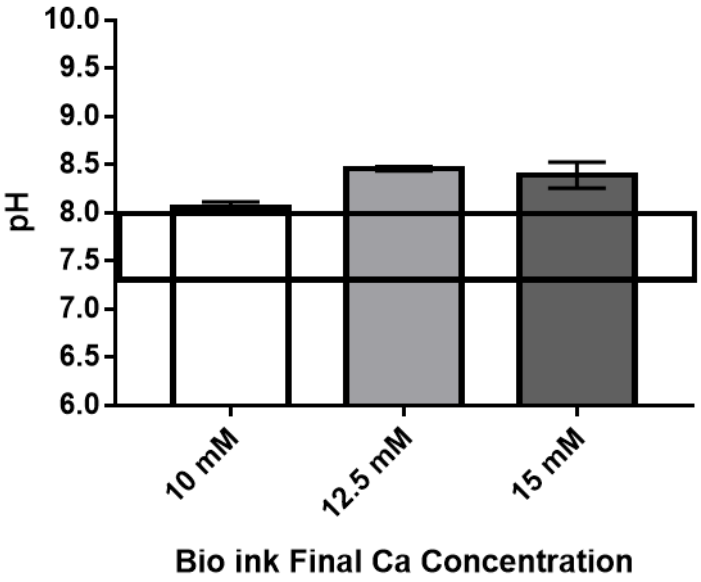

Figure 4.2.8 Increasing Calcium Concentration in the CLEX SLAM system.

To investigate whether the low calcium ion concentration compared to the final zinc concentration was causing the shift in pH, bioinks made 60, 75 and 90mM $CaCl_2$ were prepared to so that the final concentrations would equal 10, 12.5 and 15mM. The inks were made with HEPES and started at 37°C and incubated at 37°C. n=3

The Hypothesis was that the non-stoichiometric ratio in final concentrations of the gelling ions within the CLEX system may be causing the shift in pH. To investigate this new bioink formulations were made with increased concentrations of CLEX A to raise the calcium concentration. The starting concentration was 60 mM to a final concentration of 10 mM, as used in the previous HEPES v MOPS Figures (4.2.4, 4.2.6, 4.2.8). This had a final pH concentration of 8.05 (+/- 0.05) within the range as seen in Figure 4.2.9. When the final calcium concentration was raised to 12.5 mM stoichiometric to the zinc concentration, the pH rose with to a final pH of 8.46 (+/- 0.02). The concentration dependent rise in pH was not seen in the 15 mM which the pH stabilised at a similar level to 12.5 mM and had a pH of 8.39 (+/- 0.11). Therefore the subsequent formulations of the bioink remained at starting concentration of 60 mM $CaCl_2$.

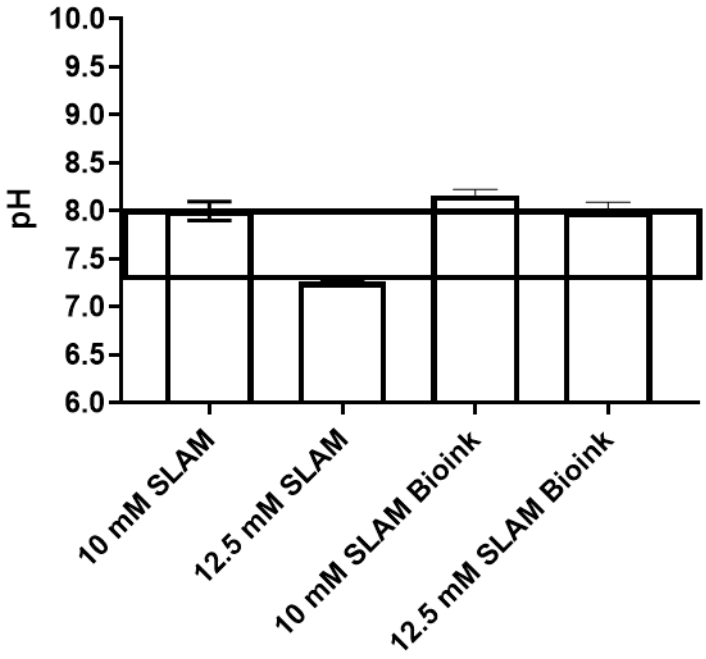

Figure 4.2.9 Effects of lowering SLAM CLEX B final zinc concentration to 10mM.

The final zinc ion concentration in the SLAM B was lowered from 12.5 mM to 10 mM to be stoichiometric as originally designed for the reaction and compared to the current working final concentration of 12.5 mM zinc. All conditions contained HEPES buffer, pH 7.0 CLEX components, started at 37^{o}C and incubated at 37^{o}C. n=3

The CLEX reaction was developed as a stoichiometric ratio between the Ca ions in part A and the Zn ions in part B. For the bioprinting development this ratio has shifted to a final 1:1.125 molar ratio Ca:Zn ions. In Figure 4.2.9 the ratio has been shifted back to 1:1 to see whether the uneven ratio is responsible for the rise in pH. When the zinc concentration was lowered to 10 mM, the initial pH was 8.00 (+/- 0.05) which is at the maximum of the target range while the 12.5 mM was below the target range at to 7.26 (+/- 0.008). After incubation both conditions rose with the 10 mM rising above the target range and 12.5 mM being just within (7.98 +/- 0.09).

4.2.2.1.3 Lowering pH

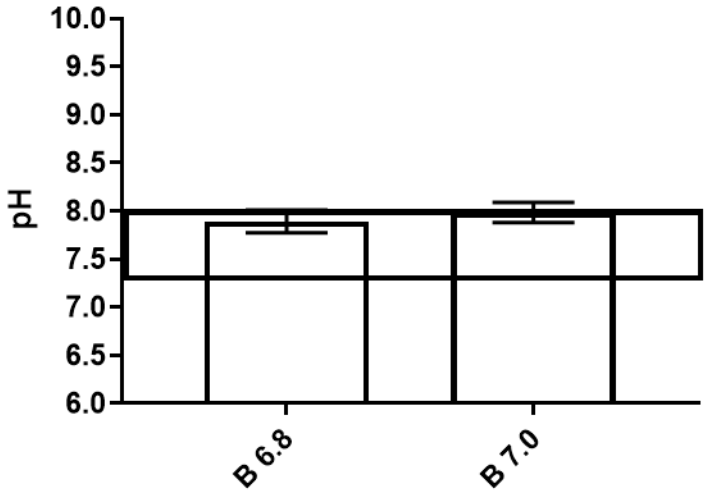

Figure 4.2.10 pH after incubation of CLEX SLAM + Bioink when only CLEX B components are lowered to pH 6.8.

The CLEX B component of the gelling system was lowered to a starting pH of 6.8 while the CLEX A components in the bioink remained at pH 7.0 due to the bioink containing cells. n=3

The CLEX B components were buffered to a pH of 6.8 which were then incorporated into the SLAM agarose. This lowering of the CLEX components brought down the starting pH within the targeted pH range. When compared to the SLAM bath made with CLEX components buffered to pH 7.0 (7.99 +/- 0.09), there was minimal difference between the final pH post incubation when switched to pH 6.8 (7.89 +/- 0.10) and both were within the target range. As the pH 6.8 buffered SLAM bath has a lower pH, this was used to continue the development of the system.

4.2.2.1.4 Proliferation media v Differentiation media

To investigate whether the media composition used in the bioinks had an effect on the pH, the systems were compared when formulated with proliferation αMEM or Differentiation media. Additionally, the concentration of Zinc in the SLAM CLEX B was lowered from 12.5 mM to 10 mM. As Figure 4.2.11 demonstrates that all conditions exceed the targeted pH ranges other than αMEM 12.5mM which had a final pH of 7.94 (+/- 0.057).

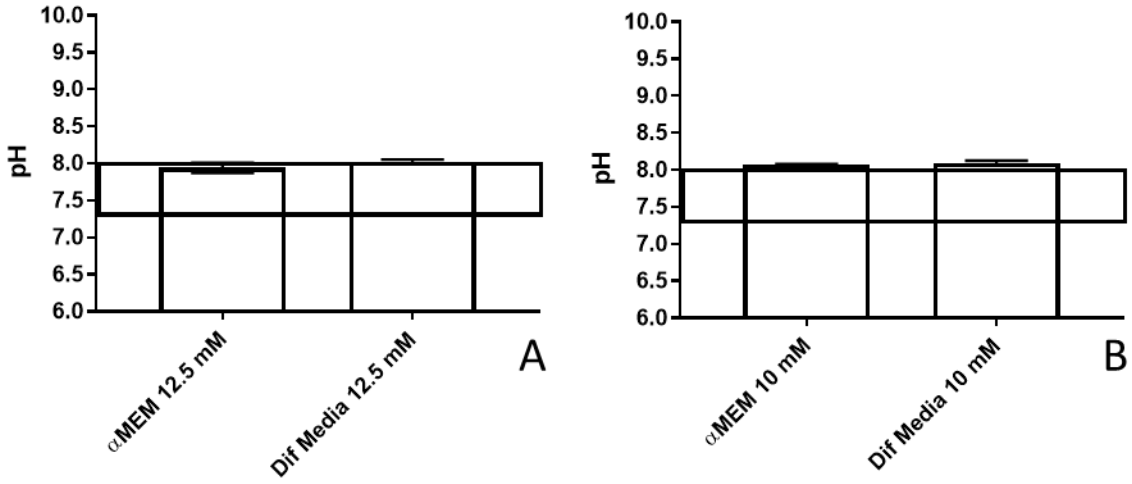

Figure 4.2.11 Effects of differentiation media and proliferation media and lowering final zinc concentration in the SLAM bioink system.

In both figures, the starting pH of the CLEX B bath was 6.80 and the bioink was 7.0, the SLAM and ink were incubated at 37°C to 37°C for 2h. The effects of osteogenic differentiation media was tested and compared to proliferation. The effect on pH of lowering zinc concentration from 12.5 mM to 10 mM were also investigated. n=3

A. The effects of the media components on the pH of the bioink and SLAM CLEX when changed from proliferation to Differentiation media
B. The effects of the media components on the pH of the bioink and SLAM CLEX when changed from proliferation to Differentiation media when the final Zinc concentration changed from 12.5 to 10 mM.

4.2.2.1.5 Reformulation to include diglycine

The final reformulation of the bioink was to swap the glycine in the CLEX B to diglycine. This swap retained the zinc chelation within the B yet chemically halved the amount of free glycine released into the system after the ligand exchange had occurred. In all conditions the final pH after incubation remained stable within the targeted pH range and close to 7.4 which is the desired pH for cell culture. The effect of changing the final zinc concentration and the media composition within the bioinks had minimal effect on the final pH. This allows for a lower 10 mM final zinc concentration to be used as well as the incorporation of differentiation media into the system.

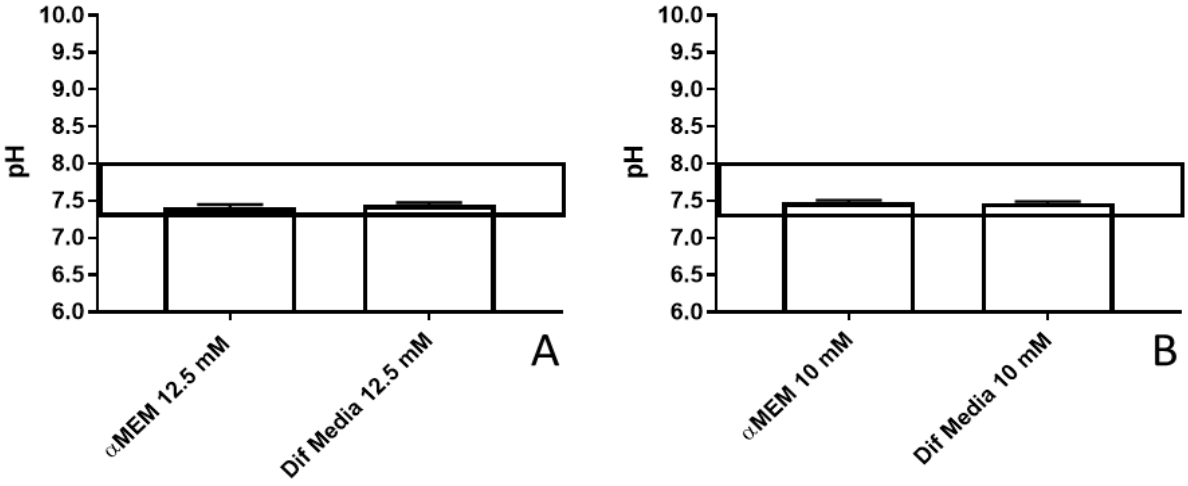

Figure 4.2.12 Reformulating CLEX SLAM from Glycine to Diglycine.

To lower the amount of free glycine released into the SLAM bath after crosslinking, the zinc chelator glycine was preplaced for diglycine. In both figures, the starting pH of the CLEX B bath was 6.80 and the bioink was 7.0, the SLAM and ink were incubated at 37°C to 37°C for 2h. The effect of osteogenic differentiation media was tested and compared to proliferation. The effect on pH of lowering zinc concentration from 12.5 mM to 10 mM were also investigated. n=3

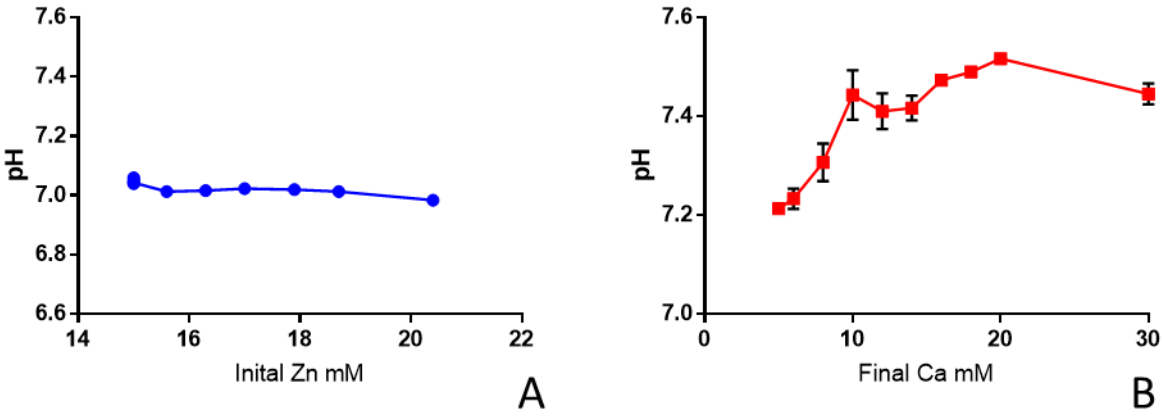

Figure 4.2.13 Effect of the crosslinking cation concentration on pH.

A. Zinc concentration effect on pH for SLAM B bath before bioink is added.
B. Calcium concentration effect on pH after ink added and incubated for 2h.

A range of concentrations of total zinc contained within the CLEX B incubated at 37°C were tested to determine the effects of diglycine on pH. The concentration was varied by adjusting the volume of agarose added to the SLAM so the resulting concentration would always be 12.5 mM. The bioink was added and incubated at 37°C for 2h and the resulting pH was measured. The Ca concentration within the bioink was constant for all conditions and the total volume of ink added was changed to change the total final Ca concentration. n=3

To investigate whether the starting Zn was the driver behind the pH rise or the released glycine was triggering the rise a concentration pH investigation was performed. SLAM CLEX B baths were made in a ranges of concentration between 12.5 mM and 20.4 mM. The SLAM and the Ink were made with the same starting stock solutions as previously used but the volume of each component shifted to vary the concentration Table 4.2.1. For all starting zinc conditions, the final total concentration after the bioink was added was 12.5 Mm. As Figure 4.2.13A shows, the starting Zn concentration had no effect on the starting pH of the SLAM bath. Figure 4.2.13 B shows that at optimal pH stability conditions, raising the final concentration of calcium within the system causes a rise in pH. As the final concentration of calcium rises as does the concentration of released EDTA a direct molar ratio. The greater the EDTA concentration in the system the more zinc cleaved from the glycine and therefore a greater free glycine concentration. Therefore the rise in pH is linked to the glycine

concentration, this in conjunction with data in Figure 4.2.11 and 4.2.12 shows that for the final system SLAM B should be made with diglycine.

4.2.2.1.6 Formulations of bioinks

To demonstrate the dynamic nature of the CLEX SLAM combination and the changing ions the CLEX ratios used in Figure 4.2.13 can be seen in Table 4.2.1. All conditions had a final zinc concentration of 12.5 mM with only the starting concentration shifted. There was minimal change in pH throughout the whole zinc mM range Figure 4.2.14A. The optimal gelling calcium concentrations are between 10 and 18 mM calcium with a drop in construct integrity after 20 mM, this could be due to the low ratio of bioink to SLAM and the limited diffusion of the CLEX components.

Table 4.2.1. Different formulations and ratio of gelling conditions used for figure 4.2.13. An overview of the two moving parts of concentration and volume ratio of the CLEX components and the bioink/SLAM.

Final Ca mM	Ink vol µL	SLAM Starting mL	SLAM Starting Zn mM	SLAM Final Zn mM	Ca:Zn ratio	Ink to SLAM Vol	Ink to Total vol	Ink Gelled
5	200	2.00	15.0	12.5	1:2.50	1:10	1:12	-
6	240	2.00	15.0	12.5	1:2.08	1:8.3	1:10	+
8	320	2.00	15.0	12.5	1:1.56	1:6.2	1:7.5	+
10	400	2.00	15.0	12.5	1:1.25	1:5.0	1:6.0	++
12	480	1.92	15.6	12.5	1:1.04	1:4.2	1:5.0	++
14	560	1.84	16.3	12.5	1:0.89	1:3.6	1:4.3	++
16	640	1.76	17.0	12.5	1:0.78	1:3.1	1:3.8	+++
18	720	1.68	17.9	12.5	1:0.69	1:2.8	1:3.3	+++
20	800	1.60	18.7	12.5	1:0.63	1:2.5	1:3.0	+
30	1230	1.17	20.4	12.5	1:0.42	1:1.6	1:1.9	-

Key	
No Gelling	-
Partial gelling	+
Gelled but weak	++
Fully Set	+++

4.3 Discussion

The key aims of this research was to develop an *in vitro* model of bone, this required a bioink system that incorporated an *in situ* alginate gelling system that allowed for the printing of very weak bioinks and collagen fibril formation that is entirely compatible with live cell encapsulation. To achieve this, the previously existing techniques of competitive ligand exchange and suspended layer additive manufacturing were combined to create a novel *in situ* gelling system for 3D printing hydrogels..

Competitive ligand exchanged (CLEX) is a strategy that allows for the controlled release of gelling ions within aqueous polymer solutions [124]. The strategy was designed as a stoichiometric system using an alginate phase in both part A and in part B, to allow for this to be 3D printed with the suspended layer additive manufacturing technique (SLAM) this to be reformulated due to the disparity in volumes between the bioink added and the SLAM support bath [120]. Initially the strategy was designed to work with 60 mM calcium ions and EDTA in part A and 60 mM zinc ions with 120 mM in part B [124]. The systems used for the CLEX SLAM had a starting concentration of 60 mM for calcium ions and EDTA in the bioink and 12.5 mM zinc ions 25 mM glycine or 12.5 mM diglycine depending on the formulation. These would result in final concentrations of 10 mM calcium ions and EDTA, and 10 mM zinc ions and 20 mM glycine or 12.5 mM di glycine. Though the final concentrations end up in a balanced ratio the starting concentration are disproportionate.

Some of the advantages of CLEX over standard alginate crosslinking is the controlled release of gelling ions, this can be modulated through pH and reformulation to have a gelling of two CLEX based alginate gels of between 2.7 seconds to 57 minutes [124]. Alginate gelling with calcium chloride is a very quick process that crosslinks the hydrogel almost immediately [110,141]. While this rapid gelation has applications such as with droplets into a bath solution or casting, this has serious limitations with 3D printing and extrusion-based cell encapsulation as it can cause premature gelling and blockages[53,56]. To overcome this, typically when 3D printing with alginate the construct is 3D printed and crosslinked after[116]. While this technique can product high resolution constructs, it is typically limited to the use in high concentrations of alginate and smaller less complex shapes[116]. The major advantage of using an *in situ* gelling system is that when alginate crosslinks it contracts, with 2% alginate contracting approximately 48% [142]. Due to the gelling front caused by crosslinking ions diffusing through the gel when constructs are immersed in a crosslinking bath [143], a printed construct can suffer distortion during the crosslinking. Additionally lower concentration alginates can spread after printing [120], thus further reducing the resolution. Using the CLEX SLAM system reduces the impact of shrinking on construct resolution due to the contraction happening homogeneously and at

a controlled rate during the printing process. This allows for greater resolution of low concentration alginate 3D printing.

When initially testing incorporating the CLEX strategy higher CLEX concentrations were used as this sped up the cross linking and allowed for faster retrieval from the SLAM. Toxicity was seen when using CLEX at these higher concentrations (Figure 4.2.1), this toxicity was hypothesized to be due to the zinc in the system. While in where should be no free zinc in the system it is unlikely that all the zinc remains bound to all the glycine or EDTA all the time and even free zinc concentrations as low as 100 nM are toxic to cells in vitro [144].

Previous publications using CLEX are typically formulated using EDDA as the zinc chelator [79],[124]. While this was initial tested as a formulation during CLEX SLAM incorporation no crosslinking would occur in the SLAM. This may be in part due to the material properties of the SLAM being a fluid gel so limited diffusion would occur through the system [120]. Therefore, the zinc chelator in CLEX B was swapped from EDDA to glycine, this allowed for in situ gelling to occur. This is in part due to glycine having a lower relative affinity for zinc than EDDA. EDDA has a log *K* of 11.1 for Zn^{2+} whereas glycine is 3.04. Additionally, two glycine molecules are required to chelate one zinc ion, therefore only one glycine unit needs to be cleaved to release the zinc into the system. This easier zinc release as well as being compatible with *in situ* gelling may also be the cause of the toxicity seen in the higher concentrations of CLEX components containing zinc which is not previously reported.

Other suspended later printing systems are reported, the most notable one is FRESH printing (Freeform Reversible Embedding of Suspended Hydrogels) [145]. This system has many of the same advantages of SLAM in supporting 3D printed constructs. FRESH printing uses a gelatin microparticle support bath which bioinks are extruded into, the bath temperature is then increased to 37 ^{o}C which melts away the supporting bath material releasing the construct [146]. While this has been shown to produce large complex structures such as an entire heart, which demonstrates the flexibly of suspended layer 3D printing[145] The FRESH supporting material is very expensive and retails for $300 USD for 20mL which takes it out the budget of less well funded projects whereas agarose based SLAM can be made for a fraction of that cost. Due to the reversable temperature required for removal of FRESH, this makes it unsuitable for materials that requires specific temperatures for extrusion and crosslinking, such as GelMA which requires extrusion at 37 ^{o}C and collagens which require crosslinking at these temperatures.

Though swapping from EDDA to glycine modified the CLEX system to be compatible with SLAM to allow for *in situ* gelling, this swap triggered a rise in pH after gelling had occurred (Figure 4.2.4 and

4.2.5). Multiple avenues of investigation were pursued from reformulating the CLEX components to having a lower pH.

One of the initial changes was switching from a MOPS buffered system to a HEPES system. Buffers go through a temperature dependent shift in buffer range (Figure 4.2.4, 4.2.6) [147]. MOPS buffer has been shown to have an effect temperature range of between 25 – 37 °C [148]. MOPS has a buffer range of pH 6.5- 7.9 but the pKa at 25 °C is 7.20 and at 37 °C is 7.02 indicating that as the temperature rises the buffer is less able to buffer the pH at the upper end of is range thus causing the rise in pH after incubation. HEPES has a buffer range of pH 6.2 to 8.2 which is greater than the range of MOPS. Its is also usable at lower temperatures than MOPS having a pKa of 7.85 at 0°C and has a higher pKa 7.55 at 20 °C, 7.48 at 25 °C and 7.31 at 37 °C [147] indicating that HEPES is the better buffer choice for the CLEX system.

Throughout section 4.2 different approaches were taken to lower and stabilize the pH of the CLEX SLAM bioink such as reformulating the gelling ion ratios within the system (Figure 4.2.8) and modifying the media component (Figure 4.2.11) of the bioink. While these all had a minimal effect on modulating the post incubation pH, the biggest affect was from reformulating the gel to use diglycine (Figure 4.2.11 and 4.2.12). This swap halved the amount of free glycine released into the system due to the conjugation of the glycine units. Therefore, an equimolar ratio of glycine to zinc was able to be used for the CLEX system, this caused a lower final pH of the system due to, the free glycine and diglycine released into the system after crosslinking has buffer capabilities.

Glycine has two buffer ranges, an acidic range, and a basic range. The acidic range for glycine at 25 °C is pH 2.2-3.6 with a pKa of 2.35 and the basic range of 8.8-10.6 with a pKa of 9.78 at 25 °C [149] and 9.30 at 37 °C [150]. Di glycine, like its mono version has two buffer ranges, and acidic range and a basic range. The acidic range for di glycine is 2.5-3.8 with a pKa of 3.14 at 25 °C. Interestingly, di glycine as a basic range very similar to the target range of the post incubation CLEX SLAM of 7.5-8.9 and a pKa of 8.25 at 25 °C. Di glycine was one of the original buffers, along with HEPES, tested by Goods to determines the Goods buffers where di glycine was shown to have a pKa of 9.0 at 0 °C, 8.4 at 20 °C and 7.9 at 37 °C [147].

This indicates that combining the HEPES buffer with the di glycine in the CLEX system is the reason for the stabilization of the pH after incubation at 37 °C. When glycine was used, the abundance of free glycine released into the system raised the pH to within the buffer ranges of glycine and above that of the HEPES due to glycine have a pKa of 9.30 at 37 °C. Whereas when the di glycine was used the pH remained within the buffer range of both di glycine and HEPES, with a pKa of 7.9 and 7.31 respectively, this aided in keeping the pH within the target range of 7.4 to 8.0. Therefore, when

designing bioinks, especially with complex or *in situ* crosslinking systems it is important to take into consideration any products produced by the process. As with 3D, there is a lower diffusion compared to 2D, so removal of byproducts takes longer and is a more involved process than conventional cell culture.

Incorporating CLEX with the SLAM system was an important step to facilitate the bioprinting of weak low viscosity bioinks. SLAM uses an agarose fluid gel as a self-healing supporting layer to facilitate extrusion of low viscosity biopolymers and bioinks [120]. These properties made SLAM an attractive method for extrusion of low concentration alginate collagen hybrid gels. Other support layer additive manufacturing techniques exist yet have fundamental limitations when incorporation collagen constructs. The incorporation of CLEX into the SLAM system was due to the addition of calcium chloride to the SLAM to crosslink the alginate within the agarose as reported in the original paper [120] disrupted the resolution of the print. This was in part due the alginate concentrations originally described being far greater than in the bioink. Therefore, an *in situ* crosslinking was required to release constructs from the SLAM bath and maintain the resolution.

The CLEX SLAM system is a co-polymerization system with the chemical CLEX system and the thermally dependent collagen crosslinking occurring simultaneously. This co-polymerization obviates the need for gelatin support bath layers such as FRESH (Freeform Reversible Embedding of Suspended Hydrogel). The temperature dependent phase change of FRESH interfered with the collagen fibril formation which is optimal at 36.5 ^{o}C [151,152] and is the temperature required to dissociate FRESH support bath[146]. Additionally, the temperature shift would affect the pH stabilization of the CLEX system (Figure 4.2.5, 4.2.7). SLAM printing has other benefits over FRESH, with a lower viscosity at low sheers rates than FRESH, suggesting less distortion during the printing process [120]. PVA polymer granules have also been used as a suspended support layer for 3D printing, though the limitations are very low movements through the medium of up 0.9 mm/s compared to the 30 mm/s used in the CLEX SLAM system, this slow printing could interfere with the temperature stability of the bioink and cause premature collagen polymerization. The PVA granules are pH sensitive and swell under different pH, with the maximum swell being at physiological pH. The pH shift undergone through the CLEX reaction would cause the particles to change size and thus distort the print, therefore rendering the technique not suitable for the CLEX and collagen system[153].

To overcome the limited cell attachment of unmodified alginate gels [76], type 1 collagen was incorporated into the bioink with the aims of forming an interpenetrating network of collagen fibrils within the ink to act as scaffold for the cells to attach to. Collagen had to be incorporated within the

alginate bioink as 3D printing collagen based gels has previously been reported to be challenging [154],[58], [113]. The major limitations of collagen as a bioink in itself are the slow crosslinking times, low viscosity when in its liquid phase and therefor fails to retain shape and requires a stable pH [58]. Despite the limitation of its printing characteristics collagen remains the gold standard for tissue engineer due to its high abundance within the body, ready cell attachment, and provides structural support[155]. Therefore to overcome these limitations collagen is typically combined with other hydrogel that have material properties that are suitable for printing [156], [110], [157], [111].

5 Optimising cell differentiation for 3D bioprinted culture

5.1 Introduction

Bone tissue is made up of three main cell populations: osteocytes, osteoclasts, osteoblasts, which are briefly summarised below. Osteoblasts and osteoclasts work in conjunction at the bone surface, continually remodelling bone through formation and absorption respectively. This process is largely orchestrated by osteocytes, which are embedded within the bone tissue. One of the aims of this project is to reliably recapitulate these remodelling processes in a synthetic spatially controlled environment. To achieve this, this chapter focuses on the cellular integration within the developed bioink.

As described in chapter 1, the complex hierarchical micro architecture of bone, is in part, where the innate strength of bone emanates from, this complexity is unfeasible to replicate synthetically. Therefore, the approach used is to continually develop the bioink post printing by providing all the building blocks of bone required within the bioink. After 3D printing, the constructs are continuously cultured in an environment conducive for the cells to remodel the bioink. This continually develops the printed construct at a scale elusive to modern 3D printing techniques. As the focus is on developing a biological tissue model of bone, having an ultimate tensile and compressive strength, orders of magnitude away from native bone tissue is not a hinderance if the biological pathways creating both native and engineered tissue are comparable.

5.1.1 Biology of Bone

Osteoblasts account for approximately 5% of the total cells present in bone and are of a mesenchymal lineage [3]. Their morphology is a cuboidal epithelial cell with their organelles featuring a well-developed golgi, with plentiful rough endoplasmic reticulum and secretory vesicles typical of secretory cells. Osteoblasts are polar cells and through their contact with bone extracellular matrix (ECM) secrete osteoid onto the bone matrix, osteoid consists of unmineralized collagen and collagen-like proteins which are later mineralised with hydroxyapatite by osteoblasts [158].

Osteoclasts are differentiated from a haemopoietic/macrophage lineage. Their morphology is large, multinucleated and have a well-developed golgi, plentiful smooth endoplasmic reticulum, and a significant presence of mitochondria and lysosomes. Osteoclasts have a membrane bound H^+ ATPase pump used for acid production for hydroxyapatite reabsorption and produce MMP and cathepsin K for organic bone matrix protein reabsorption. The reabsorbed materials are packed into vesicles and exocytosed by the osteoclasts [158].

Osteocytes are mature osteoblasts which have become encased in bone matrix, where they can remain encapsulated for up to 25 years [3]. Upon differentiating into an osteocyte, the characteristic organelles of an osteoblast are lost and diverge away from a secreting cell format. Despite being the most prevalent cell type in bone (~95%) the exact mechanisms of osteocytogenesis are still disputed and not fully characterised. Some osteoblasts are passively encapsulated by other osteoblasts in osteoid, which is subsequently mineralised, trapping the osteoblast in the bone matrix. This space is called the lacunae, here it either undergoes apoptosis or differentiates into an osteocyte [11]. While others mature into osteocytes through more active genesis, this is regulated through multiple genes and growth factors. MT-MMP1, O-Y4, OTS-8, gp38, PA2.25, E11 [11], more recently FGF-2 has been shown to upregulate E11 and drive osteoblasts into osteocytogenesis [159].

The cells incorporated within the bioink are osteoblasts. Ideally, they will continually develop within the construct and secret *de novo* bone tissue, further adding to the components incorporated. There is scope to co-culture osteoclasts to remodel and create a homeostatic environment at a later stage [160,161]. For consistency when developing the model, a commercially available and ubiquitously used bone cell line MC3T3-E1 subclone 4 was used. Firsts described by Sudo *et al* in 1983, MC3T3-E1 are osteoblast progenitors harvested from newborn mouse calvaria and have been shown to have ideal characteristics for bone tissue culture, being able to differentiate into both osteoblasts and later osteocytes. Through depositing collagen fibrils and hydroxyapatite crystals they were able to form calcified bone tissue *in vitro* [162]. These qualities are highly desirable traits in bone tissue engineering and since their discovery over 7000 articles have been published citing them.

While MC3T3s have been an invaluable resource in bone research, they are not the only cell line available. Osteoblast cell line IDG-SW3 has been shown to undergo osteoblast to osteocyte transition and produce ECM. Due to this being an immortalised cell line and requiring different culture temperatures, it was excluded due to the temperature sensitivity of the bioink shown in chapter 4 [163]. MLO-A5 is another potential candidate cell line as it can deposit bone ECM without β-glycerophosphate (β-GP) and ascorbic acid. Made from a transgenic mouse, it is in multiple stages of osteoblast/ preosteocyte differentiation [164], therefore may not provide the reproducibility desired for a tissue model. Widely cited cell lines such as osteocyte cell line MLO-Y4 and osteosarcoma derived Saos-2 cells were omitted due to the developmental nature of the project focusing on osteoblast integration and their inconsistency in long term culture [165,166].

5.1.2 Genes of interest

In this chapter, nine transcription factors of interest are used to investigate the osteogenic potential of the investigated conditions. They are separated into three phases of osteoblast differentiation with MSX2, RUNX2 and SP7, indicating early stages of osteoblast differentiation. COL1A1, ALPL and SPP1 are all matrix associated genes and are involved with cell attachment. PDPN, BGLAP and SPARC are late-stage osteoblast and early osteocyte genes. This separation may not be specifically accurate with many of the genes linked in feedback mechanisms and regulation of each other.

Msh Homeobox 2 is a gene encoded by MSX2 which is a pivotal transcription factor of bone [167]. It has a wide range of interactions, in the scope of bone and osteogenesis its linked to bone morphogenic proteins (BMP) which strongly control and promote bone formation where MSX2 is indication of BMP2 activity. MSX2 activity is strongly linked to osterix activity and primarily its role in bone formation is that of a regulator [168]. When it is dysfunctional it leads to insufficient proliferation of bone progenitors and defects in the subsequently formed bone, in both human and murine development [169, 170].

Runt-related transcription factor 2 (RUNX2) is a transcription factor that is a key marker of osteogenesis as it upregulates matrix forming genes, alkaline phosphatase, collagen type 1 and osteopontin [171]. RUNX2 is stimulated by BMPs and MSX2 and its inhibition restricts osteoprogenitors from differentiating into osteoblasts [172,173].

The function and regulation of transcription factor SP7 (also called osterix), is closely linked with RUNX2. It is a transcription factor highly associated with osteoblasts differentiation from preosteoblasts and from osteoblast to osteocytes. Embryos deficient of osterix typically fail to form any bone [174].

Collagen type 1 is the most profuse protein in the body and a major component of bone tissue. It is made up of three intertwined chains, two of which are pro-α1(I), encoded by COL1A1 [175]. With up to 90% of the organic matrix of bone comprised of collagen its presence is key when developing new bone tissue [176]. Its dysfunction can lead to diseases such as osteogenesis imperfecta [177] and dysregulation to osteoarthritis [178].

Mineralisation is a hallmark of bone tissue, one of the key proteins involved with matrix mineralisation and hydroxyapatite deposition is alkaline phosphatase (ALP), which is encoded by the gene ALPL. The mechanisms controlling ALPL expression are complex, but the upstream BMP/RUNX2/osterix network signalling cascade that control osteoblast differentiation are linked to ALPL expression [179].

Osteopontin (SPP1) is a matricellular protein associated with integrin binding and involved in the cellular and protein homeostasis of the ECM [180]. Osteopontin can be expressed by most bone cell types and progenitors, within its structure it contains the RGD motif enabling cell adhesion. When knocked down, it can block the stimulation of alkaline phosphatase and osteocalcin, reducing mineralization [181].

Podoplanin (E11) is a protein expressed by the PDPN gene, it has many functions all over the body. Expression of podoplanin is typically low in osteoblast culture, but expression increases over time and in relationship to supplementation of osteogenic media. Therefore, it is used as a marker of differentiation. Osteocyte-like cell lines typically have higher expression and its inhibition has been shown to reduce osteocytogenesis [182,65]. Podoplanin is also shown to increase in expression when under mechanotransduction which may be useful as a biomarker when engineering 3D bone tissue environments [183].

Osteocalcin is an osteoblast-specific protein encoded by BGLAP that modulates endocrine sugar homeostasis [184,185]. In the role of bone its often used as a biomarker for bone formation, with new research suggesting that overall bone metabolism is an indicator of homeostatic demands. Levels of insulin, leptin and adiponectin are all linked to osteocalcin expression, which is stimulated *via* an increase in bone metabolism [186].

Osteonectin, encoded by the SPARC gene, is a calcium-binding matricellular protein whose expression typically mirrors that of COL1A1 [187]. Osteonectin can bind to both collagen and hydroxyapatite, which suggests it has a key role in the production of functional bone tissue [188].

Two housekeeping genes were analysed for all experimental reverse transcriptase quantitative polymerise chain reaction (RT-qPCR) conditions in case of any shift. The purpose of a housekeeping gene is to be a reference gene that has stable and consistent expression irrespective of the external stimulus on the cells and can be used to benchmark relative increases and decreases in expression markers.

18s is a ribosomal subunit protein that is highly conserved throughout the cell cycle and with external stimulus, making it an excellent normalisation housekeeping gene [189,190].

β2 microglobulin (B2M) is part of the MHC class 1 complex and it is present on all nucleated cells [191]. It is often used as a housekeeping normalisation gene due to its ubiquity, though it should be used more selectively than 18s due to its variation partially in tumorigenic cell lines [192,193].

5.1.3 Aims and Hypothesis

The aims of this chapter are to investigate the optimal culturing conditions of MC3T3-E1 osteoblasts within the developed novel CLEX based bioink, as described in chapter 4. To achieve this the following were accessed.

1. Investigate mineralisation capability of MC3T3-E1 osteoblasts under 2D conditions, in three different osteogenic media formulations, using alizarin red staining.
2. Characterise the transcriptional expression of osteoblast markers in MC3T3-E1 osteoblasts under 2D conditions at timepoints between 7 and 28 days with three different osteogenic media formulations.
3. Characterise the transcriptional expression of osteoblast markers in MC3T3-E1 osteoblasts under 3D culture conditions at timepoints between 7 and 28 days. Using the optimal media formulations as determined from 2D investigation.

The hypothesis is that the addition of dexamethasone will have an effect on the mineralisation capacity of the cells and that the 3D encapsulation will have an influence on the expression profiles of the cells.

5.2 Results

5.2.1 Optimising differentiation media for ink

To optimise the osteogenic media formulation used for continuous culture after bioprinting, three formulations that are heavily cited in the literature were chosen. All three had 284 µM of L-ascorbic acid, with only the phosphate levels changing. The 3 compositions were 10 mM β-glycerophosphate (shown as 10 mM in subsequent figures), 2 mM β-glycerophosphate (shown as 2 mM) and 100 nM dexamethasone with 10 mM β-glycerophosphate (shown as Dex 10 mM).

Initially, to test the optimal media for mineral deposition, MC3T3-E4 cells were cultured in 2D with each media for 28 days, media changes were performed as previously stated every 3-4 days as per section 2.1.10 page 16. At 7-day time points, the secreted mineralisation was visualised with alizarin red to qualitatively demonstrate mineralisation. The deeper the red colour the more alizarin red bound and therefore within the well the more mineral present. The earlier the mineral is present, and its abundance, was used to determine which media triggered the greatest mineralisation from the cells.

The alizarin red staining in Figure 5.2.1 indicates that the addition of dexamethasone to the media inhibits the early production of mineralisation by the cells. Sporadic mineralisation pockets can be seen at day 28 in the dexamethasone treated cells, whereas cells exposed to the same osteogenic media except without dexamethasone had prolific mineralisation by this timepoint. Conversely, when the β-glycerophosphate concentration is lowered, mineralisation occurs earlier and can be seen at day 14 in 2 mM treated cells. Whilst 2 mM treated cells show earlier mineralisation, by days 21 and 28, both concentrations of β-glycerophosphate have induced similar deposition of mineral.

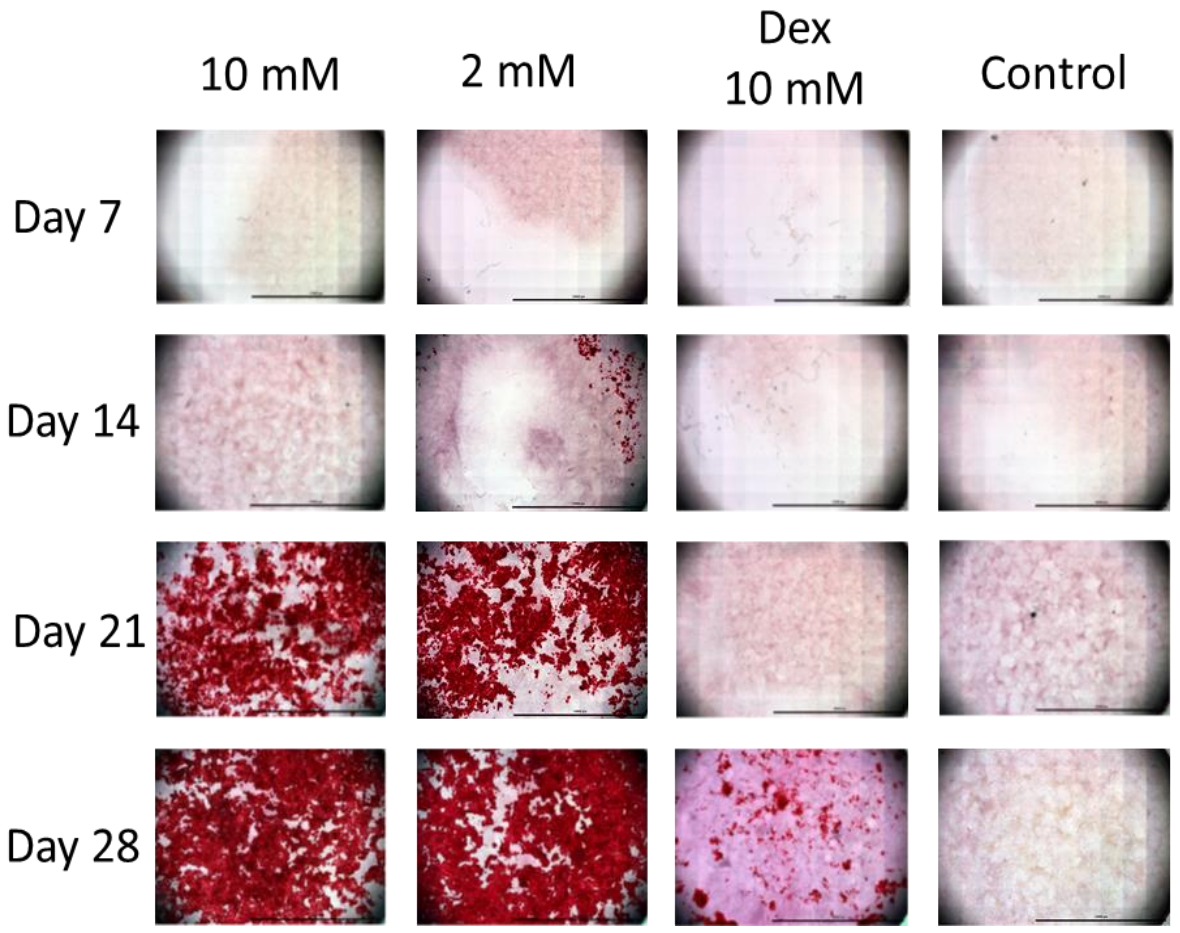

Figure 5.2.1 A panel view of cell mineralisation at 7-day intervals over 28 days. Three osteogenic media formulations and proliferation control media were used. All three osteogenic media formulations contained 284 µM of L-ascorbic acid, with only the phosphate levels changing: The 3 compositions were 10 mM β-glycerophosphate (10 mM), 2 mM β-glycerophosphate (2 mM) and 100 nM dexamethasone with 10 mM β-glycerophosphate (Dex 10 mM). Control media contained no L-ascorbic acid, β-glycerophosphate or dexamethasone.

Alizarin red staining for calcium deposits produced by cells in culture. Increased red staining indicates greater the deposition of calcium and therefore mineralisation of the extracellular matrix. Scale bars = 1cm.

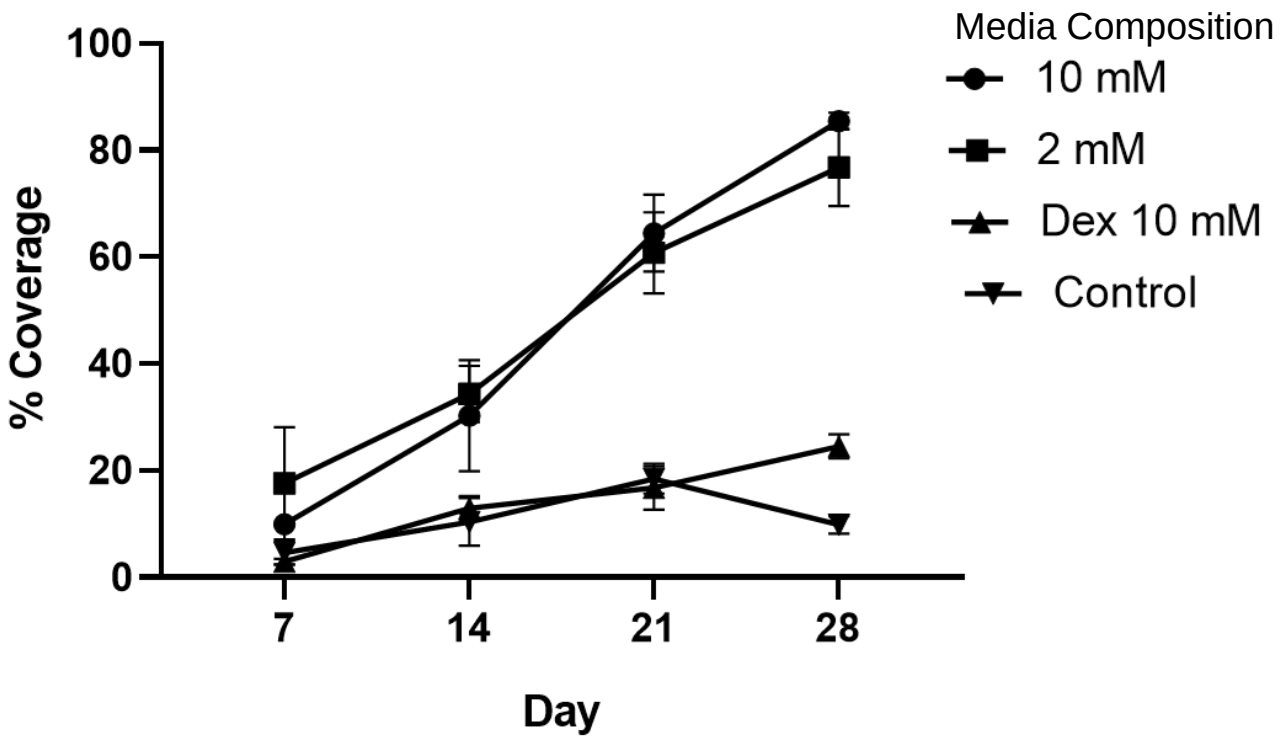

Control vs	D7	D14	D21	D28
10 mM	ns	***	****	****
2 mM	*	****	****	****
Dex 10 mM	ns	ns	ns	**

Figure 5.2.2 Image J analysis of the alizarin red coverage with each media formulation.

The alizarin red percentage coverage of the well plates was analysed on image J by colour thresholding, to determine the % coverage of the plates, as shown in the graph. To determine significance all conditions were compared to control by two-way ANNOVA with Dunnett's multiple comparison test. n=3 Levels of significance (p-value) are shown in the embedded table: ns = non-significant; * = 0.05; ** = 0.01; *** = 0.001; **** = 0.0001.

The percentage coverage of each well with alizarin red was measured and analysed using image J. As seen in Figure 5.2.2, at day 7 all conditions had minimal coverage with 2 mM having a slightly greater coverage than the other conditions and was significantly different from control. At days 14, 21 and 28, cells exposed to 10 and 2 mM β-glycerophosphate continued to demonstrate increased coverage of the well plate, while the coverage on the control and dexamethasone-treated cultures were far less. Dexamethasone was significantly different from control.

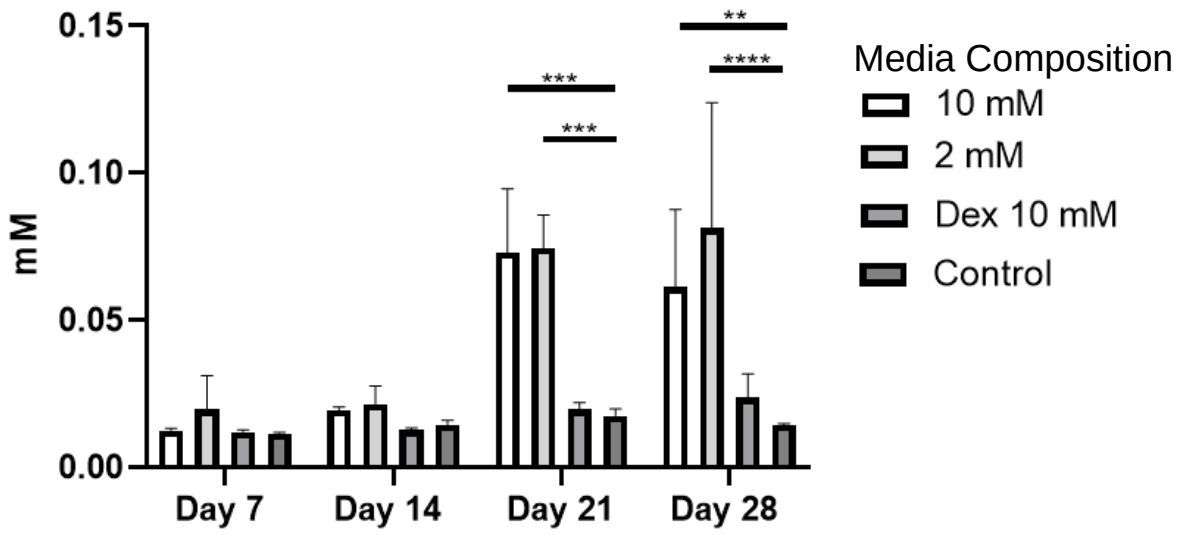

Figure 5.2.3 Alizarin red extractions from the well plates of the cells treated with the 3 media formulations and control.

Alizarin red was extracted from the culture plates and measured on a plate reader at 405 nm and compared to a known standard for a quantifiable output of mineralisation. Two-way ANNOVA with Bonferroni's multiple comparisons test was performed for all treatments at each timepoint, compared to control. n=3 Where no stats are shown there is no significant difference; $p < 0.05$ *; $p < 0.005$ **; $p < 0.0005$ ***; $p < 0.0001$ ****

The alizarin red mineralisation was quantified through acid extraction and measured on a plate reader. The trends seen in Figure 5.2.3 reflect the trends seen in Figures 5.2.1 and 5.2.2: Minimal mineralisation detected at day 7 and 14. At day 21, 2 and 10 mM had a significant rise in concentration of over 4 times compared to control. This was maintained at 28 days for 10 mM and 2 mM, rising to over 5 times the concentration of control. At all timepoints, dexamethasone treatment in combination with 10 nM β-glycerophosphate inhibited mineralisation, with no significant increase when compared to control.

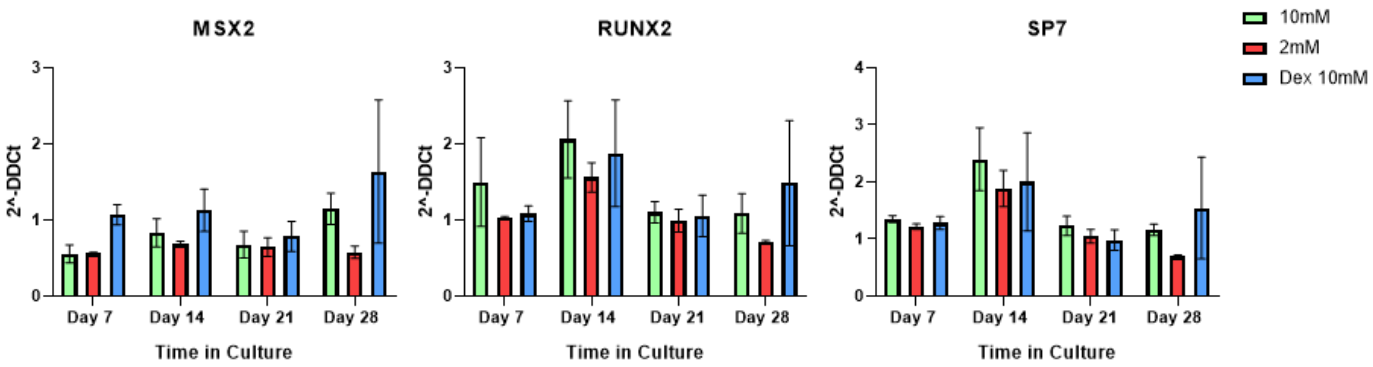

Figure 5.2.4 Real-time RT-PCR analysis of the expression of pre-osteoblast genes, normalised to housekeeping gene and expressed as relative fold change in gene expression ($2^{\wedge -DDCt}$). The 3 compositions were 10 mM β-glycerophosphate (10 mM), 2 mM β-glycerophosphate (2 mM) and 100 nM dexamethasone with 10 mM β-glycerophosphate (Dex 10 mM). Control media contained no L-ascorbic acid, β-glycerophosphate or dexamethasone.

Cells were exposed to 3 different osteogenic media formulations. All conditions are normalised to 18S and relative fold change to proliferation media. Genes of interest are presented order of early to late osteoblast differentiation. N=2, Mean +/- range.

Figure 5.2.4 demonstrates the gene expression of 3 early osteoblast markers. While expression levels fluctuated throughout the time course the only statistical difference seen was at day 28 between 2 mM and Dex treated cells for the gene MSX2.

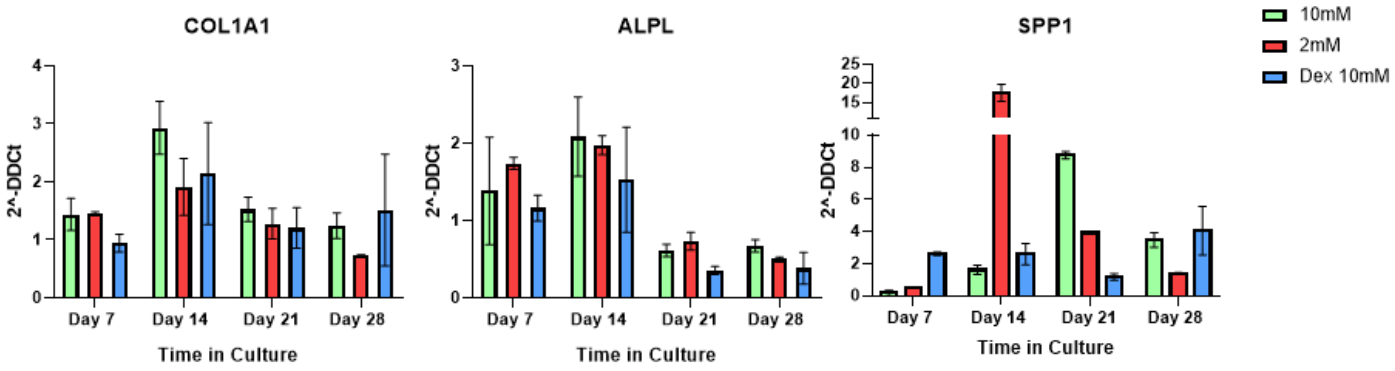

Figure 5.2.5 Real-time RT-PCR analysis of the expression osteoblast genes normalised to housekeeping gene and expressed as relative fold change in gene expression ($2^{\wedge -DDCt}$).

Cells exposed to 3 different osteogenic media formulations. All conditions are normalised to 18S and relative fold change to proliferation media. Genes of interest are presented order of early to late osteoblast differentiation. N=2, Mean +/- range.

Figure 5.2.5 shows the expression levels of some key matrix and ECM production genes used as indicators of osteoblast differentiation. For Col1A1, there is a spike around day 14 with 10 mM having the highest expression and by day 28, 2 mM was waning far below the other two conditions. A similar spike at day 14 is seen with ALPL whereby all three conditions spike at day 14 with 10 mM rising the most. After day 14 all conditions drop to a consistent level. SPP1 maintained the trend of peaking at day 14 for 2 mM which greatly rose and was statistically significant from both the 10 mM and the Dex treated cells. Cells treated with 10 mM took 21 days to spike in SPP1 expression, this rise is significantly different from 2 mM and Dex treated cells, there is no significant difference between 2 mM and Dex. The highest value for Dex treated cells was at day 28 but this was still well below the spikes seen by 2 and 10 mM at earlier days and there was no significant difference between the conditions at day 28. The timings of the spikes in SPP1 expression correlated with the early mineral production seen in 5.2.1 for 2 mM and 10 mM and with the lack of mineral produced in Dex treated cells.

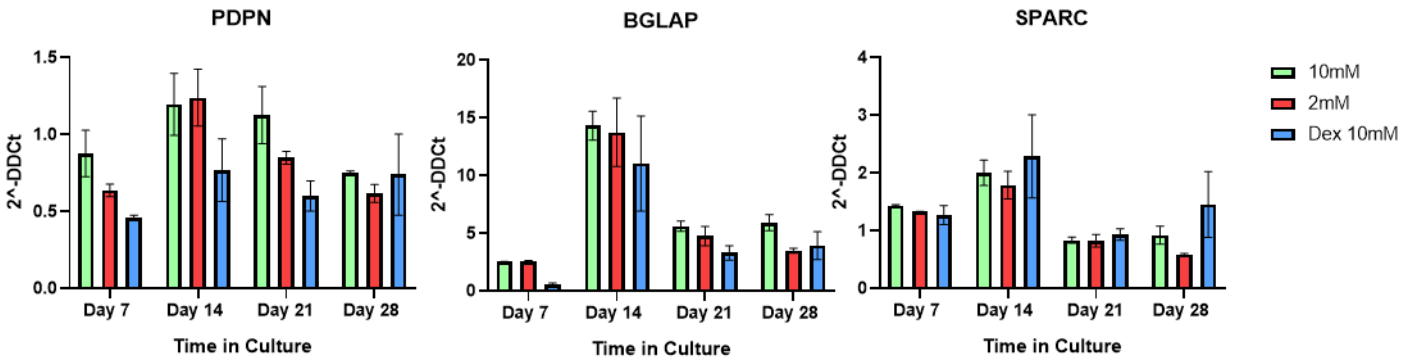

Figure 5.2.6 Real-time RT-PCR analysis of the expression of late osteoblast genes, normalised to housekeeping gene and expressed as relative fold change in gene expression ($2^{\wedge -DDCt}$).

Cells exposed to 3 different osteogenic media formulations. All conditions are normalised to 18S and relative fold change to proliferation media. Genes of interest are presented order of early to late osteoblast differentiation. N= 2, Mean +/- range. Where no stats are visible there is no significant difference.

Figure 5.2.6 shows the expression of late osteoblast genes, as with 5.2.5 and 5.2.4 there is a prominent spike in expression at day 14. This is rise in expression is seen in all in media conditions and is particularly prevalent in BGLAP which expression has a minimum of a 5-fold increase for media conditions. While still expressing a peak at day 14, the relative expression is consistent at all days for PDPN and SPARC with a small rise at day 28 for Dex.

5.2.2 Cell differentiation within constructs

Using the optimal osteogenic media formulations, cell differentiation within bioinks was tested. Initially, bioinks made with αMEM proliferation media were printed. This was to test the osteoconductive potential of the bioink alone.

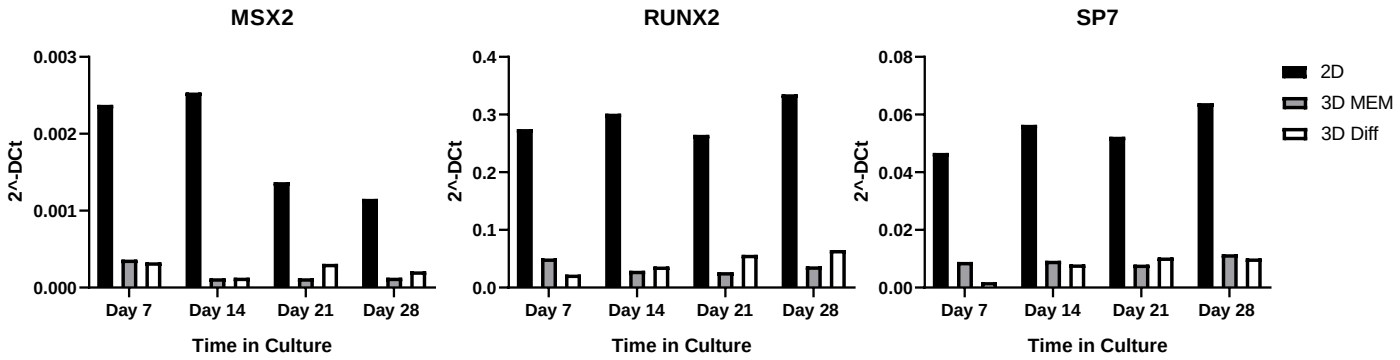

Figure 5.2.7 Real-time RT-PCR analysis of the expression pre osteoblast genes expressed as relative gene expression compared to B2M housekeeper ($2^{\wedge -DCt}$). The three formulations are cell cultured conventionally on 2D tissue culture plastic with αMEM, cells cultured in 3D printed bioink with αMEM and cells cultured in 3D printed bioink with αMEM differentiation media supplemented with 2 mM β-glycerophosphate and 284 µM of L-ascorbic acid. n=1

Relative gene expression of cells cultured with in 2D with αMEM proliferation media, 3D printed bioink construct cultured with αMEM and 3D printed bioink construct cultured with differentiation media over 28 days of culture. All conditions are normalised to B2M within their respective condition. N=1

3D printed bioink constructs were cultured in either αMEM or osteogenic differentiation media, the relative gene expression of early osteoblast genes can be seen in Figure 5.2.7. With all conditions, 2D had the greatest relative gene expression compared B2M housekeepers. MSX2 showed a time dependant decline in expression for 2D with both 3D conditions showing no clear trends in this n=1 experiment.

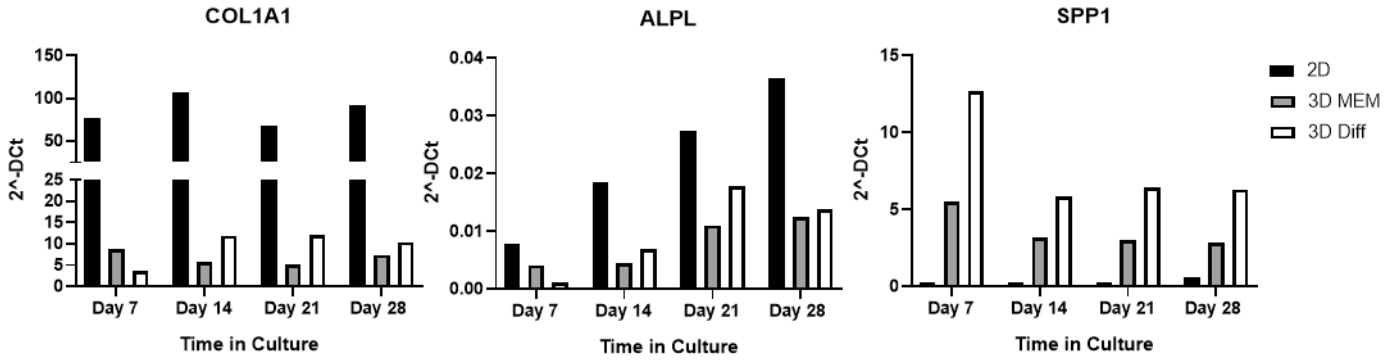

Figure 5.2.8 Real-time RT-PCR analysis of the expression osteoblast genes expressed as relative gene expression compared to B2M housekeeper ($2^{\wedge -DCt}$).

Relative gene expression of cells cultured with in 2D with αMEM proliferation media, 3D printed bioink construct cultured with αMEM and 3D printed bioink construct cultured with differentiation media over 28 days of culture. All conditions are normalised to B2M within their respective condition. N=1

Figure 5.2.8 shows the expression levels of some key matrix and ECM production genes used as indicators of osteoblast differentiation. COL1A1 is highly expressed in all conditions with the 2D cells having the greatest expression, approximately ten times that of the 3D cultured cells, and remains consistently high at all weeks. Early indications suggest that when 3D cultured in αMEM proliferation media, cells typically show lower expression than when 3D cultured in differentiation media. For ALPL, all conditions demonstrated a time dependant response to expression, which was especially evident in 2D cultured cells. The two 3D cultured also showed a trend towards increased expression of ALPL over time in culture. There is the suggestion from this n=1 experiment that expression in 3D culture trend plateaus after day 21, but further experiments are required to confirm this. Unlike all the other genes tested, SPP1 was more highly expressed in 3D cultures than 2D.

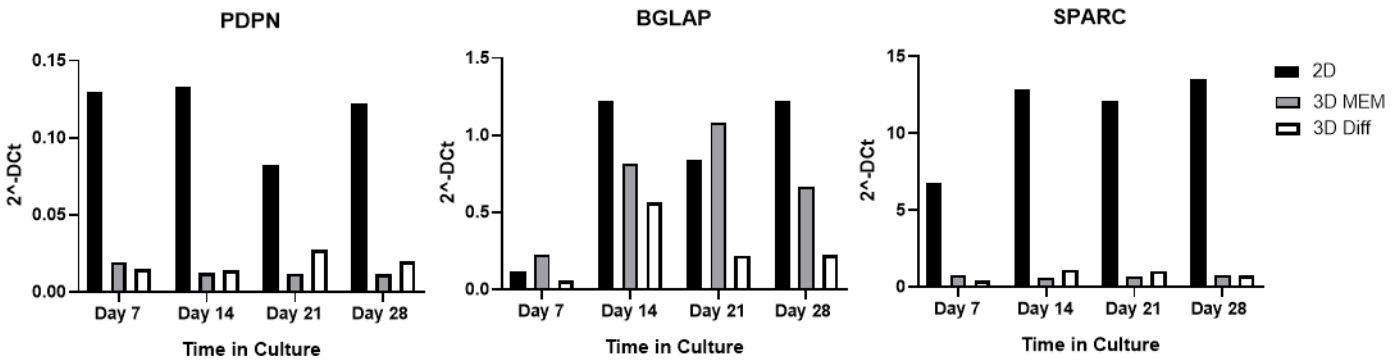

Figure 5.2.9 Real-time RT-PCR analysis of the expression of late osteoblast genes, expressed as relative gene expression compared to B2M housekeeper($2^{\wedge -DCt}$).

Relative gene expression of cells cultured in 2D with αMEM proliferation media, 3D printed bioink construct cultured with αMEM and 3D printed bioink construct cultured with differentiation media over 28 days of culture. All conditions are normalised to B2M within their respective condition. N = 1

Late-stage osteoblast genes for PDPN and SPARC are up-regulated in 2D cultured cells compared to 3D. BGLAP expression increases after 7 days in culture. Further experiments are required to identify whether the reduced expression seen in differentiation media at later timepoints is reproducible.

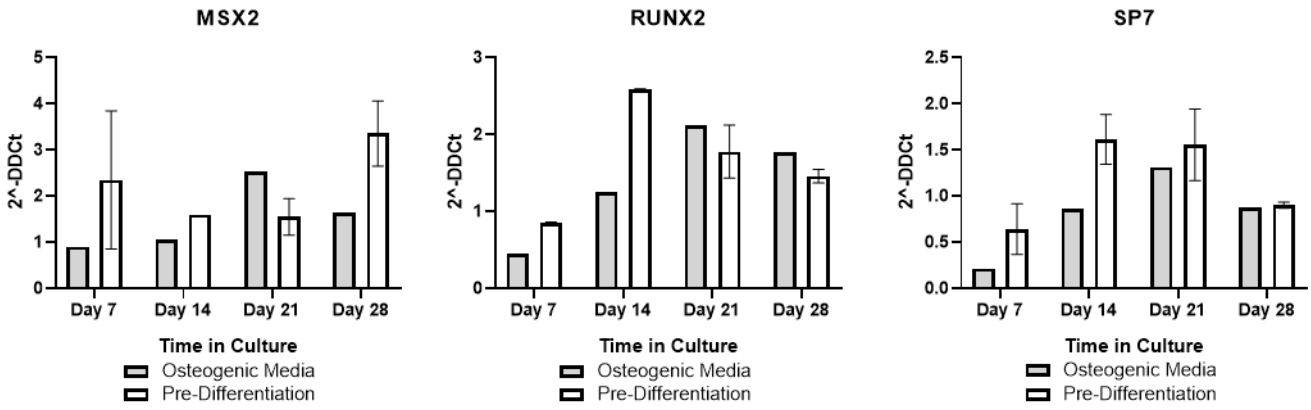

Figure 5.2.10 RT-qPCR analysis of the pre osteoblast gene expression, shown as relative fold change in gene expression of cells in 3D culture with 2 different osteogenic conditions compared to proliferation media($2^{\wedge -DDCt}$).

Relative fold change in gene expression of cells from constructs cultured with osteogenic media. Two conditions were used: Cells were either exposed to osteogenic media (2 mM β-glycerophosphate and 284 µM of L-ascorbic acid) for 7 days in 2D culture before incorporation into the bioink and printed and continually cultured for 28 days (Pre-Differentiation) or exposed to osteogenic media after printing and continually cultured for 28 days (Osteogenic Media). All conditions are normalised to B2M and relative fold change to cells from a printed construct cultured with αMEM proliferation. n=1 for osteogenic media and n=2 for pre-differentiation media. Mean +/- range.

To investigate the optimal 3D culture conditions to differentiate osteoblasts encapsulated within 3D printed constructs, cells were either cultured as per normal expansion techniques and then introduced to osteogenic media when encapsulated or expanded and pre-differentiated for 7 days in 2D culture before being removed and encapsulated. These two conditions were then normalised to cells expanded as per normal cell culture condition and then continually cultured in proliferation media when encapsulated to validate that differentiation could occur within the bioink.

The early differentiation markers RUNX2 and SP7 both show a spike in relative expression at days 14 to 21, but further experiments are required to identify whether this is seen consistently.

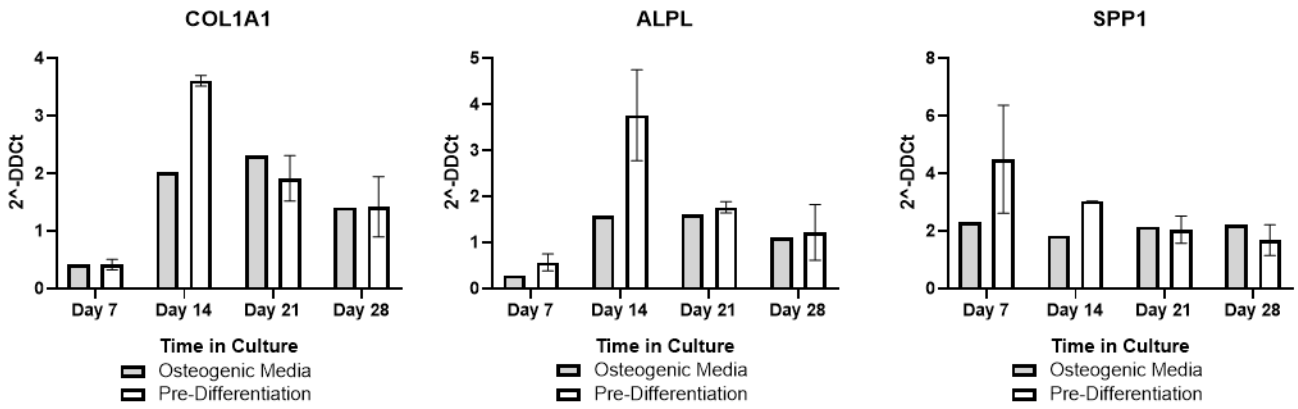

Figure 5.2.11 RT-qPCR analysis of the osteoblast gene expression, shown as relative fold change in gene expression of cells in 3D culture with 2 different osteogenic conditions compared to proliferation media ($2^{\wedge -DDCt}$).

Relative fold change in gene expression of cells from constructs cultured with osteogenic media. Two conditions were used: Cells were exposed to osteogenic media for 7 days in 2D culture before incorporation into the bioink and printed and continually cultured for 28 days (Pre-Differentiation) or exposed to osteogenic media after printing and continually cultured for 28 days (Osteogenic Media). All conditions are normalised to B2M and relative fold change to cells from a printed construct cultured with αMEM proliferation. n=1 for osteogenic media and n=2 for pre-differentiation media. Mean +/- range.

Figure 5.2.11 shows the genes commonly associated with osteoblasts. All the genes show a similar trend in their expression with the most notable outcome that pre-differentiation cells have a higher relative expression and the rise in expression are more pronounced. COL1A1 and ALPL demonstrated increases in expression at the days 14 and 21 in culture which is seen in previous figures. While SPP1 expression seems muted compared to previous conditions, the conditions here are relative to 5.2.8 where the 3D MEM condition has large spike in expression therefore there still is a notable fold change in expression. The rise in SPP1 is sustained consistently for the differentiation media treated whereas the pre-differentiated cells have a large spike at day 7 and less so but still present at day 14. Though more repeats are required to confirm this observation.

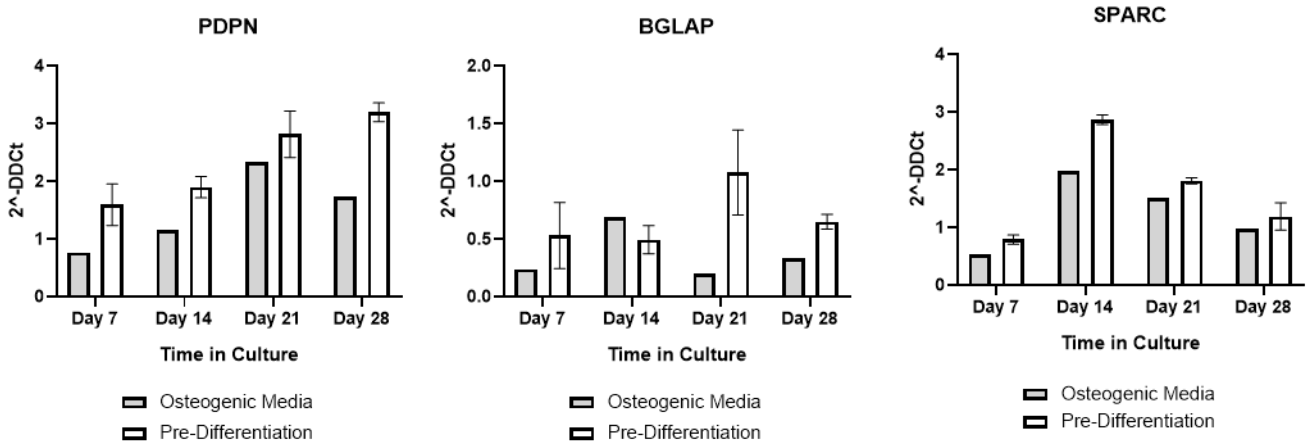

Figure 5.2.12 RT-qPCR analysis of late osteoblast gene expression, shown as relative fold change in gene expression of cells in 3D culture with 2 different osteogenic conditions compared to proliferation media ($2^{\wedge -DDCt}$).

Relative fold change in gene expression of cells from constructs cultured with osteogenic media. Two conditions were used: Cells were exposed to osteogenic media for 7 days in 2D culture before incorporation into the bioink and printed and continually cultured for 28 days (Pre-Differentiation) or exposed to osteogenic media after printing and continually cultured for 28 days (Osteogenic Media). All conditions are normalised to B2M and relative fold change to cells from a printed construct cultured with αMEM proliferation. n=1 for osteogenic media and n=2 for pre-differentiation media. Mean +/- range.

The pre differentiated cells show a clear positive trend for relative expression of PDPN from day 7 to 28, which appears less consistent in cells cultured in osteogenic media. Further experiments are required to confirm this. BGLAP expression is consistent between both conditions until day 21 where predifferentiated samples have an increase in expression while the osteogenic only cells have a drop in expression. The trends seen in SPARC expression are identical for both conditions.

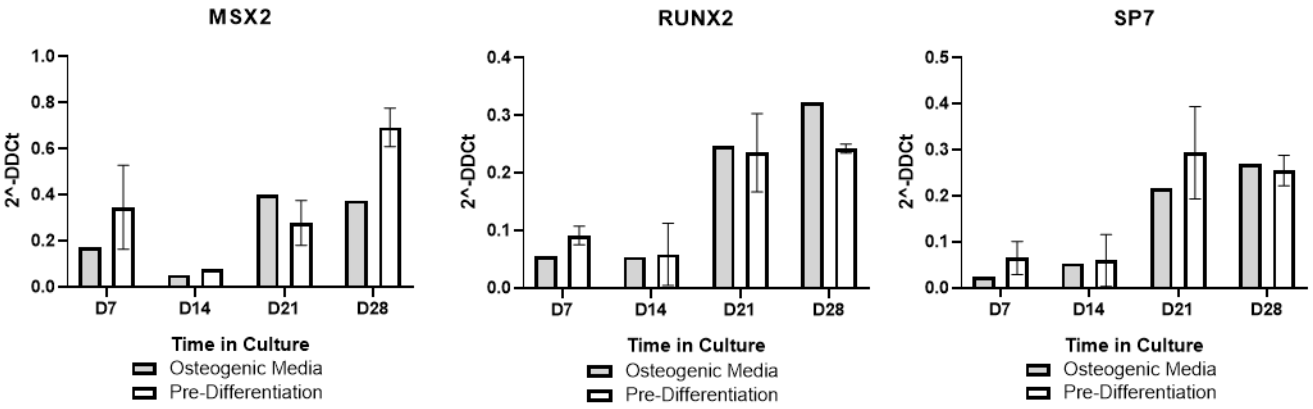

Figure 5.2.13 RT-qPCR analysis of the relative expression of early osteoblast genes expressed as relative fold change in gene expression of cells cultured with osteogenic in 3D compared to 2D ($2^{\wedge -DDCt}$).

Relative fold change in gene expression of cells from constructs cultured with osteogenic media. Two conditions were used: Cells were either exposed to osteogenic media (2 mM β-glycerophosphate and 284 µM of L-ascorbic acid) for 7 days in 2D culture before incorporation into the bioink and printed and continually cultured for 28 days (Pre-Differentiation),or exposed to osteogenic media after printing and continually cultured for 28 days (Osteogenic Media). All conditions are normalised to B2M and relative fold change to 2D cells cultured in osteogenic media. n=1 for osteogenic media and n=2 for pre-differentiation media. Mean +/- range.

Figures 5.2.10-12 show the relative expression of two 3D osteogenic conditions to a 3D non osteogenic condition. The subsequent Figures of 5.2.13-15 show the relative expression of the same 3D osteogenic conditions to a 2D osteogenic condition. The condition used is the 2mM β-glycerophosphate previously shown in Figures 5.2.1-6. For MSX2, RUNX2 and SP7, both conditions show a positive trend for time spent in culture.

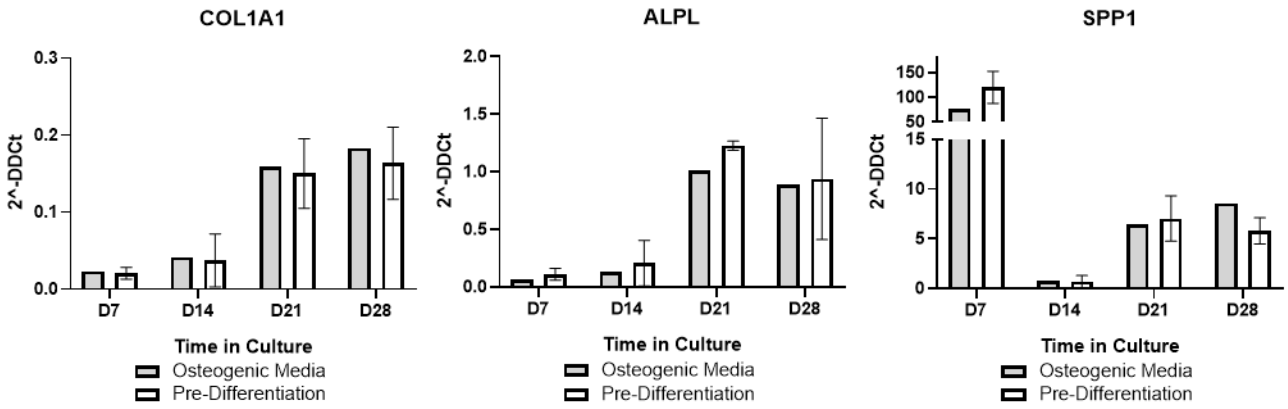

Figure 5.2.14 RT-qPCR analysis of the osteoblast gene expression, shown as relative fold change in gene expression of cells cultured with osteogenic in 3D compared to 2D.

Relative fold change in gene expression of cells from constructs cultured with osteogenic media. Two conditions were used: Cells were either exposed to osteogenic media for 7 days in 2D culture before incorporation into the bioink and printed and continually cultured for 28 days (Pre-Differentiation), or exposed to osteogenic media after printing and continually cultured for 28 days (Osteogenic Media). All conditions are normalised to B2M and relative fold change to cells from a printed construct cultured with 2D with osteogenic media. n=1 for osteogenic media and n=2 for pre-differentiation media. Mean +/- range.

In Figure 5.2.14 both COL1A1 and ALPL show clear positive trends with time spent in culture. As with previous conditions (Figures 5.2.5, 8 and 11), SPP1 had the highest expression, with a sharp rise in expression at day 7 in the osteogenic cultured and pre differentiated cells which spike at 77.0 and 153.0-fold change compared to 2D respectively (Figure 5.2.14). For the 2D conditions, the spike was at day 14 and day 21 but for the 3D conditions the increase in expression was at day 7. The apparent sharp drop seen in Figure 5.2.14 is due to that it is a relative expression compared to 5.2.5 where there is a spike in expression at day 14, mostly notably, the expression in the 3D cultured cells was relatively increased when compared to than the spike in expression for the 2D sample indicating that this is the preferred condition for the cells. This is even more evident when you factor in that the pre-exposed cells had double the relative expression compared the standardly exposed differentiated cells. Other than in SPP1 day 7, for all conditions in Figure 5.2.14, there was minimal difference between the 3D cultured osteogenic cells.

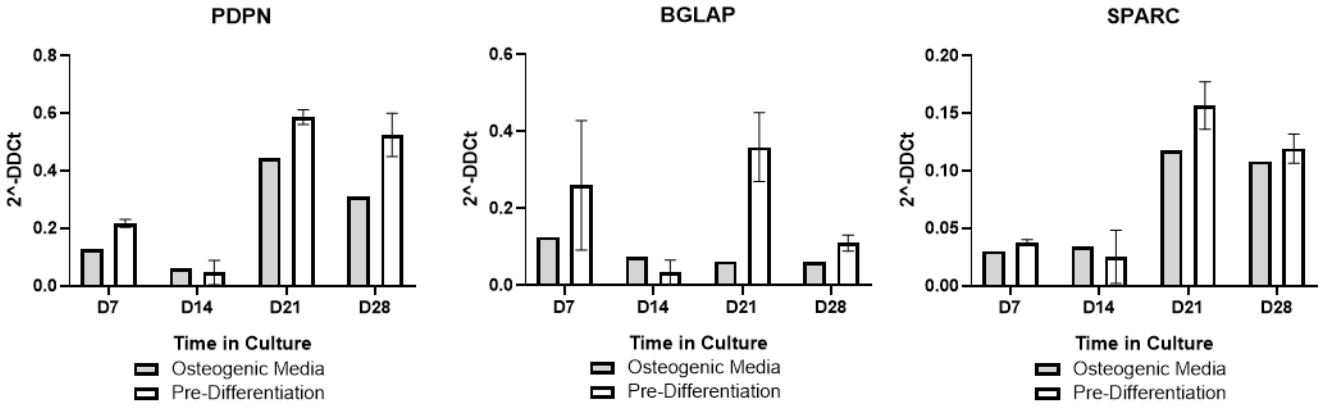

Figure 5.2.15 RT-qPCR analysis of late osteoblast genes expression, shown as relative fold change in gene expression of cells cultured with osteogenic in 3D compared to 2D.

Relative fold change in gene expression of cells from constructs cultured with osteogenic media. Two conditions were used: Cells were either exposed to osteogenic media for 7 days in 2D culture before incorporation into the bioink and printed and continually cultured for 28 days (Pre-Differentiation), or exposed to osteogenic media after printing and continually cultured for 28 days (Osteogenic Media). All conditions are normalised to B2M and relative fold change to cells from a printed construct cultured with 2D with osteogenic media. n=1 for osteogenic media and n=2 for pre-differentiation media. Mean +/- range.

The late-stage osteoblast genes PDPN and SPARC show clear positive trend for length in culture with both conditions having a rise in relative expression at the day 21 time point. BGLAP expression appears more variable and further experiments are required to identify the robustness of these data.

5.3 Discussion

One of the key aims of this chapter was to determine the optimal osteogenic formulation and conditions for the MC3T3's used to develop the bioprintable model of bone. Literature on this is variable and its translation through to our 3D culture system was unknown [91,194,195,196].

Osteogenic media formulations are widely published and typically contain three main components: A phosphate donator, in this case β-glycerophosphate; a collagen formation supplement, in this case L-ascorbic acid; and a glucocorticoid such as dexamethasone. The concentration of these components varies throughout the literature and this appears to be specific to the species from which the cells are sourced.

Dexamethasone is omitted entirely from many studies, particularly those using mouse-sourced cells, yet it is used in some studies using primary mouse osteoblasts [64,197]. Dexamethasone has been stated as required, especially from rat [198] and human cell sources [199].

The concentrations of the osteogenic supplements varies depending on the cell type and even the sub clone [163,200,201]**.** This conflicting information on osteogenic media is seen throughout the literature and shows no clear consensus, therefore the optimal media for the cell type used in this model was investigated. The cells used here (MC3T3-E1) are a widely used cell line, that are maintained in a pre-osteoblastic phenotype for expansion purposes and the addition of the osteogenic supplements promotes their differentiation into osteoblasts. When differentiated, the cells are able to express and produce bone matrix and deposit extracellular matrix (ECM) which can be characterized through gene expression and with alizarin red, which stains the mineral components of the excreted ECM (Figure 5.2.1) [91,194].

MC3T3-E1 cells have been shown to be inconsistent in culture with variable gene expression and mineralisation, highly dependent on subclone [64]. The subclone used in the model is subclone 4 which is regarded as the most suitable for mineralisation and bone formation investigations [202, 203,204,205]. Given that a requirement of this work is to have a cell line that could mineralise in a 3D environment, the evidence of ample, mineralised ECM production in 2D (Figure 5.2.1) appears to validate the choice of cell line and subclone.

Three different media formulation were investigated for cells cultured in 2D. The concentration of L-ascorbic acid varied little throughout the literature. It is required for mineralisation to occur, specifically the L-enantiomer of ascorbic acid, also know and Vitamin C [194]. The role of L-ascorbic acid is well characterized and acts as a precursor for collagen production, a major component of bone

ECM [176]. For all conditions, MC3T3-E1 cells were plated onto 12 well plates and proliferated using basal proliferation media for three days. When the cells were confluent, the media was changed out for osteogenic of the chosen formulation and the control was basal proliferation media.

The most cited formulation was 10 mM β-glycerophosphate + (284 μM) L-ascorbic acid. This formulation is used widely for human, rat and mouse cells (both primary and commercial cell lines) [154,198,206,207].

The RNA extraction protocol used here was based on the whole cell extraction methods developed in chapter 3. Though this meant that the cells were exposed to a sodium citrate chelator, they were released viable and intact, still attached to elements of the collagen and mineral added. The exposure to the chelator would have minimal effects on the expression profiles as the RNA was immediately extracted from the released cells. Though not a specific aim of this project, it is a useful tool when developing the model further to readily and easily release whole intact cells so that further work can be done to characterise them.

5.3.1 Limitations of mineralization work

The predominate limitation of this work is the lack of replicates with the qPCR work only having an n=2. Though some trends were seen, and these were great enough to show a difference with a statical test as with MSX2 and SPP1. The fact remains that without more replicates this cannot be stated as significant, and the data should be considered pilot work until more data confirms trends seen.

Another major limitation of this work is the lack of ECM analysis. Although mineralisation is imaged and measured (Figures 5.2.1,2 and 3) the composition of the expressed mineral was not investigated nor were the specific ECM components defined. Broadbrush techniques such as the Bradford assay could be used to measure total protein expression, while more specific assays such as sirius red staining highlight the presence of collagen. Specific characterisation of the excreted ECM components could achieve using antibody staining but these techniques, while providing a greater picture of cellular mechanics are unnecessary for a cell type as widely characterized as MC3T3s. Some physical characterisation techniques were attempted, such as XRF to determine difference between the mineral expressed with the different glycerophosphate concentrations, but this showed no difference between the samples and each sample exhibited significant background noise, therefore were omitted. Though the RT-qPCR analysis shows some interesting trends with some indicating significance, this work is fundamentally limited by the lack of replicates and more technical repeats are required to add robustness to the trends and significance of the data.

5.3.2 3D constructs

To compare the expression profiles of 3D bioink cultured cells in proliferation media or 2 mM β-glycerophosphate differentiation media for 28 days, the relative expression of the two conditions and 2D proliferation media was plotted. This was to see whether the 3D encapsulation within the bioink had an effect on the cell expression markers and whether the differentiation media would enhance this (Figure 5.2.7-9). The 2D cells had the highest expression for all most of the genes of interest throughout the time points. This changed dramatically for the intermediate expression markers which are all involved in ECM production. COL1A1, which encodes collagen type 1 is highly expressed in all conditions, while 2D cultured cells have the highest expression overall. The same applies for ALPL, Alkaline phosphatase ligand, a key protein involved with mineralization and typically used as a hallmark of ossification [208]. SPP1 conversely to all other genes was highly expressed in both of the 3D conditions and the with the MC3T3 used in this investigation is the gene most indicative of osteoblast differentiation and matrix production.

To compare the differences in differentiation potential with 3D encapsulation, two different differentiation conditions were tested. 3D printed cell-laden constructs that were either cultured in osteogenic media as previously optimised in Figures 5.2.1-5 or predifferentiated in osteogenic media for 7 days before encapsulation. The hypothesis was that the predifferentiation would speed up the differentiation in 3D culture. While Figures 5.2.1-5 show that peak mineral expression occurs at 21 days in culture, cell monolayer could not be consistently removed from 2D culture past 7 days. The cells required manual removal with a cell scraper, extended enzymatic dissociation and came away in clumps, making accurate counting almost impossible. Because of these limitations, the day 7 time point was chosen, in line with the literature which shows that 10 days in culture is enough time to form complete intact sheets of cells [91]. For further study, exploring the use of cell aggregates and masses into the bioink could provide better insight into cell attachment and integration within the bioinks.

For the 3D differentiation conditions, initially there appears to be very little difference between the pre differentiated cells and the standard osteogenic media cultured cells. With all early-stage osteoblast genes following the same trend of a slight rise in expression for 21 and 28 days in culture. It's worth noting that these are relative expression compared to 2D osteogenic media cultured cells that have been shown to express and deposit ECM. While minor, the trend does suggest that the 3D encapsulation increased the osteogenesis of the cells but there is not enough data to distinguish a difference between the samples (Figure 5.2.13).

The large relative increase in expression seen with the predifferentiated and osteogenic media cultured 3D constructs compared to that seen in 2D suggests that osteoblasts, especially MC3T3s are a suitable cell type for 3D culture systems (Figure 5.2.14). With SPP1/ osteopontin function involved with ECM structure it's upregulation in expression suggests an increase in ECM production, this does correlate to how the cells respond in 2D (Figure 5.2.1) [209]. This is further concluded by the rise in SPP1 expression when cultured in 3D without osteogenic media (Figure 5.2.8).

5.3.4 3D culture limitations

The serious limitations on the conclusions drawn for the 3D conditions are the same in the 2D conditions; a lack of ECM analysis and a lack of replicates to statistically validate the trends seen. Some alizarin staining was attempted on 3D constructs, but the washes and fixing steps required for the protocol dissociated the alginate and the constructs lacked the structural integrity to be analysed. Microcomputed tomography (µCT) was attempted on the samples as this is a less destructive technique. Though the constructs survived the technique, there was insufficient signal to distinguish between ECM and noise, therefore the output was inconclusive and omitted. Immunofluorescence was used to determine *de novo* collagen deposition, the collagen within the construct is rat tail and the cells are murine. Unfortunately, the antibody was not specific enough to determine the difference between the two collagens and the data was inconclusive with all collagens labelled. With refinement it may be able to provide further insight to the optimal culture conditions for collagen production and ECM deposition in 3D.

While repeating the work with the MC3T3s would provide technical replicates to validate the methods and protocols developed, the best practice would be repeating the work with multiple biological replicates, either with primary mouse osteoblasts or primary human osteoblasts and in an ideal situation both. This would not only validate the protocol but that culturing cells in 3D with this bioink increases the osteogenic potential of those cells. Biological replicates from primary mouse osteoblasts cultured within the bioink constructs compared to *in vivo* osteoblasts would be the initial approach to validate the systems. An ideal tissue model would closely model the expression of cells in their native environment and only comparing the two would truly validate a tissue model.

6 Optimization of Collagen and Hydroxyapatite Incorporation and 3D Printing Conditions

6.1 Introduction

6.1.1 3D Printing

Additive manufacturing or more conventionally known as 3D printing is a technique to manufacture three dimensional objects via mechanically controlled layer upon layer deposition. There are a variety of different methods to achieve this, but they broadly work the same: a print head, precisely controlled in the x and y axes by electric motors deposits material or a binding agent, onto a print bed. A layer of material is printed, and then either the print bed or head moves in the Z axis to start a new layer, and the next layer is then printed. This process is repeated to build up the 3D object. The rate of the deposited material can be controlled through several mechanisms, two very easy to control parameters which determine the density of deposited material are movement rate and extrusion rate. Feed rate is a term that is used differently by different manufacturers, for some use it as a term for movement speed while others use it as the rate at which the total processes happen so if a movement speed is at 30 mm/s at 50% feed rate the actual movement speed will be 15 mm/s [210]. The RegenHU system uses feed rate as term for movement speed so that is the definition used in this chapter, a higher feed rate the print head or print bed move relative to each other, the higher the movement rate the less material deposited at each location. The other parameter is extrusion rate, this is the rate at which material is fed through the print head so as this rate increases more material is deposited. To ensure that the best possible resolution of printed constructs is achieved, these two parameters are typically modulated.

With the focus on bioprinting to recapitulate anatomical components either at full scale with a regenerative medicine focus or redesigned into a schematic layout for research purposes, then 3D files sourced from MRI, CAT and ultrasound can be used for accurate dimensions [211]. Alternatively, as with this project a bespoke model can be created with computer aided design (CAD) software allows for greater freedoms when creating constructs. Typically, CAD software such as Autodesk Fusion 360, Inventor or Solidworks are focused mostly on the creation of solid parts made out rigid materials such as metals and plastics and do not take in the considerations of soft materials particularly those used in tissue engineering and bioprinting [212],[213]. With greater research interest in bioprinting, bespoke bioprinting CAD software's are available which have greater focus on the layer control and interstitial dimensions. While conventional software can be attained for free in basic forms and is universal across most printing platforms, the bioprinting bespoke software is typically made by bioprinting companies specifically for their machines [214],[215].

After CAD designing the next step before bioprinting is slicing. The 3D model can be exported multiple file types with the most common being an STL file, this is a specialized file type that

converts designs generated with CAD into a series of topographical triangles ignoring the internal space. Slicing software breaks down the triangular mesh network into sliced sections horizontally to the build plate, the size of each section is determined in the slicing software and is dependent on the extruder size and printer capabilities.

The slicing software uses the information from the STL file to create a machine code called G-Code which is a series of X and Y coordinates which controls the 3D printer. G-code is a series of commands which tell the printer how to move, which print head to select, time intervals, temperature, feed rate, home commands and which defines the print area[216].

The 3D bioprinter used in this investigation was a RegenHU Discovery 3D, this bioprinter has the advantage of being contained within a Biosafety Class 2 safety cabinet which has been modified for 3D printing. Bespoke systems such as this often have the schematic layouts of tissue culture plates integrated within them which aids in the bioprinting process, which is a major sterility and cell culturing advantage over conventional slicing software. Bioprinters such as the RegenHU allow for greater flexibility when bioprinting compared to convention 3D printing. Many of them are capable of printing in multiple ways due to their modular designs and multi-printhead formats [214] which allows for great flexibility when designing a bioprinting 3D culture environment.

6.1.2 Bioink Properties

To create a 3D environment to grow cells in typically there are two options available, either create a scaffold in the desired shape and then seed cells onto this or 3D a bioink with cells seeded inside [117]. While the scaffold and see approach has its advantages particularly when using materials that in the curing or printing process are not compatible with viable cells such as titanium implants or plastics [217]. The approach developed in this thesis is a bioink printed with cells integrated within the construct. Therefore, this approach limited the types of 3D printing available.

Typically, when bioprinting at physiological conditions three main types of printing are use. The early bioprinters were modified conventional inject jet printers [218]. These use either a piezoelectric, thermal or electromagnetic forces to break up a stream of bioink into droplets that can be deposited. Though this method can lack precision and accuracy when building up large more complex structures.

A bioprinting technique that has higher resolution than inkjet but still uses droplets is Laser assisted 3D bioprinting (LAB). LAB printing uses a laser to selectively heat up a small surface of a ribbon that which has bioink suspended from it, where the laser hits a small volume is vaporized and knocks off a droplet of bioink [219]. While this technique has far higher resolution than inkjet and has been shown

to be viable with cells [220], due to the complexity of printing and the localized heating involved, this was excluded from this investigation. Both inkjet and LAB printing are limited to slow deposition rates.

The most prominent form of bioprinting is extrusion, this technique uses either pneumatic or mechanical force to dispense the bioink through a nozzle. This technique is highly versatile as it allows a range of variables to be easily modified to suit each formulation such as extrusion pressure and nozzle diameter, often which are commonly used needle gauges. Due to the continuous depositions facilitated with extrusion-based printing, incorporation of larger polymers, high cell densities and non-uniform entities such as mineral formations can be incorporated into the bioinks, a function that is highly desirable in the bioink used in this project.

6.1.3 Collagen and Hydroxyapatite

Collagen is a key component of the ECM which acts as an anchor point for cells and provides much of the tensile strength of tissues and as much as 30% of bone is collagenous proteins [136]. There are currently 28 known types of collagen and the type predominantly found in bone is type 1. Type 1 collagen can self-form fibrils into the triple helix and the fibrils are approximately 300 nm long and 1.5 nm wide [137]. The structure of collage type 1 consists of two α1 chains and one α2 chain which when self-assembled form tropocollagen a left-handed triple helix. These tropocollagens cross link with their terminal telopeptide and build up into the collagen fibrils. The terminal telopeptides can be cleaved using acid it conditions allowing for the solubilisations and repolymerisation of collagen fibrils in solutions or bioinks [138],[49].

To create the interpenetrating network (IPN) of collagen for the tissue model, ideal fibrillogenesis needed to be determined with pH, temperature, salinity, and buffering all playing a key role in fibril formation [221]. These variables were all controlled for in chapter 4 where a well buffered, pH and temperature stable environment that was developed. The only extraction method which produces fibril collagen is acid extraction which can form gels at as low as 1 mg/mL which is the starting concentration used for the bioink [222].

Collagens at low concentration are weak and even at higher concentrations cannot form a strong structure until self-assembled which can be challenging to 3D print. Therefore collagen is typically co-printed with another stiffer polymer which provides the structural integrity such as alginate, hydroxyapatite, pluronic f 127, [27],[90],[111]. While this enables the composite formation of collagen incorporated into the constructs it can limit the free formation of the collagen around the secondary polymers. The approach taken in this project is to use the alginate as a templating reversable

scaffold and using the methods developed in chapter 3 reverse gelled leaving behind the fibrillar collagen structure.

A widely used bone mineral substitute that is stable at in physiological yet can be reabsorbed and remodeled by osteoclasts is β-tricalcium phosphate (β-$Ca_3(PO_4)_2$). Though being highly porous and osteoinductive it has shown to have inconsistencies in culture [223]. Other calcium phosphate forms such as brushite ($CaHPO_4 \cdot 2H_2O$) are used in bone defects as cements and have been used as mineral scaffold for osteoblast culture [224,225]. Hydroxyapatite ($Ca_{10}(PO_4)_6(OH)_2$) is the native calcium phosphate phase found in bone with a Ca/P ratio of 1.67. It is stable at physiological conditions and biocompatible without causing a immune response [226]. Hydroxyapatite compressive, shear and tensile behavior are biomimetic of bone than other calcium phosphate phases, which has attracted its uses as a cement for bone defects [227]. These properties along with the osteoinductivness of hydroxyapatite make it a strong candidate for bone tissue engineering [228].

Bioink for bone typically contain a calcium phosphate/ hydroxyapatite component. This reflects the native tissue environment of bone and provides an ion source for remodeling. The main approaches for this of using a cement or paste based system which has high viscosity and represents the rigidity of bone tissue. Due to the harsh nature of producing calcium phosphate when creating a 3D construct the calcium phosphate can be cast or printed into the desired shape and then seeded with cells after or the calcium phosphate is broken into small enough particles to be incorporated into a bioink, either cell laden or not [229, 230].

Hydroxyapatite micro tubes were incorporated into the bioink. These are a recently developed cell scaffold which facilitate the attachment of cells within the bioink. The tubes are grown chemobrionically and self-assemble forming a lumen of approximately 50 µm bringing them into the size ranges of a haversian canal [4,62]. The small size diameter of the tubes suggest they are compatible with bioprinting with most nozzle diameters between 20 G and 27 G, 603 µm to 210 µm, respectively. The incorporation of these biomimetic microtubes within a bioink for the development of bone has not been previously described to the authors' knowledge, therefore a key element of this investigation is to see whether the MC3T3s are able to attach to the tubes as an anchor point, if the tubes survive the printing process, and if this interferes with collagen fibril formation.

6.1.2 Aims and Hypotheses

The aims of this chapter are to show the developed bioink has the printable resolution required for bioprinting and that the integrated collagen and hydroxyapatite tubes are compatible with the printing process.

1. Optimise the extrusion conditions by modulating nozzle diameter, movement speed, and extrusion pressure to give the most consistent print resolution.
2. Show the optimal collagen incorporation conditions and test the concentration ranges of collagen compatible with the ink.
3. Ensure the biomimetic hydroxyapatite tubes remain intact after extrusion and integrate within the model and do not interfere with the collagen formation.

The hypothesis are that the nozzle diameter and movement speed will both have an impact on the size of the extruded filament. The formation of collagen fibrils is dependent on alginate concentration within the bioink. That the incorporation of the hydroxyapatite tubes will have no effect on collagen fibril formation within the optimal fibril forming formulation.

6.2 Results

6.2.1 Printing resolution

The approach of using the SSL chip and bead encapsulation is no longer usable as mentioned in chapter 3, a new construct shape for the 3D printed constructs for long term culture was needed. The shape used is a hollow cylinder which was created using RegenHU Biocad software, the external diameter was 14 mm with 3 inner shells and a lumen of 10 mm with the centre point of each extruded cylinder 1 mm away from the centre point of the other cylinders (Figure 6.2.1). The shape was chosen as tube are a difficult shape to 3D print so would test the suitability of the CLEX SLAM system and has large surface area for nutrient exchange for the cells within the construct The 3D printed cylinder had 18 layers stacked on top of each other; to ensure the stability of the structures post printing, the layers must interlock to form one continuous construct, therefore the extruded layer height needs to be known.

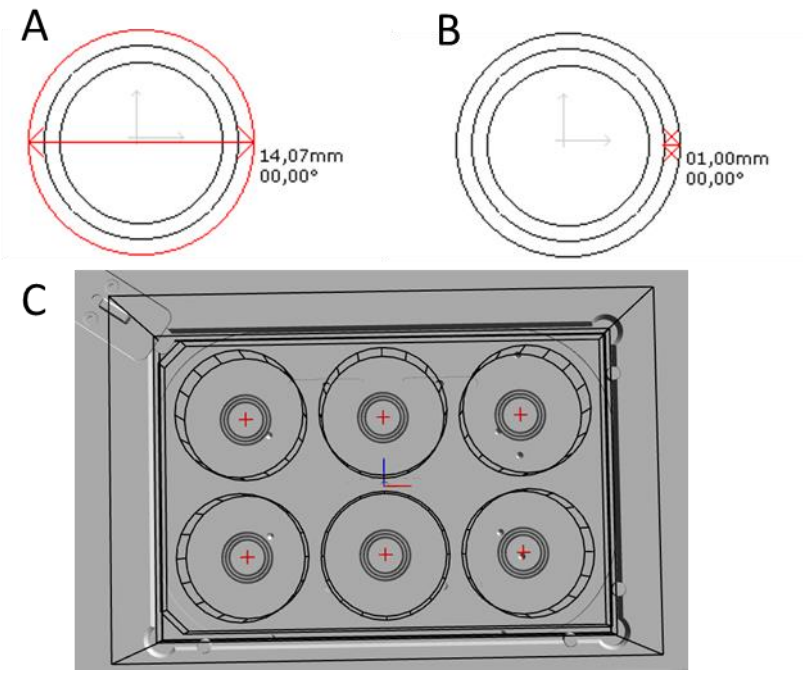

Figure 6.2.1 A schematic CAD layout of the printed cylinder design.

A.) Hollow cylinder designed in bespoke bioprinting CAD software.

B.) The dimensions are a diameter of 14.07 mm and made of three lines equally spaced 1 mm apart

C.) The hollow cylinder as printed in a 6 well plate with the center point of the plate dead center of the cylinder set within a 6 well plate.

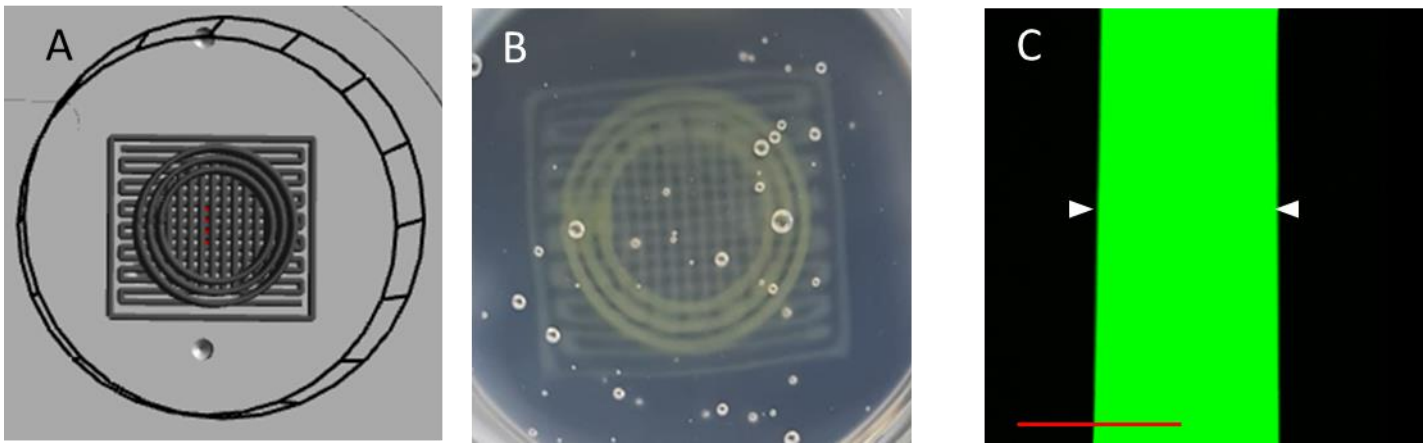

Figure 6.2.2 Bioink extrusion conditions calibration.

A. A schematic repeating back and forth layout used to calibrate continuous flow form the printer
B. Fluorescence loaded dye printed into SLAM
C. Confocal image of printed fluorescent green filament used to determine size, the white arrows are indicating the outside edges of a printed line of ink. Scale bar 1000 µm

To determine optimal printing resolution, fluorescent dye was loaded into alginate bio inks. Flow rates were preliminary optimised by printing 2 parallel lines and adjusting the extrusion pressure until a continuous unbroken filament was extruded. A crosshatch pattern was added below the printed construct for ease of imaging as the circular shape of the cylinders was difficult to accurately measure. The design in Figure 6.2.1 was still extruded on top of this to ensure that a full construct could be printed with the conditions.

Then either the extrusion pressure, movement speed or needle gauge was changed to produce the most consistent flow for reliable bioprints. Figure 6.2.2 A shows the schematic shape used for the calibration of the printer, a continuous back and forth pattern was used on the base to provide multiple points of measurement. Figure 6.2.2 B shows the resulting 3D printed gel loaded with fluorescent dye and printed in SLAM, the schematic print is designed to have space between the filaments so that accurate measurements can be taken. Figure 6.2.2 C shows that confocal microscopy provided sharp lines to accurately determine the outside edge of the ink, between 8 and 18 measurements were taken though the full size of the print depending on the quality of the images.

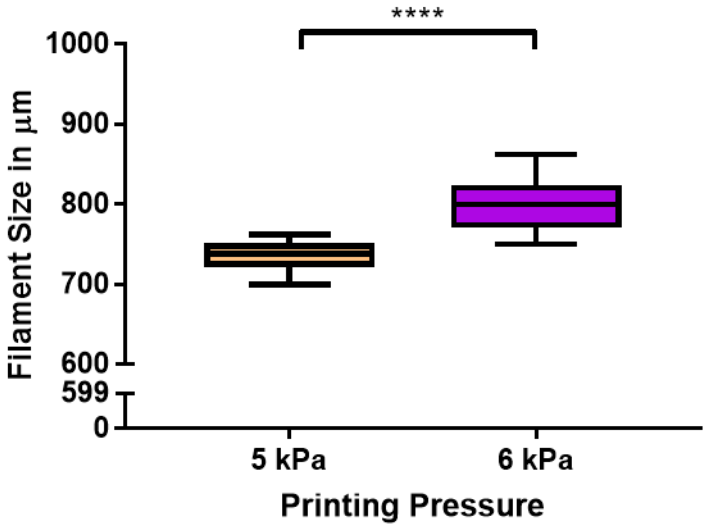

Figure 6.2.3 0.6% alginate filament extruded through a 22 G needle at varying pressures.

0.6% alginate with fluorescein was extruded through a 22 G 1.5-inch blunt needle in a set pattern and the filament diameter was measured using a confocal microscope at x4 magnification, at a standard feed rate of 30 mm/s. N=3, 6 measurements per sample. Error bars are Tukey standard error. $p < 0.05$ *; $p < 0.005$ **; $p < 0.0005$ ***; $p < 0.0001$ ****

Initially 0.6% w/v alginate made with αMEM as per the bioink formulation and additional fluorescein was printed. When extruded through a 22 G 1.5-inch blunt needle at the machine default of 30 mm/s, only two pressures were found to be practical to achieve reliable bioprinting. When the extrusion pressure was at 4 kPa, no continuous filament was formed and did not produce any printable shapes. At 7 kPa extrusion pressure, the flow was too high, resulting in poor resolution as printed lines began to merge together. Even though the filaments printed at the pressures had similar diameters of 737 µm +/- 16 for 5 kPa and 803 µm +/- 30 for 6 kPa, they are still significantly different and are both considerably larger than the internal diameter of the 22 G needle (0.413 µm ± 0.019).

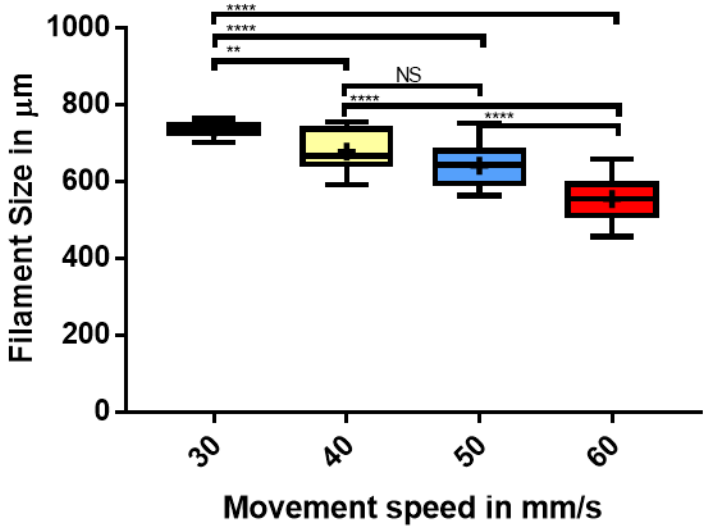

Figure 6.2.4 0.6% alginate filament extruded through a 22 G needle at varying nozzle movement speeds at 5 kPa extrusion pressure.

0.6% alginate with fluorescein was extruded through a 22 G 1.5-inch blunt needle in a set pattern filament diameter was measured using a confocal microscope at x4 magnification. N=3, 6 measurements per sample. Error bars are Tukey standard error. . $p < 0.05$ *; $p < 0.005$ **; $p < 0.0005$ ***; $p < 0.0001$ ****

Using a fixed extrusion pressure of 5 kPa as used in Figure 6.2.4 the nozzle movement speed was increased. The default movement speed of the machine is 30 mm/s and this is what was used in the previous experiment (Figure 6.2.3). When lowered to 20 mm/s all resolution between the printed filament was lost so therefore it was excluded as not viable due to 5 kPa being the lowest suitable extrusion pressure. As the print head movement speed was increased, the size of the filament decreased but the distribution of the diameter also increased. Therefore, the greater the movement speed the reproducibility of the print decreased. For 50 and 60 mm/s multiple attempts had to be made until an entire intact print could be produced for measurement. 30 mm/s had the largest average filament diameter at 737 µm but had the lowest distribution with a standard deviation of +/- 16 µm and was significantly different from all the other printing speeds. The diameter of filament printed at 40 and 50 mm/s were not significantly different from each other (677 µm and 640 µm respectively) and also had similar deviations of +/- 54 and 53 µm respectively.

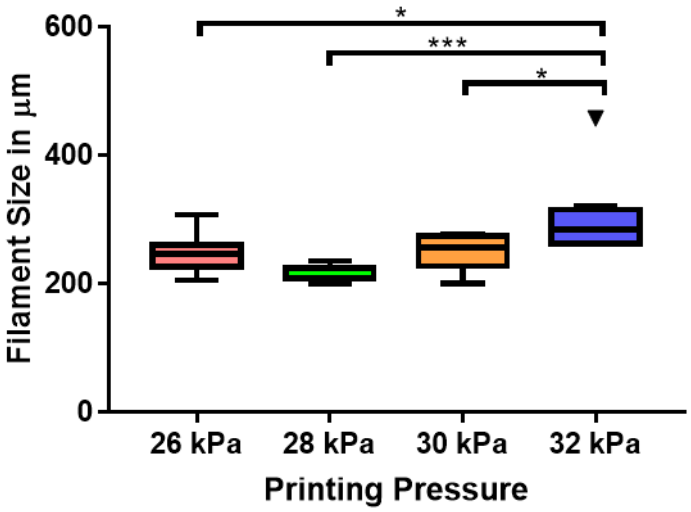

Figure 6.2.5 Bioink made with working concentrations of Collagen, Biomimetic tubes, CLEX, and alginate were printed using a 22 G needle.

The working bioink formulation containing alginate, collagen and hydroxyapatite was extruded through a 22 G blunt needle at a range of extrusion pressures to determine how the addition of the collagen and mineral would affect the bioprinting properties. N= 3, 6 measurements per sample. Error bars are Tukey standard error with the triangle representing an outlier. $p < 0.05$ *; $p < 0.005$ **; $p < 0.0005$ ***; $p < 0.0001$ ****

Working formulation of bioink minus cells was made with the fluorescein dye to determine how the additional of collagen and hydroxyapatite affected the extrusion. The printed constructs required a much greater extrusion pressure to print than 0.6% alginate alone (Figure 6.2.5). Below 26 kPa there was patchy and inconsistent flow and therefore excluded. Beyond 32 kPa the needle would drip bioink when there was no printing and therefore these pressures were excluded. There was no significant difference in filament diameter between 26 kPa and 28 kPa, nor was there between 28 kPa and 30 kPa or 30 kPa and 26 kPa, however 32 kPa being significantly different from all the extrusion pressures. The biggest limitation with using the 22 G needle was that all the working filament sizes were smaller than the needle size which has an outer diameter of 717 µm and an inner diameter of 413 µm.

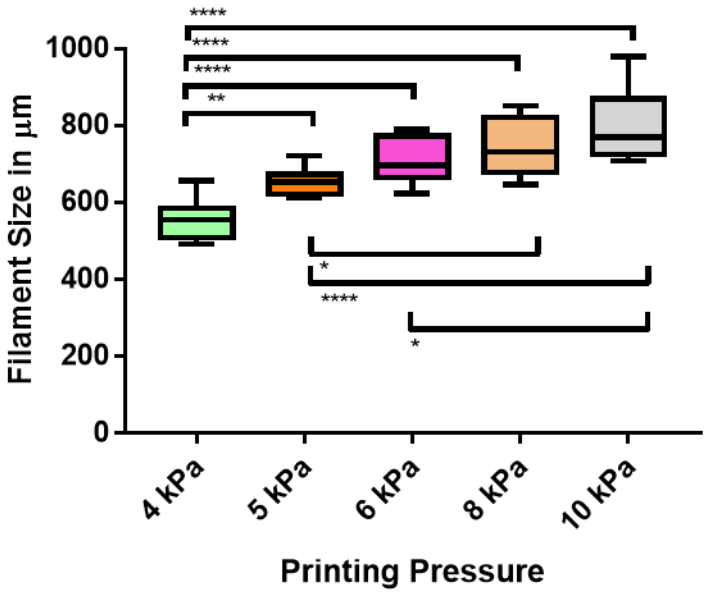

Figure 6.2.6 Filament diameter for working bioink composition using a 20 G needle. All at 30 mm/s.

The working bioink formulation was extruded through a 20 G blunt needle at a range of extrusion pressures to determine how the addition of the collagen and mineral would affect the bioprinting properties. n= 3, 6 measurements per sample. Error bars are Tukey standard error with the triangle representing an outlier. $p < 0.05$ *; $p < 0.005$ **; $p < 0.0005$ ***; $p < 0.0001$ ****

With the 22 G needle filament not being suitable for printing due to the large disparity between needle size and resulting filament diameter, a larger 20 G needle was used. This has an external diameter of 908 µm and an internal diameter of 603 µm. Using a 20 G needle, 5 kPa was found to be the optimal extrusion pressure with an average diameter of 654 µm (+/- 34 µm). As well as having the most consistent print of all the conditions, it was also closest to the internal diameter of the needle as well. Though the extrusion pressure here was far lower than that used for the 22 G needle (Figure 6.2.3) there was still a clear upward trend within the data that clearly indicated increasing printing pressure increased filament diameter as well as distribution of size. Though 4 kPa had the smallest filament size of 555 µm it did not follow the trend of having a lower size distribution of +/- 45 µm which is a variation of 8.1% compared to 5 kPa which had a variation of 5.2%.

6.2.2 alginate concentration limits

To determine the optimal alginate concentration within the bioink that is compatible with fibril collagen formation was investigated. This is one of the key aims of this chapter and thesis, a fixed collagen concentration of 1 mg/mL was used and formulated with a range of alginate concentrations from 0.2 – 1.6% w/v. Due to the concentration of incorporated CLEX gelling components, the αMEM based alginate and collagen the testable range was between 0.2% and 1.6%.

To determine the alginate concentrations compatible with collagen fibril formation, a range of bioinks with different alginate concentrations were made. Labelled 488 nm collagen was later incorporated within the bioinks so that the fibril structure could be visualised inside the crosslinked bioink. Table 6.2.1 demonstrates the different bioink formulations used, due to the maximum producible concentration of the CLEX A and the alginate gel, the maximum concentration of the alginate was 1.6% within these parameters.

Table 6.2.1 Formulations of bioinks used to determine collagen fibril formation within alginate concentrations ranging from 0.4% to 1.6%.

To determine optimal alginate concentration for collagen fibril formation a range of bioinks made using CLEX SLAM were made. The concentration of collagen and labelled collagen used remain consistent with the volume of alginate in the ink adjusted. Max concentration of 1.6% due to a 4% alginate stock used. inks were incubated for 2h at 37°C and then imaged on confocal.

	Alginate Concentration						
Ink components	0.4%	0.6%	0.8%	1.0%	1.2%	1.4%	1.6%
CLEX A x4	375 µL	375 µL	375 µL	375 µL	375 µL	375 µL	375 µL
Collagen 3mg/ml	475.5 µL	475.5 µL	475.5 µL	475.5 µL	475.5 µL	475.5 µL	475.5 µL
Labelled Collagen 6.19mg/ml	24 µL	24 µL	24 µL	24 µL	24 µL	24 µL	24 µL
1M NaOH	12.18 µL	12.18 µL	12.18 µL	12.18 µL	12.18 µL	12.18 µL	12.18 µL
4% Alginate	**150 µL**	**225 µL**	**300 µL**	**375 µL**	**450 µL**	**525 µL**	**600 µL**
αMEM	**462.7 µL**	**387.7 µL**	**321.7 µL**	**237.7 µL**	**162.7 µL**	**87.7 µL**	**12.7 µL**

Initially two zinc concentrations were used for the CLEX SLAM system of 12.5 mM and 25 mM to see whether this affected the retrieval of the constructs and the collagen fibril formation. As table 6.2.2 shows there was no effect of the increased zinc concentration on the retrieval of the constructs or the fibril formation but as determined previously (Figure 4.2.2) the higher zinc concentration had a negative effect on the cell viability so therefore 25 mM was no longer used, and all collagen fibril formation work was done only using 12.5 mM. No images were able to be obtained of 0.2% and 0.4% due to the constructs being too weak to remove from the SLAM bath even with the a 100 mM calcium chloride incubation.

Table 6.2.2 An overview of the collagen fibril formation and gel state after crosslinking using the CLEX SLAM system.

Bioinks formulated with alginate concentrations from 0.2 to 1.6% as shown in table 4.2.2 were used and two Zinc concentrations in the CLEX SLAM system of 12.5 mM and 25 mM. The intactness of the constructs was determined whether a printed construct could be removed from the SLAM bath. Initially fibrils where determined using a polarised light microscope and later confocal microscopy.

	Intact construct			
	12.5 mM	25 mM	Fibrils	Comments
0.2%	No	No	Yes	Gel too weak to form any form a solid struture
0.4%	No	No	Yes	Very weak gel, held structure after printing, fell apart during retrieval
0.6%	Yes	Yes	Yes	Soft gel, held its shape after printing in both conditions. Able to retrieve intact construct
0.8%	Yes	Yes	Some	Similar to 0.6%, slightly firmer gel but not as clear fibril formation
1.0%	Yes	Yes	Some	Strong set gel, able to be removed from bath with ease. Fibrils are small and bunched up
1.2%	Yes	Yes	Only at edge	Very strong gel, minimal fibril formation, only at edge of gel
1.4%	Yes	Yes	No	Very strong gel, minimal fibril formation, only at edge of gel
1.6%	Yes	Yes	No	Very strong gel, minimal fibril formation, only at edge of gel

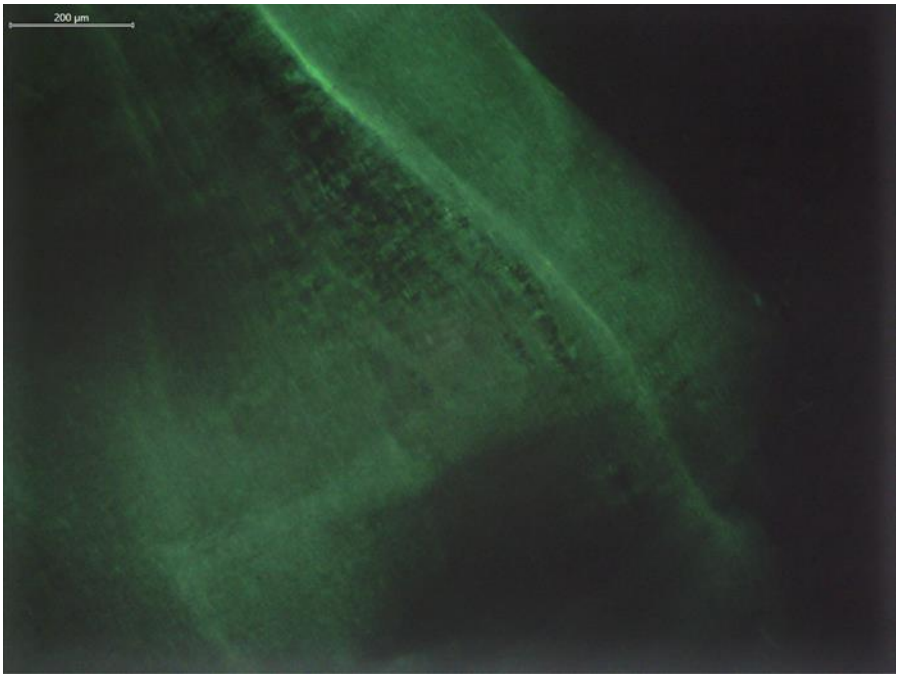

Figure 6.2.7 Polarised light microscope of collagen within an 0.6% alginate construct.

0.6% w/v alginate 0.1% w/v collagen CLEX based bioink seen under a polarised light microscope, the collagen fibrils scatter the light so that it can be seen through the polarised filters shown as the light grey area indicating collagen filaments. X4 Magnification, scale bar 200 µm.

Initially, collagen fibril analysis was performed using a polarised light microscope. When the collagen forms fibrils these then scatter the light which is picked up using the polarised filters to be visualised. Due to the depth of the constructs required to visualise the collagen images could only be taken at x4 magnification. While broad collagen formation could be determined within the constructs, at this low magnification fine fibral collagen structures could not be visualised therefore further fibril analysis was used using a fluorescent label.

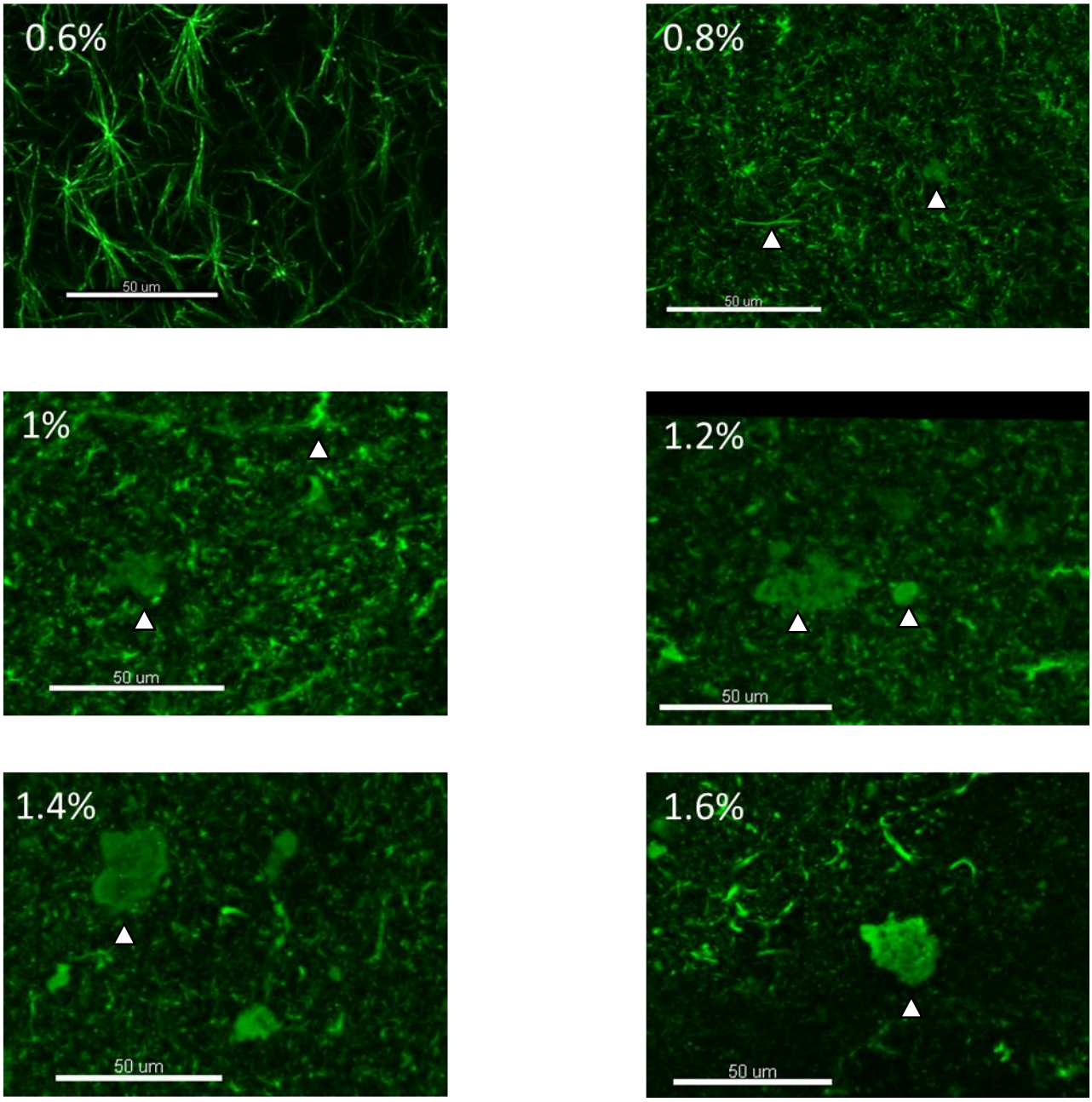

Figure 6.2.8 Effects of alginate concentration from 0.6% to 1.6% on collagen fibril formation.

Alginate collagen CLEX based bioink formulations as shown in Table 4.2.2 imaged with confocal microscopy. The morphology of 488 labelled collagen incorporated in the ink acts as a representation of total collagen behaviour. The increased alginate concentration reduces collagen fibril formation, size and distribution within alginate based bioinks. The white triangles demonstrate where collagen has formed globular clumps rather than fine fibrils. All at x40 magnification, 488 labelled collagen, scale bar 50 µm.

To determine the optimal alginate concentration for fibril formation in the bioink a range of bioinks were made with different concentrations of alginate. The formulations of the bioinks can be seen in Table 4.2.2. The bioinks were cross linked for 2h in SLAM CLEX B for 2 h, after 100 mM $CaCl_2$ was added to the wells and incubated for 5 min before retrieval of constructs Table 4.2.4. Figure 4.2.16

shows that beyond 0.6% w/v alginate, the fibril formation of collagen within the alginate declines as the concentration increases. No clear homogeneous fibril formation can be seen beyond 1.0% alginate. Some fibrils can be seen in 0.8% w/v alginate, the fibrils are smaller and tighter compact than 0.6% with some clumping and sheets visible and no homogeneous long fibrils can be seen. In 1.2-1.6% alginate constructs, minimal fibril formation is seen, and the collagen typically presents with large sheets of collagen forming in the gel rather than fine fibrils, some fibrils were seen at the edge of the construct, but the main body of the construct had minimal fibrils seen. As the collagen is labelled pre-polymerisation it is able to be visualised in all states whether fibril, globular or a sheet. Using the CLEX gelling agents and 4% w/v alginate limited the maximum concentration to 1.6%, 0.2% and 0.4% w/v were also tested but were unable to be removed intact after gelling due to the gel being too weak to form a uniform structure Table 6.2.2 and therefore were excluded from further investigation.

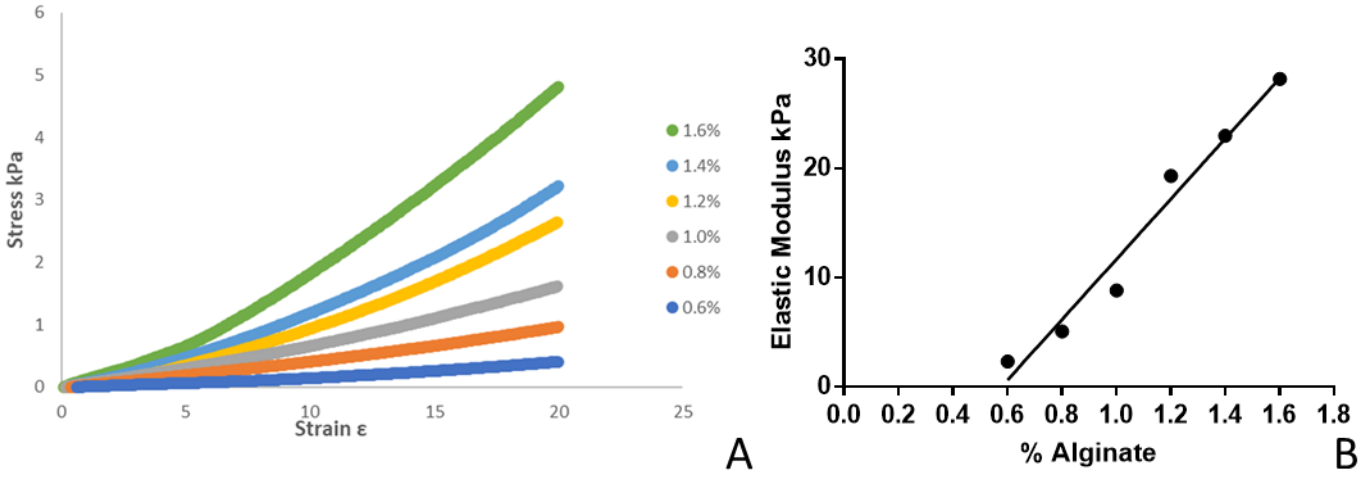

Figure 6.2.9 Mechanical analysis of alginate CLEX bioinks without collagen.

Stress strain analysis was performed on alginate only CLEX bioinks used in figure 4.2.16. 20% compression used to determine the material characteristics of each concentration. An elastic modulus for each concentration was determined to demonstrate the large change material character with a small change in concentration.

A. Stress strain curves of alginates gels between 0.6% and 1.6% w/v.
B. Elastic modulus of alginates between 0.6% and 1.6% w/v.

The material properties of the alginate components of the bioinks were measured to determine the range that is useable for collagen fibril formation. With Figure 6.2.8 demonstrating that 0.8% is the maximum usable concentration for collagen fibril formation and that 0.6% is optimal. This trend of a large difference in collagen formation from a relatively small difference in concentration change relates to the sharp increase in the stress strain curve and the elastic modulus with concentration increase Figure 6.2.9A, B. From the figure, it can be determined that the range for collagen fibril formation within alginate would suggest that the bioink needs to have an elastic modulus of between 2.34 kPa (0.6%) and 5.09 kPa (0.8%).

6.2.3 collagen concentration limits

In order to develop the bioink further, increased collagen concentration was explored. To achieve this, an alternative source of collagen was used with a concentration of 9.1 mg/mL. Due to the fixed concentrations of other CLEX components, this limited the maximum concentration available to 0.6% (6 mg/mL). As determined previously, 0.6% alginate is the optimal concentration for collagen fibril formation, so this was used as a standard throughout. The fluorescently labelled collagen used in chapter 4 was also used to determine fibril structure.

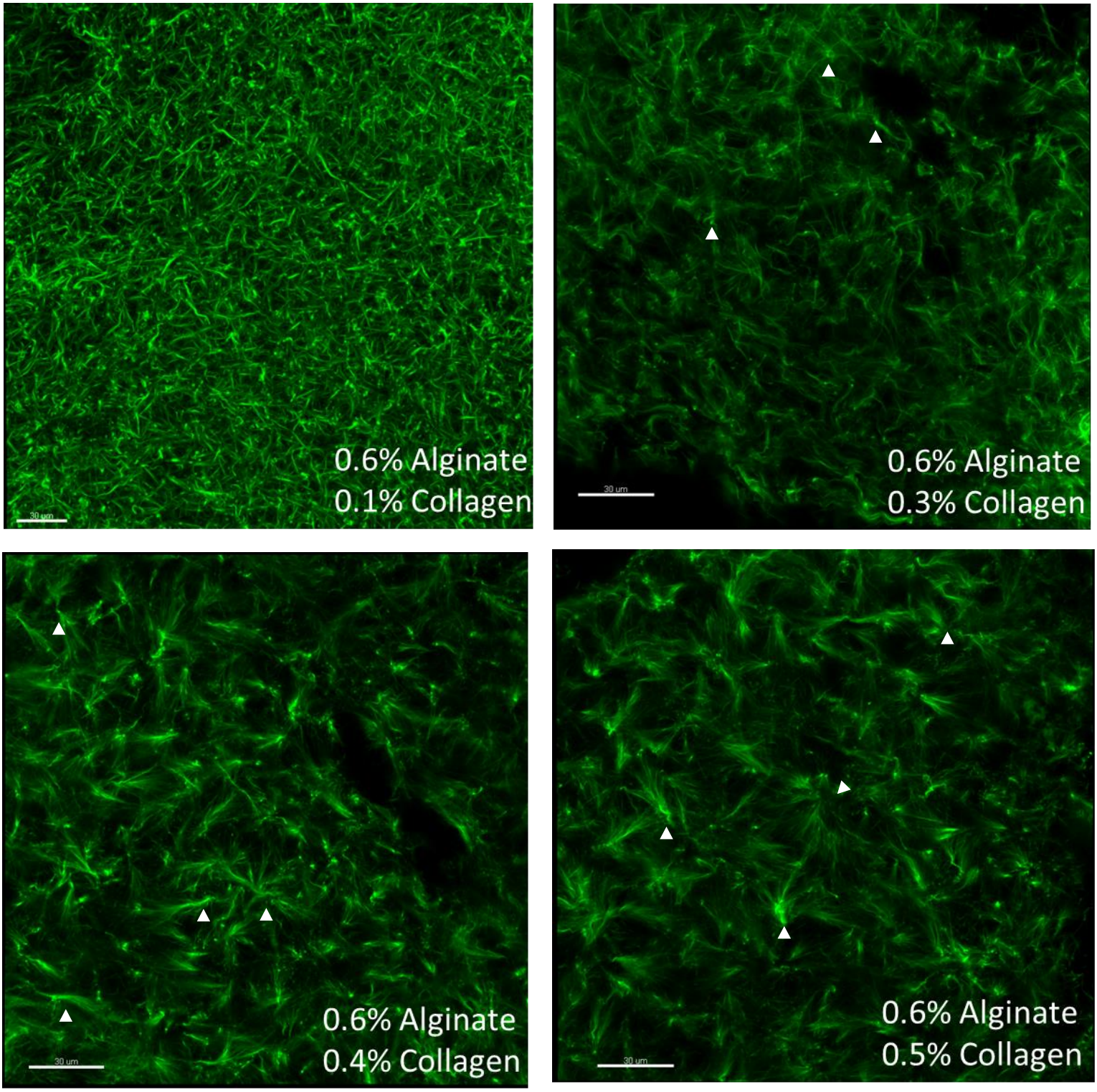

Figure 6.2.10 Collagen behaviour within bioink at increasing concentrations.

The current bioink formulation is at 0.1% (1 mg/ml) which forms fibrils of collagen as seen in the top right image. Collagen concentrations increased within the CLEX alginate bioink was increased to determine whether an increased concentration of collagen was able to form fibrils within the bioink. As the concentration of collagen increased the morphology of the collagen changes from a fibrillar to a spherite shape forming from a central point with branches emanating from this. All scale bars are 30 µm.

To validate that the different starting concentration and supplier of collagen was able to form fibrils within the alginate, the same conditions from Figure 6.2.8 were repeated. Notably the collagen was able to form fibrils in a similar manner to previous experiments. The fibrils observed in Figure 6.2.10 0.1% collagen are individual, isolated, and homogenously distributed throughout the sample. Whereas in Figure 6.2.8 0.6% the collagen formed star shaped bundles with a central nucleus from which the fibrils branch out from, leading to more small dense clusters of collagen fibrils with a heterogeneous distribution throughout the sample. Most importantly, the collagen was able to form clear fibrils within the bioink.

When the concentration of collagen was increased to 0.3% w/v, the fibril structure presented as singular fibrils but with some central nucleation points (Figure 6.2.10 0.3% white arrows). Fundamentally, collagen fibrils were still able to form. Though the green intensity in Figure 6.2.10 0.3% is less intense than Figure 6.2.10 0.1%, this is due to that the same ratio of collagen in stained so there is 3 times the signal of collagen in Figure 6.2.10 0.3%B compared to Figure 6.2.10 0.1%. The confocal settings were adjusted for the greater signal intensity and to still be able to interpret the fibril morphology. Therefore the intensity of green is only relevant within each figure and not able to be compared between the conditions.

As seen in Figure 6.2.10 - 0.4%, the increasing concentration of collagen leads to fibrils forming from a singular nuclear point. The shapes are less spherical than Figure 6.2.10 - 0.3% and are more densely clustered into triangular and ‘bow tie’ double triangular shapes. Some of the larger structures form into large branching continuous trees of collagen (white arrows).

The collagen fibril structures observed in Figure 6.2.10 - 0.4% and Figure 6.2.10 - 0.5% are very similar, though, the clusters of collagen and how they stem from the central nucleus present subtly differently. The clusters of collagen in Figure 6.2.10 - 0.4% are smaller than in Figure 6.2.10 - 0.5% and are more widely distributed. The higher concentration of collagen appears to cause the collagen to cluster together and form large networks with fibrils projecting of branches rather than resulting in a homogeneous interpenetrating next work as seen in Figure 6.2.10 - 0.1%

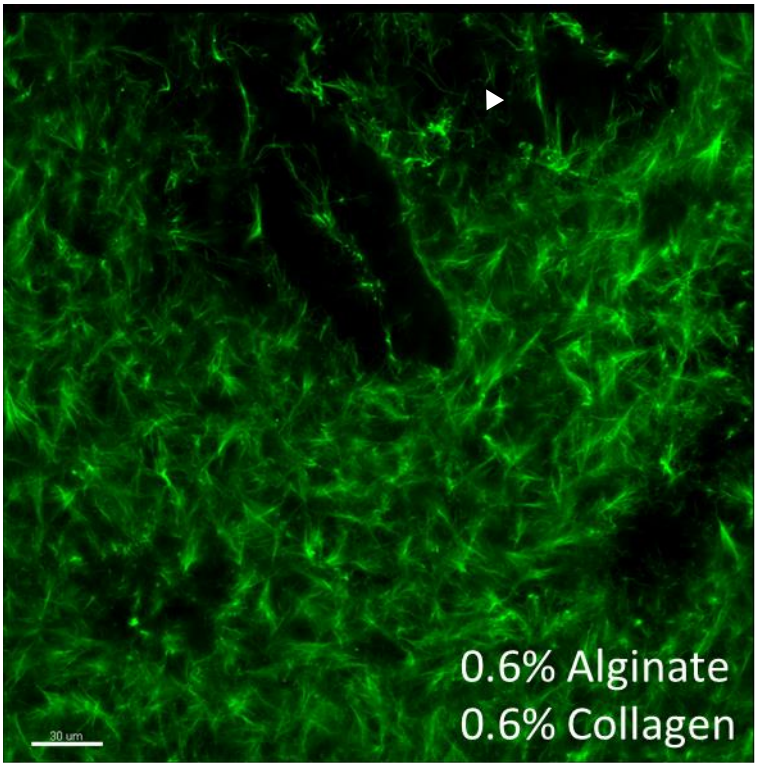

Figure 6.2.11 Maximum permissible collagen concentration within the bioink as formulated.

Using the stock solutions available, a 1:1 ration of collagen and alginate was made. The morphology of the collagen structures is vastly different than seen in previous high concentration collagen bioinks. The individual fibrils are overlapped heavily and hard to distinguish within the ink. Scale bar 30 µm

The concentration of collagen was raised to 0.6% w/v, the maximum allowed by the stock solutions and 1:1 with the alginate. With this increase, the collagen presented almost entirely from singular nucleation points. At the top right-hand side of Figure 6.2.10, some lone individual collagen fibrils can be seen (white arrows). Excluding these, all of the collagen presents with the triangular, double triangle 'bow tie' and branching morphology. Though due to the high concentration of collagen present it is difficult to determine the full extent of fibril formation.

6.2.4 Calcium phosphate biomimetic tubes incorporation

Biomimetic calcium phosphate tubes were incorporated into the bioink to act as mineral reservoirs for the cells and addition adhesion points for the cells to attach to. To determine whether the tubes interfered with the formation of the collagen fibrils, fluorescently labelled collagen was used. Tubes were incorporated into the bioink at approx. 4 mg/mL. To determine the orientation and distribution throughout the ink tubes were fluorescently labelled with calcein blue for visualisation.

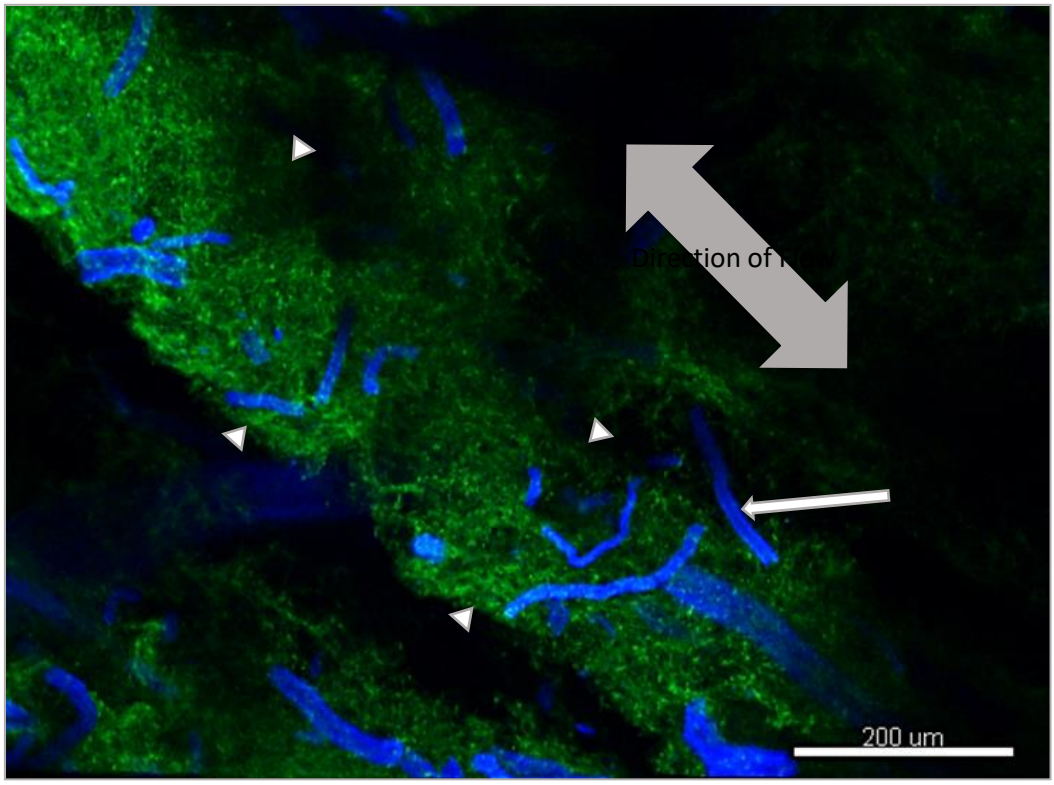

Figure 6.2.12 Calcium phosphate tubes integration into bioink.

Intact calcium phosphate tubes (blue) embedded in an alginate collagen CLEX based bioink with labelled collagen (green). The small white triangles indicate the external edge of the filament and that large arrow indicate and intact tube with lumen. Direction of flow is indicated by large double ended arrow. x10 magnification. 10 µm slice intervals 30 stacks. Scale bar 200 µm.

The outline of the printed bioink can be clearly seen in Figure 6.2.12 with the white triangles highlighting the edge of the filament. The bioink filament was printed using a RegenU Discovery bioprinter with a 22 G needle which has an internal diameter of 413 µm which is approximately. double the diameter of the printed filament at which had an average thickness of 219.8 µm. This can be visualised by the sharp edges of the collagen (green). The tubes (blue) are homogeneously distributed throughout the ink with the orientation appearing random with tubes both parallel and perpendicular to the flow of the ink (grey arrow). Importantly, the tubes remained intact throughout the incorporation into the bioink, extrusion and retrieval retaining their biomimetic shape. The lumen of one of the tubes can be seen highlighted by the small white arrow, the more intense colour on the outside of the tube with less colouration in the middle is indicative of a hollow cylinder. As with the collagen, the tubes were prelabelled with calcein blue before incorporation into the bioink, therefore all tubes present are labelled and Figure 6.2.12 can be considered a representative sample of printed bioink.

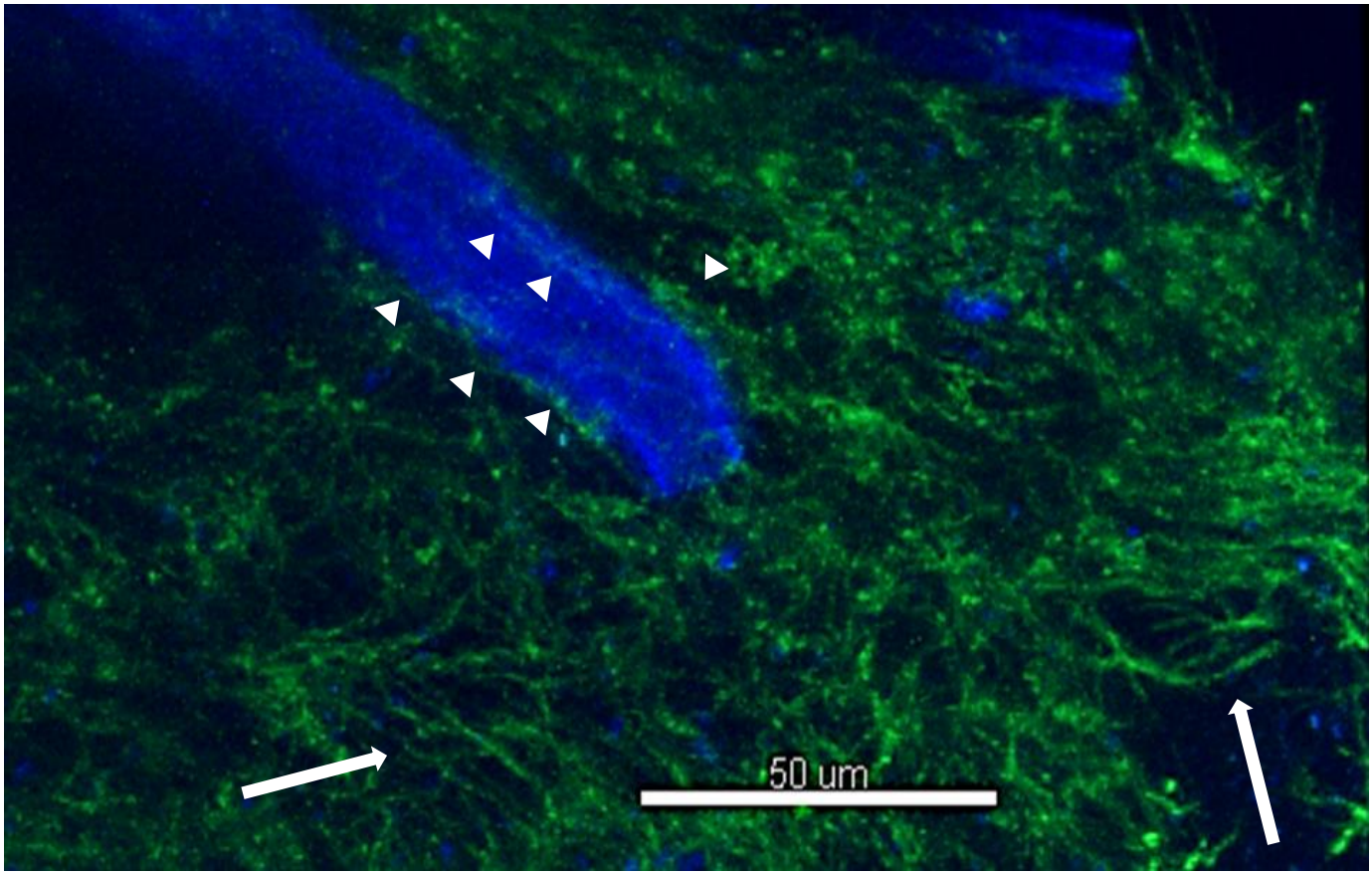

Figure 6.2.13 An intact calcium phosphate tube integrated into the fibril collagen network.

Calcium phosphate tube (blue) with clear lumen can be seen with labelled collagen (green) interacting with the tube highlighted by white triangles. Fibrils are highlighted with white arrows. X40 4 µm slice intervals 20 stacks, scale bar 50 µm.

While Figure 6.2.12 show a global integration of tubes into the bioink and the intact deposition of the tube, due to the low magnification used the fibril structure of the collagen cannot be clearly determined not can the interaction between the two components. Figure 6.2.13 is of a much higher magnification and clearly shows that the collagen fibril formation is not disrupted by the presence of the tubes (white arrows). Additionally around the tubes itself collagen can been seen to attach or directly integrate onto the tube structure (white triangles). Some fibrils can be seen above and below the tube structure suggesting that the collagen has formed around the tube, but further investigation is required to determine this as it may be an artifact of the z stacking.

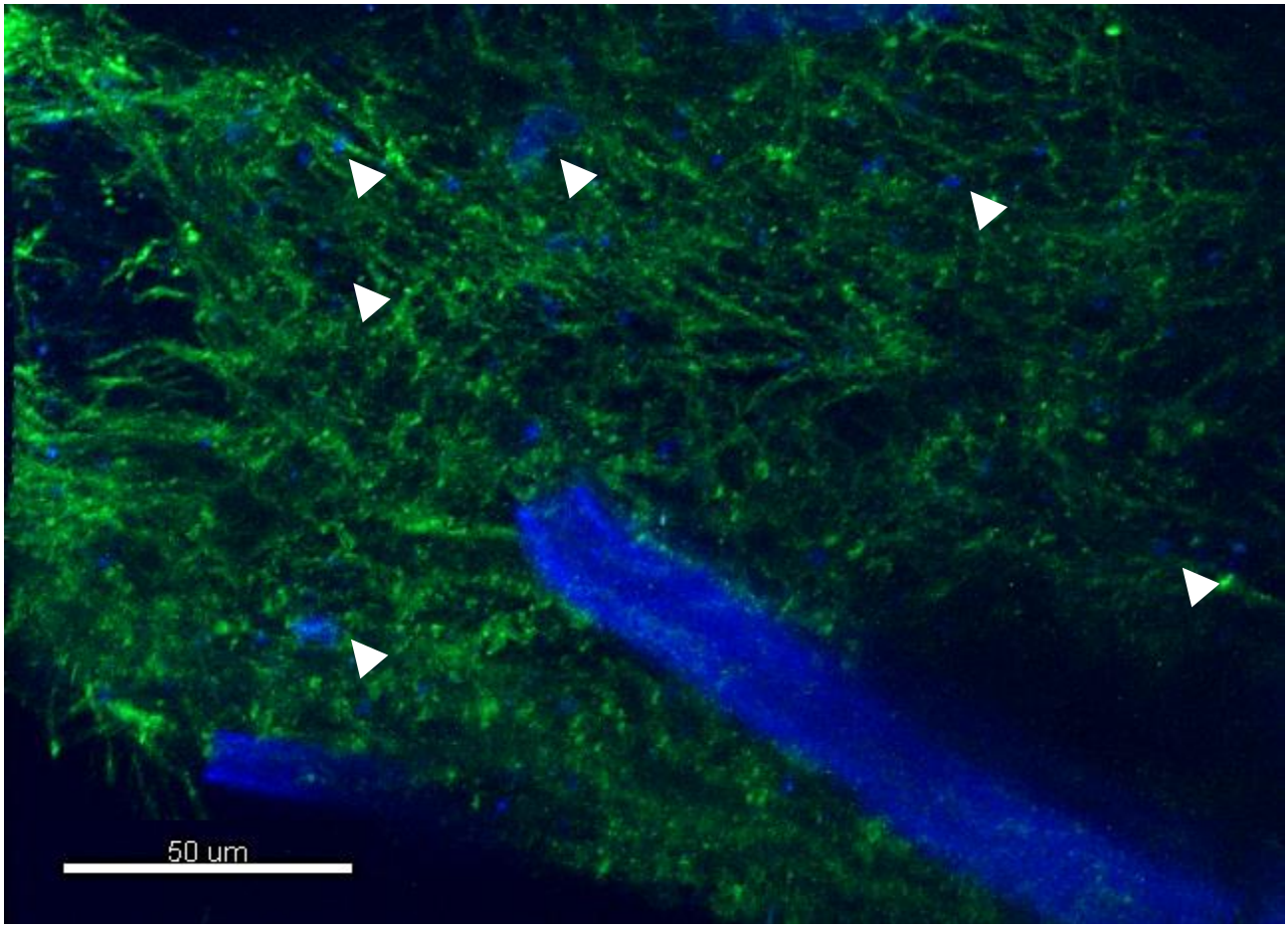

Figure 6.2.14 Calcium phosphate tube integrated into the fibril collagen network with fragments.

Fibril collagen can be seen around the tubes with small fragments of hydroxyapatite embedded within the collagen network (Arrows). X40 4 µm slice intervals 20 stacks, scale bar 50 µm

As shown in Figure 6.2.13, the collagen is able to interact with the tubes and form around the biomimetic whole tube constructs. During the tube encapsulation some calcium phosphate fragments are also incorporated into the ink and collagen matrix (white arrows) (Figure 6.2.14). Further suggesting that the collagen IPN is able to form around calcium phosphate bodies within the ink.

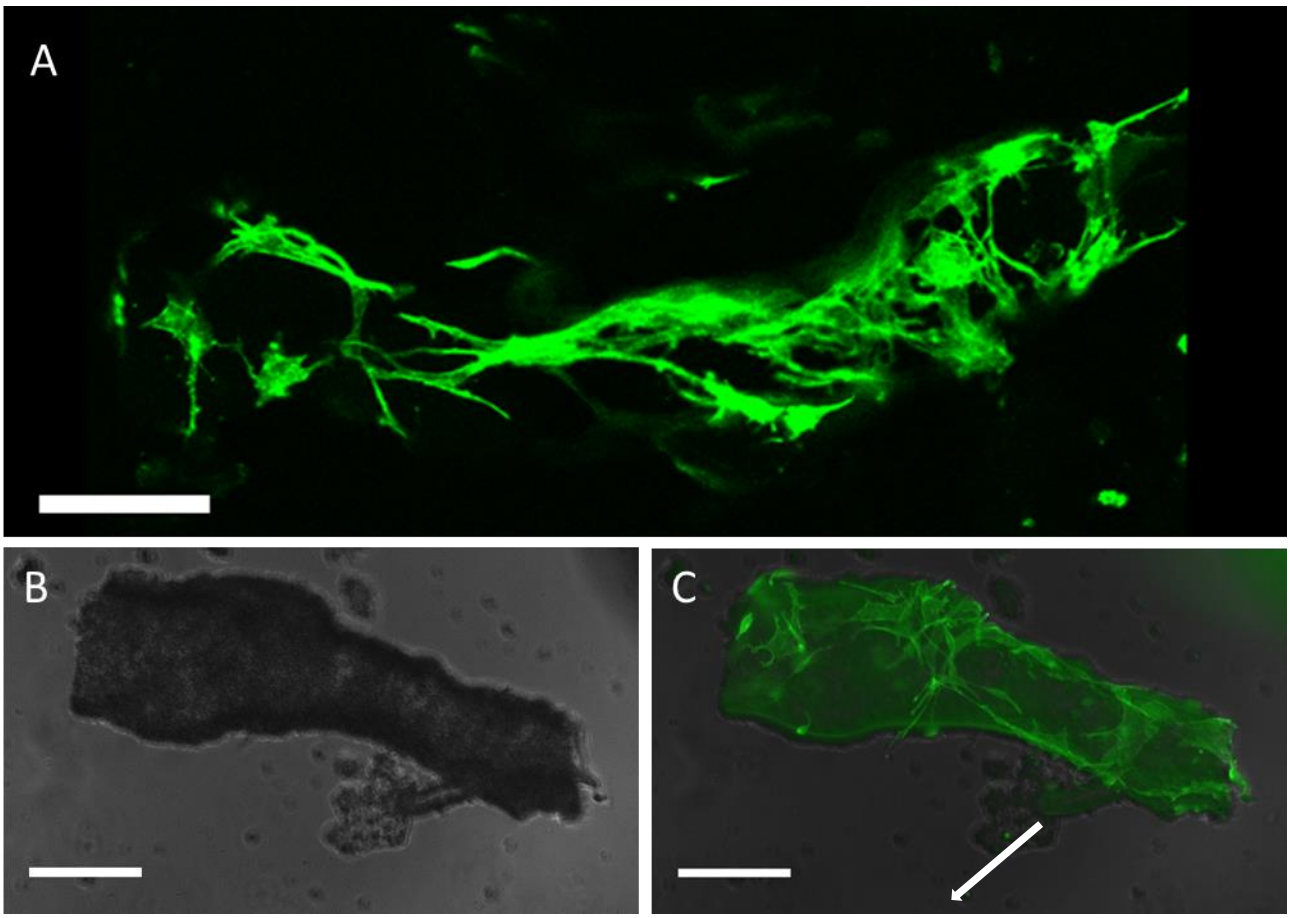

Figure 6.2.15 Calcium phosphate tubes with MC3T3-E1 cells attached labelled with phalloidin.

Phalloidin 488 labelled cells attached to calcium phosphate tubes. Same tubes previously incorporated into alginate collagen CLEX based bioink with cells seeded onto tubes to determine whether the cells can attach to the tubes. All scale bars are 100 µm.

A. Confocal image of a tube with cells attached
B. Phase contrast image of calcium phosphate tube with cells attached
C. Image B with fluorescent lamp on highlighting cell attachment to the tubes.

Cell attachment to the calcium phosphate tubes can be seen in Figure 6.2.15. In Figure 6.2.15A, the lumen of the tube is shown by the cells forming a circular shapes around the entrance of the tube (white arrow). The cells can be seen to have a dendritic like morphology with finger like projections attaching at multiple points along the exterior surface of the tube. Figures 6.2.15B&C are phase contrast and fluorescent microscope images of a tube respectively. In Figure 6.2.15B the cells are indistinguishable from the tubes and are adhered to the external surface of the tube. In Figure 6.2.15C, the actin labelled actin cytoskeleton of the cells can be visualised. There are no cells visibly attached to the surrounding TC plastic with the cell having an apparent preference for the calcium phosphate tubes.

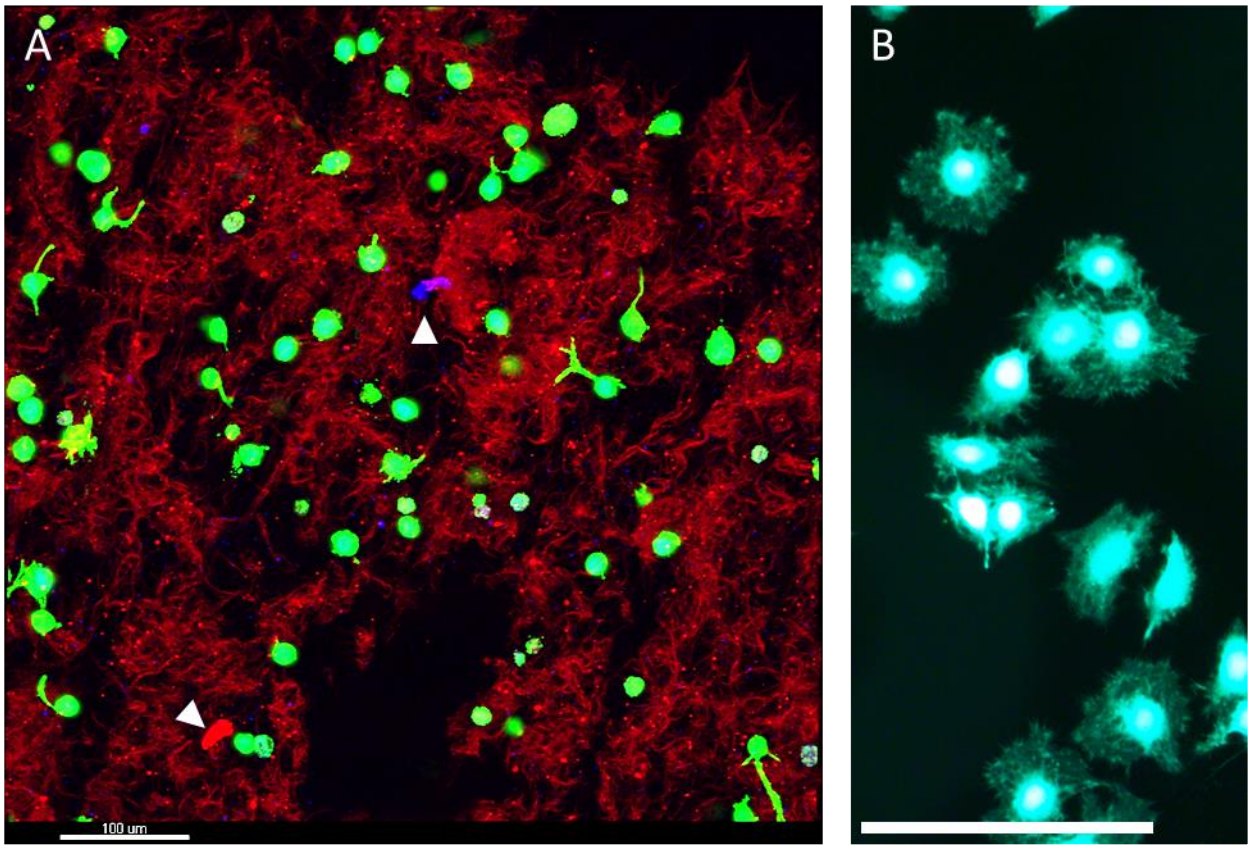

Figure 6.2.16 Live cell image of 3D printed CLEX SLAM bioink containing cells

A. Live confocal z stack 3D cells labeled with Calcein AM (green) to indicate metabolic activity and outline cell morphology. The collagen (red) has been labelled and presents as the large mesh in which the cells are integrated. Hoechst (blue) was used to confirm presence of cells and can be seen on some none or low metabolically active cells (white triangle). Propidium iodide(red) was also used and indicates a dead cell (white triangle). Scale bar 100 µm, 20 slices at 4 µm spacing
B. Live 2D cells cultured on cell culture plastic labeled with Calcein AM (Green) to indicate metabolic activity and outline cell morphology. Scale bar 100 µm

In the combined 3D printed bioink using the CLEX slam developed in Chapter 4 and the media in chapter 5, the large black areas in the bottom centre and top right of Figure 6.2.16 A are the non-labelled tubes incorporated into the ink. The live cells labelled green can be seen to project throughout the alginate-based ink and integrate within the collagen. The morphology of the cells is vastly different from the alginate only encapsulated cells (Figure 3.5.1 D) and that of cells cultured on 2D tissue culture plastic in Figure 6.2.16B. The bioink encapsulated cells show long projections into the bioink matrix with attaching to the collagen, the cells seem to have a central nuclear point and project out from that, while some of the cells appear rounded they are in fact projecting directly in line with the Z axis.

6.3 Discussion

A key characteristic of a successful bioink is the printability of the material, in chapter 4 *in situ* crosslinking chemistry was developed, in chapter 5 the osteogenesis and cell response of the ink was investigated and in this chapter the printability of the ink and all its components will be investigated.

6.3.1 Printing resolution

Initially a schematic diagram using bespoke bioprinting CAD software was used, this allows for layer-by-layer control of the print head rather than a standard .STL file which uses a triangular mesh to slice the constructs. Therefore, deposition is controllable on each layer, an important tool when building up complex biological tissues. When extruding bioink, keeping the sheer forces within the ink as low as possible is key as high sheer has been shown to induce cell death [142],[121]. Additionally, the CLEX SLAM bioink had two crosslinking mechanisms, the CLEX system as described in chapter 4 and collagen polymerization both of which are optimal at approx. 37 ^{o}C [152]. The modular RegenHU printer used can have cooled print heads and heated print beds which would facilitate keeping the bioink cooled at 4 ^{o}C and the SLAM crosslinking bath at 37 ^{o}C. Due to the newness of the equipment these capabilities where not available at the time of the work being done therefore when printing the constructs, time was imperative to keep both parts and the system at the required temperature, as such the swiftest extrusion time was required.

Therefore, the aim was to print a reliable filament as close to the inner diameter as possible with as low pressure as possible speediest fashion. To achieve this the 20 G 1.5 in blunt needle was chosen as it had a low extrusion pressure of 5 kPa which deposited a line of ink at 655 µm +/- 33.9 in diameter which is close to the the outer diameter of the needle at 718 µm ± 64. Therefore, each deposited layer was not disturbed by the adjacent filament being printed. To reduce the total print time, the effect of feed rate on filament size was investigated. Using a fixed 5 kPa extrusion pressure the trend seen was that increasing the feed rate of the needle is inversely proportional to the thickness of extruded filament. Though due to the loss of precision and increased dispersion of the printed filaments when feed rate was increased, the standard 30 mm/s was used for all subsequent prints (Figure 6.2.4).

Interestingly, much of the published literature on bioprinting, the feed rate is rarely mentioned which, as the data in Figure 6.2.4 demonstrates has a statistically significant effect on the resolution of the printed constructs. With the focus typically based on the bioink composition and the extrusion pressure and nozzle size[27,114,120,231].

6.3.2 Collagen incorporation into the bioink

In the CLEX based bioinks developed in chapter 4, one of the key aims was to not only incorporate collagen in the bioink but to have the formation of collagen fibrils interpenetrating throughout the ink. This was a key distinguishment from other collagen hybrid bioinks. To determine the presence of fibril collagen a couple different techniques were trialed. Initially, polarized light microscopy was investigated. This technique uses polarizing condensers to expose the bioink to light of a uniform polarization which is unable to pass through the top condenser. If the light hits collagen fibrils, the light is scattered and no longer on the same polarizing plane and therefore can pass through the top condenser to be visualized or imaged [232]. While simple, this technique lacked the magnification power to be able to visualize the fibrils (Figure 6.2.7). Secondary harmonic generation is a technique that can be used to image type 1 collagen [233]. The fibrillar structure of collagen type allows it to be imaged, while this technique was considered it was ruled out due to secondary harmonic generation being beyond the capabilities of the equipment that could be accessed.

Scanning electron microscopy (SEM) was used to investigate whether fibrils were present. This technique was excluded due to limitation of the equipment not being able to exceed x7000 and typically collagen is imaged at x20,000 to 50,000 magnification [234,235]. Therefore, no clear resolution of the collagen could be determined. Additionally, the sample preparation required for hydrogels to be imaged with SEM is not compatible with live cell imaging, the samples prep required also limits other techniques such as atomic force microscopy and transmission electron microscopy. Furthermore, SEM is a surface imagining technique and much of the collagen is within the bioink construct. To get accurate and in-depth images sections would need to be taken to allow for manual Z stacking of the images to determine if fibrils were present. Therefore, fluorescently labelling collagen was used to determine fibril formation as this was able to be used with live cells, was nondestructive and could image inside the bioink constructs. The technique developed by Doyle 2018 and has been previously shown to be nontoxic, compatible with cell adhesion and does not interfere with the structure or fibril formation of the collagen peptide chains [236]. The great advantage of this technique of the others is that it does not require the formation of collagen fibrils for imaging. Therefore, the orientation of collagen the collagen peptides can be easily visualized irrespective of whether fibrils or globular collagen had formed, which is an advantage over conventional collagen imaging techniques.

The fluorescently labeled collagen was combined with CLEX based bioinks (Table 6.2.1) to determine the optimal alginate concentration for collagen fibril formation and the ranges that are compatible with fibril formation if reformulation was required during the development process. Initially bioinks from 0.2 to 1.6% w/v were made, 1.6% w/v is the maximum formulated concentration with the

concentration of the components used limiting anything beyond this. Very early 0.2% and 0.4% w/v were eliminated from further characterization due to poor structural integrity of the constructs and none were able to be retrieved intact for fluorescent collagen analysis (Table 6.2.2). Bioinks made with 0.6% to 1.6% w/v were imaged at x40 magnification to determine optimal alginate concentration for collagen interpenetrating fibril formation with 0.8% w/v being the upper limit for fibril collagen formation. While some fibrillar can be seen in 1% w/v, predominantly the collagen present is globular and presenting as sheets. This trend continues as the alginate concentration increases with no fine fibrils seen in the higher concentration alginates, with more large sheets of collagen seen in 1.2,1.4 and 1.6% w/v alginates. While some thick fibril structures can be seen in 1.6% w/v, this is not true of the whole construct as the only area where the collagen could be visualized was at the edge a therefore the alginate concentration may not be homogeneous and thus some fibrillar formations occurred. Additionally, 1.6% w/v is the least homogenous off all the samples with most of the collagen condensed into small regions that present with greater intensity. The optimal condition for collagen formation was 0.6% w/v alginate with the large fine fibril formations within the ink forming an interpenetrating network. There is limited work with defined collagen fibrils within alginate bioinks. The main limitations with these is that they are not 3D printed or compatible with 3D printing and therefore are cast models. Additionally, due to the pH shifts for collagen stability they are not cell compatible until after the collagen has polymerized [237, 238]. A major advantage of the CLEX SLAM based printing system is that the collagen IPN is compatible when using 0.6% w/v alginate, the bioink is 3D printable and the whole system is cell compatible therefore cells can be incorporated throughout the bioink rather than seeded on after. Typically when using collagen in 3D printed tissue constructs, the collagen used has not been characterized as fibrils or is a hydrolyzed version of collagen such as gelatin [58,119,239].

For further development of the model increasing the collagen concentration was investigated from ranges between 0.1 mg/mL to 0.6 mg/mL with the latter being 1:1 with the alginate within the system. The change in collagen from morphology from fibril to spherite indicates that IPN network forms optimally at lower concentrations (Figure 6.2.10). The higher concentrations appear to have the fibrils emanating from a central point (Figure 6.2.11). The effect this would have on the cells and the development of the model would be an interesting avenue to continue the work. Though due to the complexity of this the decisions was to continue to use 1 mg/mL for simplicity while developing all aspects of the model.

Bone tissue is a mineralised collagen matrix that consists mostly of collagen type 1 and calcium phosphate in the phase of Hydroxyapatite (HA). The Bioink has so far been shown to be non-cytotoxic, compatible with collagen fibril formation and 3D printable. To improve the osteoinductive

properties of the ink calcium phosphate chemobrionic tube structures were incorporated into the bioink. While the cells are able to produce their own mineralised ECM as shown in Figure 5.2.1 the addition of collagen and calcium phosphate tubes was to incorporate more of the building blocks of bone rather than relying on all the relevant biological material to be produced by the cells. The calcium phosphate tubes are biomimetic and provide additional adhesion points for cells to attach to (Figure 6.2.15).The tubes have been previously characterised and shown to be calcium deficient hydroxyapatite and when cells were cultured in the presence of the tubes upregulated osteogenic markers [62]. The incorporation of intact tubes and printable tubes was achieved using CLEX 0.6% w/v alginate, 0.1% w/v collagen bioink printed into CLEX SLAM with a 20 G blunt needle as shown in Figure 6.2.12. The tubes appear in be in mostly a random orientation with some aligning perpendicular to the flow of the ink (Figure 6.2.12). Importantly, the collagen initially appeared in a fibrillar phase, due to the low magnification this couldn't initially be determined from the global image. High magnification images were taken which confirmed that the collage had formed fibrils (Figures 6.2.13, 14). A key component of the bioink is to have the fibril collagen interpenetrating collagen next work with the calcium phosphate tubes both acting as biomimetic adhesion points for the cells to attach to without the need to chemically modify the alginate in anyway [98]. This aim was achieved, and the combination of viable cells attached to an interpenetrating collagen network with calcium phosphate tubes that was 3D printed with the CLEX SLAM technique can be seen in Figure 6.2.16 A.

6.4 Conclusion

This culmination of work has produced a 3D printable bone precursor bioink which has stable *in situ* gelling kinetics, fibrillar collagen, biomimetic hydroxyapatite cell anchors, consistent print resolution and compatible with cell integration and continual culture. The initial approach taken using the SSL chip and cell encapsulation as explored in chapter 3 provided much of the pilot information required to develop a bioink which sustains cell culture. Though due to the incompatibility of the encapsulation crosslinking and collagen incorporation could no longer be explored as a viable research avenue within the scope of this project. From this development, the combination of CLEX and SLAM was investigated in chapter 4, these two techniques allow for the 3D printing of very low viscosity hydrogels and liquids in a system with tunable gelling kinetics. These properties open a plethora of further investigation such as bioinks made of liquid or of very low viscosity materials which previously could not have been printed i.e fibrin, pure collagen and very weak alginate. Therefore materials matching the mechanical properties of weak tissue types such as neural and adipose are able to be printed and crosslinked.

The controlled release of calcium within the system is compatible with 3D printed collagen fibril formation, which can be used as foundation to create bioprinted tissue structures which have collagen structural formations comparable to those found in vivo, with further investigation orientation of and spatial positioning of the collagen fibrils could be investigated.

The main limitations of this thesis are found in chapter 5 which due to the Covid 19 pandemic reduced laboratory access which impeded the data collection of the long-term cultures. Though this chapter lacks the repeats necessary for statistical validation, some interesting trends were seen such as SPP1 up regulation in 3D cultures and that the cells were able to change their expression profiles within the model which eludes to the suitability of the model for further analysis. The impact of pre differentiation on the incorporated cells was investigated and indicated that this may reduce the time needed in culture for osteogenic differentiation to occur, though this needs more technical replicates and should be investigated with multiple cell sources before any conclusion can be drawn.

Chapter 6 demonstrates the application of the bioink into a 3D printable system, using the bioink and SLAM system optimized in chapter 4 and 5, this was able to be printed into a 3D shaped with a high degree of precision and accuracy. In addition to that, the compatible incorporation of fibrillar collagen and biomimetic tubes demonstrated that no only do these act as anchor points for cell attachment but survive the printing process.

The culmination of this work, in the authors opinion provides a foundation for developing 3D models of bone, not only that but the methodologies developed can also be applied to other tissue types, particularly those requiring low viscosity bioinks such as neural, adipose and hepatic tissue models.

7.Summary

This thesis was an investigation in developing 3D synthetic bone models. This had two main focuses, the first was to create a 3D spatially controlled environment that contained the building blocks of bone which are hydroxyapatite and collagen. The second was that this environment was compatible with cell incorporation, facilitated long term culture within the constructs that ultimately leads to remodeling into bone tissue.

The initial focus was on encapsulating preosteoblast cells within alginate microbeads, a starting point of 1 and 2 % alginate was chosen as these were stiffer beads which are potentially more biomimetic of hard tissue. While this direction of work was ultimately scrapped due to the incompatibility of fibril collagen under the bead formation conditions, it did show some interesting results that encapsulated cells cultured in osteogenic media retained their proliferation potential longer than cells in standard proliferation media. From this research an easy reliable protocol to release viable cells encapsulated within alginate constructs was developed, which was later used for PCR analysis on 3D printed constructs.

This led to the research focus changing to developing a 3D printable bioink. The bioink had cells incorporated within and facilitated the formation of fibril collage that forms an interpenetrating network within the printed constructs. The concentration of alginate that facilitated the optimal formation of fibril collagen was 0.6%. Though this was able to have fibrillar collagen within it, the 3D printed constructs made from 0.6% alginate did not have the structural stability to retain its shape when 3D printed unsupported. This is ultimately a limitation of 3D printing with low concentration biomaterials.

Therefore, the incorporation of a recently reported supporting agarose fluid gel bath printing system SLAM was used to facilitate the printing of the low concentration bioink. Constructs made with the low concentration of alginate bioink printed within this fluid gel system held their shape and had high resolution. Due to the low structural stability of the bioink, that inhibited the use of conventional bioprinting, when calcium chloride crosslinker was added the constructs, it would distort the structure of the bioink before the crosslinker could stiffen the constructs. To overcome this limitation of the SLAM system, incorporation of an *in situ* competitive ligand exchange crosslinking system was used. A two-part system which incorporates stoichiometrically chelated calcium within the bioink, the calcium is released when in contact with its counterpart contained within the agarose bath. This semi crosslinked the constructs to a degree that they could be

retrieved from the agarose bath intact. This is, as far as the author is aware the only system of its type and represents a novel contribution to bioprinting research. The development of this system further opens the use of low concentrations polymers for bioprinting by incorporating a crosslinking agent within the bath. This is not limited to calcium-based systems, the principle can be applied to other commonly tissue engineering materials such as fibrin/thrombin, the thermal stability of the agarose can be exploited as well by using a temperature change to polymerise materials within the bath. This technique would be a useful tool in developing soft tissues models such as neural networks and adipose formations. Additionally, a greater range of shapes and dimensions can be bioprinted as this system does not require any additional supports either internally or externally. With further development, intricate details such as vascularization within a printed construct, a gas exchange interface as within alveoli of the lungs or the fluid exchange within a kidney nephron can be modelled.

With the controllable kinetics and crosslinker concentrations of the ligand exchange system, this facilitated enough calcium to be released to partially crosslink the alginate yet prevented free calcium being released into the system. With free calcium, as shown in chapter 3 can inhibit collagen fibril formation. As the calcium is contained within the alginate bioink, lower concentrations can be used for the initial crosslinking as there is no need for a large excess of calcium to diffuse through the ink. After initial alginate crosslinking and collagen polymerisation, calcium chloride can be added to fully crosslink the bioink. The combined elements created a novel supported ionic *in situ* crosslinking bioprinting system.

Biomimetic hydroxyapatite tubes were incorporated into the bioink, these are a relatively new development in the world of bone tissue engineering and the work here demonstrates the compatibly with bioprinting as well as an easy characterization non-destructive technique to visualize the tubes within the bioink. As far as the author is aware, the incorporation of a biomimetic hollow tube form of hydroxyapatite into a 3D printed bone based bioink has not been previously described. This also represent a novel contribution to the field of tissue engineering. This technique has application beyond bone tissue, the small size of the tubes is similar to capillaries and could have uses in fine vascularization of 3D printed tissues. Another potential use could be to direct growth and development of a tissue model by using the tubes to infuse nutrients deep into a synthetic tissue and attract cells through a nutrient gradient. The directionality of the cells could be used to dictate direction of growth with cells such as neurons which could grow within the lumen of the tubes.

Though further research is required to determine the biological impact of the bioink on the cells, the work here has developed a versatile novel bioink that has potential beyond bone tissue engineering.

8 References

1. Su, N. *et al.* Bone function, dysfunction and its role in diseases including critical illness. *Int. J. Biol. Sci.* **15**, 776–787 (2019).

2. Ansari, M. Bone tissue regeneration: biology, strategies and interface studies. *Prog. Biomater.* **8**, 223–237 (2019).

3. Florencio-Silva, R., Sasso, G. R. D. S., Sasso-Cerri, E., Simões, M. J. & Cerri, P. S. Biology of Bone Tissue: Structure, Function, and Factors That Influence Bone Cells. *Biomed Res. Int.* **2015**, (2015).

4. Wegst, U. G. K., Bai, H., Saiz, E., Tomsia, A. P. & Ritchie, R. O. Bioinspired structural materials. *Nat. Mater.* **14**, 23–36 (2015).

5. Hamed, E., Jasiuk, I., Yoo, A., Lee, Y. & Liszka, T. Multi-scale modelling of elastic moduli of trabecular bone. *J. R. Soc. Interface* **9**, 1654–1673 (2012).

6. Henkel, J. *et al.* Bone Regeneration Based on Tissue Engineering Conceptions — A 21st Century Perspective. *Bone Res.* **1**, 216–248 (2013).

7. Lemaire, V., Tobin, F. L., Greller, L. D., Cho, C. R. & Suva, L. J. Modeling the interactions between osteoblast and osteoclast activities in bone remodeling. *J. Theor. Biol.* **229**, 293–309 (2004).

8. Campana, V. *et al.* Bone substitutes in orthopaedic surgery: from basic science to clinical practice. *J. Mater. Sci. Mater. Med.* **25**, 2445–2461 (2014).

9. Norman, G. A. Van. Limitations of Animal Studies for Predicting Toxicity in Clinical Trials. *JACC Basic to Transl. Sci.* **4**, 845–854 (2019).

10. Bracken, M. B. Why animal studies are often poor predictors of human reactions to exposure. 120–122 (2008). doi:10.1258/jrsm.2008.08k033

11. Bonewald, L. F. The amazing osteocyte. *J. Bone Miner. Res.* **26**, 229–238 (2011).

12. Qin, L., Liu, W., Cao, H. & Xiao, G. Molecular mechanosensors in osteocytes. *Bone Res.* **8**, 1–24 (2020).

13. Shah, K. M. *et al.* Osteocyte isolation and culture methods. *Bonekey Rep.* **5**, 1–9 (2016).

14. Sun, Q. *et al.* Ex vivo 3D osteocyte network construction with primary murine bone cells. *Bone Res.* **3**, (2015).

15. Komori, T. Animal models for osteoporosis. *Eur. J. Pharmacol.* **759**, 287–294 (2015).

16. Kruger, M. C. & Morel, P. C. H. Experimental Control for the Ovariectomized Rat Model: Use of Sham Versus Nonmanipulated Animal. *J. Appl. Anim. Welf. Sci.* **19**, 73–80 (2016).

17. Salamanna, F. *et al.* A Human 3D In Vitro Model to Assess the Relationship Between Osteoporosis and Dissemination to Bone of Breast Cancer Tumor Cells. *J. Cell. Physiol.* **232**, 1826–1834 (2017).

18. Office of the Surgeon General (US). *Bone health and osteoporosis: a report of the Surgeon General*. *US Health and Human Services* (2004).

19. Bouet, G., Marchat, D., Cruel, M., Malaval, L. & Vico, L. *In Vitro* Three-Dimensional Bone Tissue Models: From Cells to Controlled and Dynamic Environment. *Tissue Eng. Part B Rev.* **21**, 133–156 (2015).

20. Knight, E. & Przyborski, S. Advances in 3D cell culture technologies enabling tissue-like structures to be created in vitro. *J. Anat.* **227**, 746–756 (2015).

21. Kim, Y. E. *et al.* Quantitative Proteomic Analysis of 2D and 3D Cultured Colorectal Cancer Cells: Profiling of Tankyrase Inhibitor XAV939-Induced Proteome. *Sci. Rep.* **8**, 1–12 (2018).

22. Ryan, B. J. A. Evolution of Cell Culture Surfaces. 1–7 (2011).

23. Bryhan, D. (12) United States Patent. **2**, (2003).

24. Duval, K. *et al.* Modeling physiological events in 2D vs. 3D cell culture. *Physiology* **32**, 266–277 (2017).

25. Tibbitt, M W., Anseth, K. S. Hydrogel as Extracellular Matrix Mimics for 3D Cell Culture. *NIH Public Access* **103**, 655–663 (2010).

26. Raghavan, S. *et al.* Formation of stable small cell number three-dimensional ovarian cancer spheroids using hanging drop arrays for preclinical drug sensitivity assays. *Gynecol. Oncol.* (2015). doi:10.1016/j.ygyno.2015.04.014

27. Kang, H. W. *et al.* A 3D bioprinting system to produce human-scale tissue constructs with structural integrity. *Nat. Biotechnol.* **34**, 312–319 (2016).

28. Fang, Y. & Eglen, R. M. Three-Dimensional Cell Cultures in Drug Discovery and Development. *SLAS Discov.* **22**, 456–472 (2017).

29. Polakis, P. The many ways of Wnt in cancer. *Curr. Opin. Genet. Dev.* **17**, 45–51 (2007).

30. Edmondson, R., Broglie, J. J., Adcock, A. F. & Yang, L. Three-Dimensional Cell Culture Systems and Their Applications in Drug Discovery and Cell-Based Biosensors. *Assay Drug Dev. Technol.* **12**, 207–218 (2014).

31. Seyhan, A. A. Lost in translation: the valley of death across preclinical and clinical divide – identification of problems and overcoming obstacles. *Transl. Med. Commun.* **4**, 1–19 (2019).

32. Roseti, L. *et al.* Scaffolds for Bone Tissue Engineering: State of the art and new perspectives. *Mater. Sci. Eng. C* **78**, 1246–1262 (2017).

33. Andersen, T., Auk-emblem, P. & Dornish, M. 3D Cell Culture in Alginate Hydrogels. 133–161 (2015). doi:10.3390/microarrays4020133

34. Hulsart-Billström, G. *et al.* A surprisingly poor correlation between in vitro and in vivo testing of biomaterials for bone regeneration: Results of a multicentre analysis. *Eur. Cells Mater.* **31**, 312–322 (2016).

35. Wang, X. & Yang, P. In vitro differentiation of mouse embryonic stem (mES) cells using the hanging drop method. *J. Vis. Exp.* 2–3 (2008). doi:10.3791/825

36. Cui, X., Hartanto, Y. & Zhang, H. Advances in multicellular spheroids formation. *J. R. Soc. Interface* **14**, (2017).

37. Muz, B., Puente, P. de la, Azab, F. & Azab, A. K. The role of hypoxia in cancer progression angiogenesis metastasis and resistane to therapy. *Hypoxia* **3**, 83–92 (2015).

38. Petersen, O. W., Ronnov-Jessen, L., Howlett, A. R. & Bissell, M. J. Interaction with basement

membrane serves to rapidly distinguish growth and differentiation pattern of normal and malignant human breast epithelial cells. *Proc. Natl. Acad. Sci.* **89**, 9064–9068 (1992).

39. Bai, X. *et al.* Bioactive hydrogels for bone regeneration. *Bioactive Materials* (2018). doi:10.1016/j.bioactmat.2018.05.006

40. Engler, A. J., Sen, S., Sweeney, H. L. & Discher, D. E. Matrix Elasticity Directs Stem Cell Lineage Specification. *Cell* **126**, 677–689 (2006).

41. Khalili, A. A. & Ahmad, M. R. A Review of cell adhesion studies for biomedical and biological applications. *International Journal of Molecular Sciences* (2015). doi:10.3390/ijms160818149

42. Paoli, P., Giannoni, E. & Chiarugi, P. Anoikis molecular pathways and its role in cancer progression. *Biochim. Biophys. Acta - Mol. Cell Res.* **1833**, 3481–3498 (2013).

43. Ahmed, E. M. Hydrogel: Preparation, characterization, and applications: A review. *J. Adv. Res.* **6**, 105–121 (2015).

44. El-sherbiny, I. M. & Yacoub, M. H. Review article Hydrogel scaffolds for tissue engineering : Progress and challenges. (2013).

45. Guo, L. *et al.* The role of natural polymers in bone tissue engineering. *J. Control. Release* **338**, 571–582 (2021).

46. Chen, M. *et al.* Natural polymer-based scaffolds for soft tissue repair. 1–8 (2022). doi:10.3389/fbioe.2022.954699

47. Corning Inc. Corning Incorporated Life Sciences. Corning Matrigel Matrix Frequently Asked Questions. 1–8 (2019).

48. Marinkovic, M. *et al.* One size does not fit all: Developing a cell-specific niche for in vitro study of cell behavior. *Matrix Biol.* **52**–**54**, 426–441 (2016).

49. Shoulders, M. D. & Raines, R. T. Collagen structure and stability. *Annu. Rev. Biochem.* **78**, 929–958 (2009).

50. Velez, A. M. A. & Howard, M. S. Collagen IV in normal and in disease process. *N. Am. J. Med. Sci.* **4**, 1–8 (2012).

51. Shao, F. *et al.* Microfluidic Encapsulation of Single Cells by Alginate Microgels Using a Trigger-Gellified Strategy. *Front. Bioeng. Biotechnol.* **8**, 1–13 (2020).

52. Duarte, J. M., Barbier, I. & Schaerli, Y. Bacterial Microcolonies in Gel Beads for High-Throughput Screening of Libraries in Synthetic Biology. *ACS Synth. Biol.* **6**, 1988–1995 (2017).

53. Eleftheriadou, D. *et al.* An alginate-based encapsulation system for delivery of therapeutic cells to the CNS. *RSC Adv.* **12**, 4005–4015 (2022).

54. Zafeiri, I., Beri, A., Linter, B. & Norton, I. Mechanical properties of starch-filled alginate gel particles. *Carbohydr. Polym.* **255**, 117373 (2021).

55. Wang, N., Adams, G., Buttery, L., Falcone, F. H. & Stolnik, S. Alginate encapsulation technology supports embryonic stem cells differentiation into insulin-producing cells. *J. Biotechnol.* **144**, 304–312 (2009).

56. Justin, A. W., Brooks, R. A. & Markaki, A. E. Multi-casting approach for vascular networks in cellularized hydrogels. *J. R. Soc. Interface* **13**, (2016).

57. Wu, Y. *et al.* 3d printed calcium phosphate cement (CPC) scaffolds for anti-cancer drug

delivery. *Pharmaceutics* **12**, 1–15 (2020).

58. Marques, C. F. *et al.* Collagen-based bioinks for hard tissue engineering applications: a comprehensive review. *J. Mater. Sci. Mater. Med.* **30**, (2019).

59. Gallorini, M. *et al.* The open cell form of 3d-printed titanium improves osteconductive properties and adhesion behavior of dental pulp stem cells. *Materials (Basel).* **14**, (2021).

60. Yuan, H. *et al.* A novel bovine serum albumin and sodium alginate hydrogel scaffold doped with hydroxyapatite nanowires for cartilage defects repair. *Colloids Surfaces B Biointerfaces* **192**, 111041 (2020).

61. Doyle, A. Correction: Fluorescent Labeling of Rat-tail Collagen for 3D Fluorescence Imaging. *Bio-Protocol* **10**, (2020).

62. Hughes, E. A. B., Chipara, M., Hall, T. J., Williams, R. L. & Grover, L. M. Chemobrionic structures in tissue engineering: Self-assembling calcium phosphate tubes as cellular scaffolds. *Biomater. Sci.* **8**, 812–822 (2020).

63. Sawa, N., Fujimoto, H., Sawa, Y. & Yamashita, J. Alternating Differentiation and Dedifferentiation between Mature Osteoblasts and Osteocytes. *Sci. Rep.* **9**, 1–9 (2019).

64. Hwang, P. W. & Horton, J. A. Variable osteogenic performance of MC3T3-E1 subclones impacts their utility as models of osteoblast biology. *Sci. Rep.* **9**, 1–9 (2019).

65. Takenawa, T. *et al.* Expression and dynamics of podoplanin in cultured osteoblasts with mechanostress and mineralization stimulus. *Acta Histochem. Cytochem.* **51**, 41–52 (2018).

66. Thermofisher. How TaqMan Assays Work. Available at: https://www.thermofisher.com/uk/en/home/life-science/pcr/real-time-pcr/real-time-pcr-learning-center/real-time-pcr-basics/how-taqman-assays-work.html.

67. ScienCell. No Title. Available at: https://www.sciencellonline.com/PS/8678.pdf.

68. Yang, Z. & Xiong, H.-R. Culture Conditions and Types of Growth Media for Mammalian Cells. in *Biomedical Tissue Culture* **i**, 17 (InTech, 2012).

69. Kim, J., Sachdev, P. & Sidhu, K. Alginate microcapsule as a 3D platform for the efficient differentiation of human embryonic stem cells to dopamine neurons. *Stem Cell Res.* **11**, 978–989 (2013).

70. An, C. *et al.* Continuous microfluidic encapsulation of single mesenchymal stem cells using alginate microgels as injectable fillers for bone regeneration. *Acta Biomater.* **111**, 181–196 (2020).

71. Chen, B., Wright, B., Sahoo, R. & Connon, C. J. A novel alternative to cryopreservation for the short-term storage of stem cells for use in cell therapy using alginate encapsulation. *Tissue Eng. - Part C Methods* **19**, 568–576 (2013).

72. Swioklo, S., Constantinescu, A. & Connon, C. J. Alginate-Encapsulation for the Improved Hypothermic Preservation of Human Adipose-Derived Stem Cells. *Stem Cells Transl. Med.* **5**, 339–349 (2016).

73. Zhang, C. *et al.* Hydrogel cryopreservation system: An effective method for cell storage. *Int. J. Mol. Sci.* **19**, (2018).

74. Szekalska, M., Puciłowska, A., Szymańska, E., Ciosek, P. & Winnicka, K. Alginate: Current Use and Future Perspectives in Pharmaceutical and Biomedical Applications. *Int. J. Polym. Sci.*

2016, (2016).

75. Aderibigbe, B. A. & Buyana, B. Alginate in wound dressings. *Pharmaceutics* **10**, (2018).

76. Lee, K. Y. & Mooney, D. J. Alginate: Properties and biomedical applications. *Prog. Polym. Sci.* **37**, 106–126 (2012).

77. Johnston, T. G. *et al.* Compartmentalized microbes and co-cultures in hydrogels for on-demand bioproduction and preservation. *Nat. Commun.* **11**, 1–11 (2020).

78. Ruvinov, E., Leor, J. & Cohen, S. The promotion of myocardial repair by the sequential delivery of IGF-1 and HGF from an injectable alginate biomaterial in a model of acute myocardial infarction. *Biomaterials* **32**, 565–578 (2011).

79. Håti, A. G. *et al.* Versatile, cell and chip friendly method to gel alginate in microfluidic devices. *Lab Chip* **16**, 3718–3727 (2016).

80. Iansante, V. *et al.* A new high throughput screening platform for cell encapsulation in alginate hydrogel shows improved hepatocyte functions by mesenchymal stromal cells co-encapsulation. *Front. Med.* **5**, 1–11 (2018).

81. Yang, Z., Li, J. P. & Guan, H. S. Preparation and characterization of oligomannuronates from alginate degraded by hydrogen peroxide. *Carbohydr. Polym.* **58**, 115–121 (2004).

82. Public Health England, T. D. *Hydrogen Peroxide Toxicological Overview Key Points*. *PHE Centre for Radiation, Chemical and Environmental Hazards* (2009).

83. Gardner, A. M. *et al.* Apoptotic vs. Nonapoptotic Cytotoxicity Induced by Hydrogen Peroxide. *Free Radic. Biol. Med.* **22**, 73–83 (1997).

84. Cheng, Y. *et al.* Biochemical Characteristics and Variable Alginate-Degrading Modes of a Novel Bifunctional Endolytic Alginate Lyase. *Appl. Environ. Microbiol.* **83**, 1–18 (2017).

85. Zhu, B. & Yin, H. Alginate lyase: Review of major sources and classification, properties, structure-function analysis and applications. *Bioengineered* **6**, 125–131 (2015).

86. Holme, H. K., Lindmo, K., Kristiansen, A. & Smidsrød, O. Thermal depolymerization of alginate in the solid state. *Carbohydr. Polym.* **54**, 431–438 (2003).

87. Saladino, A. J. *et al.* Effects of Formaldehyde, Acetaldehyde, Benzoyl Peroxide, and Hydrogen Peroxide on Cultured Normal Human Bronchial Epithelial Cells. *Cancer Res.* **45**, 2522–2526 (1985).

88. Amaral, K. F., Rogero, M. M., Fock, R. A., Borelli, P. & Gavini, G. Cytotoxicity analysis of EDTA and citric acid applied on murine resident macrophages culture. *Int. Endod. J.* **40**, 338–343 (2007).

89. Zhao, S. *et al.* Bioengineering of injectable encapsulated aggregates of pluripotent stem cells for therapy of myocardial infarction. *Nat. Commun.* **7**, 1–12 (2016).

90. Wu, Z. *et al.* Bioprinting three-dimensional cell-laden tissue constructs with controllable degradation. *Sci. Rep.* **6**, 1–10 (2016).

91. Tevlek, A., Odabas, S., Çelik, E. & Aydin, H. M. Preparation of MC3T3-E1 cell sheets through short-term osteogenic medium application. *Artif. Cells, Nanomedicine Biotechnol.* **46**, 1145–1153 (2018).

92. Hunt, N. C. & Grover, L. M. Encapsulation and Culture of Mammalian Cells Including Corneal Cells in Alginate Hydrogels. in *Corneal Regenerative Medicine* **1014**, 201–210 (Humana Press,

Totowa, NJ, 2013).

93. Yan, X. Z. *et al.* Effects of continuous passaging on mineralization of MC3T3-E1 cells with improved osteogenic culture protocol. *Tissue Eng. - Part C Methods* **20**, 198–204 (2014).

94. Sun, Y., Ma, X., Zhou, D., Vacek, I. & Sun, A. M. Normalization of diabetes in spontaneously diabetic cynomologus monkeys by xenografts of microencapsulated porcine islets without immunosuppression. *J. Clin. Invest.* **98**, 1417–1422 (1996).

95. Mahapatra, C., Jin, G. Z. & Kim, H. W. Alginate-hyaluronic acid-collagen composite hydrogel favorable for the culture of chondrocytes and their phenotype maintenance. *Tissue Eng. Regen. Med.* **13**, 538–546 (2016).

96. Nishimura, I. *et al.* Effect of osteogenic differentiation medium on proliferation and differentiation of human mesenchymal stem cells in three-dimensional culture with radial flow bioreactor. *Regen. Ther.* **2**, 24–31 (2015).

97. Butcher, D. T., Alliston, T. & Weaver, V. M. A tense situation: forcing tumour progression. *Nat. Rev. Cancer* **9**, 108–122 (2009).

98. Grigore, A., Sarker, B., Fabry, B., Boccaccini, A. R. & Detsch, R. Behavior of encapsulated MG-63 cells in RGD and gelatine-modified alginate hydrogels. *Tissue Eng. - Part A* **20**, 2140–2150 (2014).

99. Yazid, M. D., Ariffin, S. H. Z., Senafi, S., Razak, M. A. & Wahab, R. M. A. Determination of the differentiation capacities of murines' primary mononucleated cells and MC3T3-E1 cells. *Cancer Cell Int.* **10**, 42 (2010).

100. Langenbach, F. & Handschel, J. Effects of dexamethasone, ascorbic acid and ?-glycerophosphate on the osteogenic differentiation of stem cells in vitro. *Stem Cell Res. Ther.* **4**, 117 (2013).

101. Saji Joseph, J., Tebogo Malindisa, S. & Ntwasa, M. Two-Dimensional (2D) and Three-Dimensional (3D) Cell Culturing in Drug Discovery. in *Cell Culture* **11**, 13 (IntechOpen, 2019).

102. Ye, K. *et al.* Matrix Stiffness and Nanoscale Spatial Organization of Cell-Adhesive Ligands Direct Stem Cell Fate. *Nano Lett.* **15**, 4720–4729 (2015).

103. Sun, M. *et al.* Effects of matrix stiffness on the morphology, adhesion, proliferation and osteogenic differentiation of mesenchymal stem cells. *Int. J. Med. Sci.* **15**, 257–268 (2018).

104. Piroli, M. E. & Jabbarzadeh, E. Matrix Stiffness Modulates Mesenchymal Stem Cell Sensitivity to Geometric Asymmetry Signals. *Ann. Biomed. Eng.* **46**, 888–898 (2018).

105. Sun, M. *et al.* Extracellular matrix stiffness controls osteogenic differentiation of mesenchymal stem cells mediated by integrin α5. *Stem Cell Research and Therapy* **9**, (2018).

106. Tian, K.-K., Huang, S.-C., Xia, X.-X. & Qian, Z.-G. Fibrous Structure and Stiffness of Designer Protein Hydrogels Synergize to Regulate Endothelial Differentiation of Bone Marrow Mesenchymal Stem Cells. *Biomacromolecules* **23**, 1777–1788 (2022).

107. van der Stelt, M. *et al.* Pioneering low-cost 3D-printed transtibial prosthetics to serve a rural population in Sierra Leone – an observational cohort study. *ECl1. van der Stelt, M. al. Pioneer. low-cost 3D-printed transtibial prosthetics to serve a Rural Popul. Sierra Leone – an Obs. cohort study. EClinicalMedicine 35, 100874 (2021).inicalMedicine* **35**, 100874 (2021).

108. Willemsen, K. *et al.* Challenges in the design and regulatory approval of 3D-printed surgical implants: a two-case series. *Lancet Digit. Heal.* **1**, e163–e171 (2019).

109. Zheng, F., Wang, Z., Huang, J. & Li, Z. Inkjet printing-based fabrication of microscale 3D ice structures. *Microsystems Nanoeng.* **6**, (2020).

110. Erkoc, P. *et al.* 3D Printing of Cytocompatible Gelatin-Cellulose-Alginate Blend Hydrogels. *Macromol. Biosci.* **20**, 1–15 (2020).

111. Ardelean, I. L. *et al.* Collagen/hydroxyapatite bone grafts manufactured by homogeneous/heterogeneous 3D printing. *Mater. Lett.* **231**, 179–182 (2018).

112. Sharma, R., Smits, I. P. M., De La Vega, L., Lee, C. & Willerth, S. M. 3D Bioprinting Pluripotent Stem Cell Derived Neural Tissues Using a Novel Fibrin Bioink Containing Drug Releasing Microspheres. *Front. Bioeng. Biotechnol.* **8**, 1–12 (2020).

113. Lee, A. *et al.* 3D bioprinting of collagen to rebuild components of the human heart. *Science (80-.).* **365**, 482–487 (2019).

114. Jessop, Z. M. *et al.* Printability of pulp derived crystal, fibril and blend nanocellulose-alginate bioinks for extrusion 3D bioprinting. *Biofabrication* **11**, (2019).

115. Guvendiren, M., Lu, H. D. & Burdick, J. A. Shear-thinning hydrogels for biomedical applications. *Soft Matter* **8**, 260–272 (2012).

116. Wang, J. *et al.* 3D printed agar/ calcium alginate hydrogels with high shape fidelity and tailorable mechanical properties. *Polymer (Guildf).* **214**, (2021).

117. Ramesh, S. *et al.* Extrusion bioprinting: Recent progress, challenges, and future opportunities. *Bioprinting* **21**, e00116 (2021).

118. Zołek-Tryznowska, Z. Rheology of Printing Inks. in *Printing on Polymers: Fundamentals and Applications* 87–99 (2015). doi:10.1016/B978-0-323-37468-2.00006-3

119. Alexa, R. L. *et al.* 3D-printed gelatin methacryloyl-based scaffolds with potential application in tissue engineering. *Polymers (Basel).* **13**, 1–17 (2021).

120. Senior, J. J., Cooke, M. E., Grover, L. M. & Smith, A. M. Fabrication of Complex Hydrogel Structures Using Suspended Layer Additive Manufacturing (SLAM). *Adv. Funct. Mater.* **29**, 1–10 (2019).

121. Blaeser, A. *et al.* Controlling Shear Stress in 3D Bioprinting is a Key Factor to Balance Printing Resolution and Stem Cell Integrity. *Adv. Healthc. Mater.* **5**, 326–333 (2016).

122. Hoehne, J. L. *et al.* Piezoelectric 3D bioprinting for ophthalmological applications: Process development and viability analysis of the technology. *Biomed. Phys. Eng. Express* **6**, (2020).

123. Schubert, D. W. Simple Model for the Spreading of Inks in Bioprinting—Revealing Relevant Scaling Laws—Part I Theory. *Macromol. Theory Simulations* **31**, 1–9 (2022).

124. Bassett, D. C., Håti, A. G., Melø, T. B., Stokke, B. T. & Sikorski, P. Competitive ligand exchange of crosslinking ions for ionotropic hydrogel formation. *J. Mater. Chem. B* **4**, 6175–6182 (2016).

125. Liberski, A., Latif, N., Raynaud, C., Bollensdorff, C. & Yacoub, M. Alginate for cardiac regeneration: From seaweed to clinical trials. *Glob. Cardiol. Sci. Pract.* **2016**, (2016).

126. Salvatore, S. *et al.* The Effect of Alginate in Gastroesophageal Reflux in Infants. *Pediatr. Drugs* **20**, 575–583 (2018).

127. Bedê, P. M., Da Silva, M. H. P., Da Silva Figueiredo, A. B. H. & Finotelli, P. V. Nanostructured magnetic alginate composites for biomedical applications. *Polimeros* **27**, 267–272 (2017).

128. Geckil, H., Xu, F., Zhang, X., Moon, S. & Demirci, U. Engineering hydrogels as extracellular matrix mimics.Geckil, H., Xu, F., Zhang, X., Moon, S., & Demirci, U. (2010). Engineering hydrogels as extracellular matrix mimics. Nanomedicine (London, England), 5(3), 469–84. http://doi.org/10.2217/nnm.10.12. *Nanomedicine (Lond).* **5**, 469–84 (2010).

129. Caliari, S. R., Burdick, J. A. & Terms, B. O. X. K. E. Y. REVIEW A practical guide to hydrogels for cell culture. *Nat. Publ. Gr.* **13**, 405–414 (2016).

130. Freeman, F. E. & Kelly, D. J. Tuning alginate bioink stiffness and composition for controlled growth factor delivery and to spatially direct MSC Fate within bioprinted tissues. *Sci. Rep.* **7**, 1–12 (2017).

131. Otterlei, M. *et al.* Induction of Cytokine Production from Human Monocytes Stimulated with Alginate. *J. Immunother.* **10**, 286–291 (1991).

132. Yang, D. & Jones, K. S. Effect of alginate on innate immune activation of macrophages. *J. Biomed. Mater. Res. - Part A* **90**, 411–418 (2009).

133. Deepthi, S. & Jayakumar, R. Alginate nanobeads interspersed fibrin network as in situ forming hydrogel for soft tissue engineering. *Bioact. Mater.* **3**, 194–200 (2018).

134. Melchels, F. P. W., Dhert, W. J. A., Hutmacher, D. W. & Malda, J. Development and characterisation of a new bioink for additive tissue manufacturing. *J. Mater. Chem. B* **2**, 2282 (2014).

135. Rowley, J. A., Madlambayan, G. & Mooney, D. J. Alginate hydrogels as synthetic extracellular matrix materials. *Biomaterials* **20**, 45–53 (1999).

136. Goldberga, I., Li, R. & Duer, M. J. Collagen Structure-Function Relationships from Solid-State NMR Spectroscopy. *Acc. Chem. Res.* **51**, 1621–1629 (2018).

137. Lodish H, Berk A, Zipursky SL, et al. *Molecular Cell Biology. 4th edition. Title*. (2000).

138. Miller, E. J. & Kent Rhodes, R. *[2] Preparation and Characterization of the Different Types of Collagen*. *Methods in Enzymology* **82**, (1982).

139. Pati, F. *et al.* Printing three-dimensional tissue analogues with decellularized extracellular matrix bioink. *Nat. Commun.* **5**, 1–11 (2014).

140. Rutz, A. L., Hyland, K. E., Jakus, A. E., Burghardt, W. R. & Shah, R. N. A Multimaterial Bioink Method for 3D Printing Tunable, Cell-Compatible Hydrogels. *Adv. Mater.* **27**, 1607–1614 (2015).

141. MacCallum, B. *et al.* Development of a 3D bioprinting system using a Co-Flow of calcium chloride mist. *Bioprinting* **20**, e00085 (2020).

142. Hazur, J. *et al.* Improving alginate printability for biofabrication: establishment of a universal and homogeneous pre-crosslinking technique. *Biofabrication* **12**, (2020).

143. Bjørnøy, S. H. *et al.* Gelling kinetics and in situ mineralization of alginate hydrogels: A correlative spatiotemporal characterization toolbox. *Acta Biomater.* **44**, 243–253 (2016).

144. Bozym, R. A. *et al.* Free zinc ions outside a narrow concentration range are toxic to a variety of cells in vitro. *Exp. Biol. Med.* **235**, 741–750 (2010).

145. Mirdamadi, E., Tashman, J. W., Shiwarski, D. J., Palchesko, R. N. & Feinberg, A. W. FRESH 3D Bioprinting a Full-Size Model of the Human Heart. *ACS Biomater. Sci. Eng.* **6**, 6453–6459 (2020).

146. Hinton, T. J. *et al.* Three-dimensional printing of complex biological structures by freeform reversible embedding of suspended hydrogels. *Sci. Adv.* **1**, 1–10 (2015).

147. Good, N. E. *et al.* Hydrogen Ion Buffers for Biological Research *. *Biochemistry* **5**, 467–477 (1966).

148. Roy, L. N. *et al.* Buffer standards for the physiological pH of the zwitterionic compound of 3-(N-morpholino)propanesulfonic acid (MOPS) from T=(278.15 to 328.15)K. *J. Chem. Thermodyn.* **47**, 21–27 (2012).

149. No Title. Available at: http://staff.ustc.edu.cn/~liuyz/methods/buffer.htm.

150. Sun, N. & Avdeef, A. Biorelevant pKa (37°C) predicted from the 2D structure of the molecule and its pKa at 25°C. *J. Pharm. Biomed. Anal.* **56**, 173–182 (2011).

151. Nikolaeva, T. I., Tiktopulo, E. I., Polozov, R. V. & Rochev, Y. A. Thermodynamic and structural characteristics of collagen fibrils formed in vitro at different temperatures and concentrations. *Biophysics (Oxf).* **52**, 191–195 (2007).

152. Nikolaeva, T. I., Kuznetsova, S. M. & Rogachevsky, V. V. Collagen fibril formation in vitro at nearly physiological temperatures. *Biophys. (Russian Fed.* **57**, 757–763 (2012).

153. Bhattacharjee, T. *et al.* Writing in the granular gel medium. *Sci. Adv.* **1**, 4–9 (2015).

154. Kim, Y. B., Lee, H. & Kim, G. H. Strategy to Achieve Highly Porous/Biocompatible Macroscale Cell Blocks, Using a Collagen/Genipin-bioink and an Optimal 3D Printing Process. *ACS Appl. Mater. Interfaces* **8**, 32230–32240 (2016).

155. Frantz, C., Stewart, K. M. & Weaver, V. M. The extracellular matrix at a glance. *J. Cell Sci.* **123**, 4195–4200 (2010).

156. Suo, H., Zhang, J., Xu, M. & Wang, L. Low-temperature 3D printing of collagen and chitosan composite for tissue engineering. *Mater. Sci. Eng. C* **123**, 111963 (2021).

157. Sun, Y. *et al.* 3D printing collagen/chitosan scaffold ameliorated axon regeneration and neurological recovery after spinal cord injury. *J. Biomed. Mater. Res. - Part A* **107**, 1898–1908 (2019).

158. Marquis, M.-E. Bone cells-biomaterials interactions. *Front. Biosci.* **Volume**, 1023 (2009).

159. Ikpegbu, E. *et al.* FGF-2 promotes osteocyte differentiation through increased E11/podoplanin expression. *J. Cell. Physiol.* **233**, 5334–5347 (2018).

160. Dolci, L. S. *et al.* Modulation of Alendronate release from a calcium phosphate bone cement: An in vitro osteoblast-osteoclast co-culture study. *Int. J. Pharm.* **554**, 245–255 (2019).

161. Penolazzi, L. *et al.* Establishment of a 3D-dynamic osteoblasts-osteoclasts co-culture model to simulate the jawbone microenvironment in vitro. *Life Sci.* **152**, 82–93 (2016).

162. HIROKO SUDO, HIRO-ARI KODAMA, YUJI AMAGAI, SHIGEHISA YAMAMOTO, and S. K. In Vitro Differentiation and Calcification in a New Clonal Osteogenic Cell Line Derived from Newborn Mouse Calvaria. *J. Cell Biol.* **96**, 191–1998 (1983).

163. Woo, S. M., Rosser, J., Dusevich, V., Kalajzic, I. & Bonewald, L. F. Cell Line IDG-SW3 Replicates Osteoblast-to-Late-Osteocyte. *J Bone Min. Res* **26**, 2634–2646 (2011).

164. Kato, Y. *et al.* Establishment of an Osteoid Preosteocyte-like Cell MLO-A5 That Spontaneously Mineralizes in Culture. *J. Bone Miner. Res.* **16**, 1622–1633 (2001).

165. Kato, Y., Windle, J. J., Koop, B. A., Mundy, G. R. & Bonewald, L. F. Establishment of an Osteocyte-like Cell Line, MLO-Y4. *J. Bone Miner. Res.* **12**, 2014–2023 (2010).

166. Hausser, H. J. & Brenner, R. E. Phenotypic instability of Saos-2 cells in long-term culture. *Biochem. Biophys. Res. Commun.* **333**, 216–222 (2005).

167. Zhang, J., Zhang, W., Dai, J., Wang, X. & Shen, S. G. Overexpression of Dlx2 enhances osteogenic differentiation of BMSCs and MC3T3-E1 cells via direct upregulation of Osteocalcin and Alp. *Int. J. Oral Sci.* **11**, (2019).

168. Nishimura, R., Hata, K., Matsubara, T., Wakabayashi, M. & Yoneda, T. Regulation of bone and cartilage development by network between BMP signalling and transcription factors. *J. Biochem.* **151**, 247–254 (2012).

169. Wilkie, A. O. M. *et al.* Functional haploinsufficiency of the human homeobox gene MSX2 causes defects in skull ossification. *Nat. Genet.* **24**, 387–390 (2000).

170. Han, J. *et al.* Concerted action of Msx1 and Msx2 in regulating cranial neural crest cell differentiation during frontal bone development. *Mech. Dev.* **124**, 729–745 (2007).

171. Krishnan, R. H. *et al.* Role of p300, a histone acetyltransferase enzyme, in osteoblast differentiation. *Differentiation* **124**, 43–51 (2022).

172. Komori, T. Molecular Mechanism of Runx2-Dependent Bone Development. *Mol. Cells* **43**, 168–175 (2020).

173. Shirakabe, K., Terasawa, K., Miyama, K., Shibuya, H. & Nishida, E. Regulation of the activity of the transcription factor Runx2 by two homeobox proteins, Msx2 and Dlx5. *Genes to Cells* **6**, 851–856 (2001).

174. Sinha, K. M. & Zhou, X. Genetic and molecular control of osterix in skeletal formation. *J. Cell. Biochem.* **114**, 975–984 (2013).

175. Forlino, A. & Marini, J. C. Osteogenesis imperfecta. *Lancet* **387**, 1657–1671 (2016).

176. Tzaphlidou, M. Bone architecture: Collagen structure and calcium/phosphorus maps. *J. Biol. Phys.* **34**, 39–49 (2008).

177. Willing, M. C., Deschenes, S. P., Slayton, R. L. & Roberts, E. J. Premature chain termination is a unifying mechanism for COL1A1 null alleles in osteogenesis imperfecta type I cell strains. *Am. J. Hum. Genet.* **59**, 799–809 (1996).

178. Couchourel, D. *et al.* Altered mineralization of human osteoarthritic osteoblasts is attributable to abnormal type I collagen production. *Arthritis Rheum.* **60**, 1438–1450 (2009).

179. Vimalraj, S. Alkaline phosphatase: Structure, expression and its function in bone mineralization. *Gene* **754**, 144855 (2020).

180. Lund, S. A., Giachelli, C. M. & Scatena, M. The role of osteopontin in inflammatory processes. *J. Cell Commun. Signal.* **3**, 311–322 (2009).

181. Si, J. *et al.* Osteopontin in Bone Metabolism and Bone Diseases. *Med. Sci. Monit.* **26**, 1–9 (2020).

182. Staines, K. A. *et al.* E11/Podoplanin Protein Stabilization Through Inhibition of the Proteasome Promotes Osteocyte Differentiation in Murine in Vitro Models. *J. Cell. Physiol.* **231**, 1392–1404 (2016).

183. Zhang, K. *et al.* E11/gp38 Selective Expression in Osteocytes: Regulation by Mechanical Strain

and Role in Dendrite Elongation. *Mol. Cell. Biol.* **26**, 4539–4552 (2006).

184. Lee, N. K. *et al.* Endocrine Regulation of Energy Metabolism by the Skeleton. *Cell* **130**, 456–469 (2007).

185. Moser, S. C. & van der Eerden, B. C. J. Osteocalcin — A versatile bone-derived hormone. *Front. Endocrinol. (Lausanne).* **10**, 4–9 (2019).

186. Zoch, M. L., Clemens, T. L. & Riddle, R. C. New insights into the biology of osteocalcin. *Bone* **82**, 42–49 (2016).

187. Rosset, E. M. & Bradshaw, A. D. SPARC/osteonectin in mineralized tissue. *Matrix Biol.* **52**–**54**, 78–87 (2016).

188. Delany, A. M. & Hankenson, K. D. Thrombospondin-2 and SPARC/osteonectin are critical regulators of bone remodeling. *J. Cell Commun. Signal.* **3**, 227–238 (2009).

189. Kuchipudi, S. V. *et al.* 18S rRNA is a reliable normalisation gene for real time PCR based on influenza virus infected cells. *Virol. J.* **9**, 1 (2012).

190. Bas, A., Forsberg, G., Hammarstrom, S. & Hammarstrom, M.-L. Utility of the Housekeeping Genes 18S rRNA, beta-Actin and Glyceraldehyde-3-Phosphate-Dehydrogenase for Normalization in Real-Time Quantitative Reverse Transcriptase-Polymerase Chain Reaction Analysis of Gene Expression in Human T Lymphocytes. *Scand. J. Immunol.* **59**, 566–573 (2004).

191. Bernier, G. M. β 2-Microglobulin: Structure, Function and Significance. *Vox Sang.* **38**, 323–327 (1980).

192. Ho, K. H. & Patrizi, A. Assessment of common housekeeping genes as reference for gene expression studies using RT-qPCR in mouse choroid plexus. *Sci. Rep.* **11**, 1–15 (2021).

193. NIHON-YANAGI, Y. *et al.* B-2 Microglobulin Is Unsuitable As an Internal Reference Gene for the Analysis of Gene Expression in Human Colorectal Cancer. *Biomedical Reports* **1**, 193–196 (2013).

194. Izumiya, M. *et al.* Evaluation of mc3t3-e1 cell osteogenesis in different cell culture media. *Int. J. Mol. Sci.* **22**, 1–12 (2021).

195. Li, L., Zeng, Z. & Cai, G. Phytomedicine Comparison of neoeriocitrin and naringin on proliferation and osteogenic differentiation in MC3T3-E1. *Eur. J. Integr. Med.* **18**, 985–989 (2011).

196. Xu, W., Xu, C., Yi, J. & Dai, H. The effect of different hydroxyapatite microparticles on the osteogenic differentiation of MC3T3-E1 preosteoblasts. 5234–5242 (2018). doi:10.1039/c8tb01352g

197. Ghali, O. *et al.* Dexamethasone in osteogenic medium strongly induces adipocyte differentiation of mouse bone marrow stromal cells and increases osteoblast differentiation. 1–15 (2015). doi:10.1186/s12860-015-0056-6

198. Orriss, I. R., Hajjawi, M. O. R., Huesa, C., Macrae, V. E. & Arnett, T. R. Optimisation of the differing conditions required for bone formation in vitro by primary osteoblasts from mice and rats. *Int. J. Mol. Med.* **34**, 1201–1208 (2014).

199. Song, I. H., Caplan, A. I. & Dennis, J. E. In vitro dexamethasone pretreatment enhances bone formation of human mesenchymal stem cells in vivo. *J. Orthop. Res.* **27**, 916–921 (2009).

200. Li, W., Zhang, S., Liu, J., Liu, Y. & Liang, Q. Vitamin K2 stimulates MC3T3-E1 osteoblast differentiation and mineralization through autophagy induction. *Molecular Medicine Reports* **49**, 3676–3684 (2019).

201. Fukunishi, Y. & Tabata, Y. Osteogenic differentiation enhances the MC3T3-E1 secretion of glycosaminoglycans with an affinity for basic fibroblast growth factor and bone morphogenetic protein-2. *Regen. Ther.* **8**, 58–62 (2018).

202. Wang, D. *et al.* Isolation and characterization of MC3T3-E1 preosteoblast subclones with distinct in vitro and in vivo differentiation/mineralization potential. *J. Bone Miner. Res.* **14**, 893–903 (1999).

203. Varanasi, V. G. *et al.* Si and Ca individually and combinatorially target enhanced MC3T3-E1 subclone 4 early osteogenic marker expression. *J. Oral Implantol.* **38**, 325–336 (2012).

204. Toor, R. H. *et al.* Ethyl acetate and n-butanol fraction of Cissus quadrangularis promotes the mineralization potential of murine pre-osteoblast cell line MC3T3-E1 (sub-clone 4). *J. Cell. Physiol.* **234**, 10300–10314 (2019).

205. Zhen Hua *et al.* Fabrication of Bone Morphogenic Protein-2 and Icariin-Containing Sustained-Release Microcapsule and Evaluation of its Osteogenic Differentiation Capacity in MC3T3-E1 Cells. *Polym. Sci. - Ser. B* (2022). doi:10.1134/S1560090422700270

206. Taubenberger, A. V., Woodruff, M. A., Bai, H., Muller, D. J. & Hutmacher, D. W. The effect of unlocking RGD-motifs in collagen I on pre-osteoblast adhesion and differentiation. *Biomaterials* **31**, 2827–2835 (2010).

207. Davies, O. G. *et al.* Annexin-enriched osteoblast-derived vesicles act as an extracellular site of mineral nucleation within developing stem cell cultures. *Sci. Rep.* **7**, 1–13 (2017).

208. Wrobel, E., Leszczynska, J. & Brzoska, E. The Characteristics Of Human Bone-Derived Cells (HBDCS) during osteogenesis in vitro. *Cell. Mol. Biol. Lett.* **21**, 1–15 (2016).

209. Holm, E. *et al.* Osteopontin mediates mineralization and not osteogenic cell development in vitro. *Biochem. J.* **464**, 355–364 (2014).

210. Davies, M. 3D Printer Feed Rate vs. Flow Rate – What Is the Difference? 1 (2022). Available at: https://www.3dprintbeast.com/3d-printer-feed-rate-vs-flow-rate/.

211. Ravi, T., Ranganathan, R., Pugalendhi, A. & Arumugam, S. ScienceDirect 3D Printed Patient Specific Models from Medical Imaging - A General Workflow. *Mater. Today Proc.* **22**, 1237–1243 (2020).

212. Solidworks. No Title. Available at: https://www.solidworks.com/solutions.

213. Autodesk. No Title. Available at: https://www.autodesk.com/products/fusion-360/overview?term=1-YEAR&tab=subscription.

214. RegenHU. No Title. Available at: https://www.regenhu.com/3dbioprinting-solutions/shaper-3dprinting-software/.

215. Cellink. No Title. Available at: https://www.cellink.com/product/dna-studio-4/.

216. REP RAP. No Title. *October 2022* Available at: https://www.reprap.org/wiki/G-code.

217. Mousavi Nejad, Z., Zamanian, A., Saeidifar, M., Vanaei, H. R. & Salar Amoli, M. 3D Bioprinting of Polycaprolactone-Based Scaffolds for Pulp-Dentin Regeneration: Investigation of Physicochemical and Biological Behavior. *Polymers (Basel).* **13**, 4442 (2021).

218. Karzyński, K. *et al.* Use of 3D bioprinting in biomedical engineering for clinical application. *Med. Stud.* **34**, 93–97 (2018).

219. Ventura, R. D. An Overview of Laser-assisted Bioprinting (LAB) in Tissue Engineering Applications. **10**, 76–81 (2021).

220. Koch, L., Gruene, M., Unger, C. & Chichkov, B. Laser Assisted Cell Printing. 91–97 (2013).

221. Williams, R., Gelman, A. & Poppke, C. Collagen fibril formation. Optimal in vitro conditions and preliminary kinetic results. *J. Biol. Chem.* **253**, 6578–6585 (1978).

222. Darvish, D. M. Materials Today Bio Collagen fi bril formation in vitro : From origin to opportunities. *Mater. Today Bio* **15**, 100322 (2022).

223. Bohner, M., Santoni, B. L. G. & Döbelin, N. β-tricalcium phosphate for bone substitution: Synthesis and properties. *Acta Biomater.* **113**, 23–41 (2020).

224. Hurle, K., Oliveira, J. M., Reis, R. L., Pina, S. & Goetz-neunhoeffer, F. Acta Biomaterialia Ion-doped Brushite Cements for Bone Regeneration. **123**, 51–71 (2021).

225. Bjørnøy, S. H., Bassett, D. C., Ucar, S., Andreassen, J. & Sikorski, P. Controlled mineralisation and recrystallisation of brushite within alginate hydrogels Controlled mineralisation and recrystallisation of brushite within alginate hydrogels. doi:10.1088/1748-6041/11/1/015013

226. N. Patel, S. M. Best, W. Bonfield, I. R. Gibson, K. A. Hing, E. D. & P. A. R. A comparative study on the in vivo behavior of hydroxyapatite and silicon substituted hydroxyapatite granules. *J. Mater. Sci. Mater. Med.* **13**, 1199–1206 (2002).

227. Charrière, E. *et al.* Mechanical characterization of brushite and hydroxyapatite cements. *Biomaterials* **22**, 2937–2945 (2001).

228. Woodard, J. R. *et al.* The mechanical properties and osteoconductivity of hydroxyapatite bone scaffolds with multi-scale porosity. **28**, 45–54 (2007).

229. Luo, J., Engqvist, H. & Persson, C. Acta Biomaterialia A ready-to-use acidic , brushite-forming calcium phosphate cement. *Acta Biomater.* **81**, 304–314 (2018).

230. Ma, G. Three common preparation methods of hydroxyapatite. *IOP Conf. Ser. Mater. Sci. Eng.* **688**, 033057 (2019).

231. Rhee, S., Puetzer, J. L., Mason, B. N., Reinhart-King, C. A. & Bonassar, L. J. 3D Bioprinting of Spatially Heterogeneous Collagen Constructs for Cartilage Tissue Engineering. *ACS Biomater. Sci. Eng.* **2**, 1800–1805 (2016).

232. Robinson,Philip C. Davidson, M. W. Polarized Light Microscopy. Available at: https://www.microscopyu.com/techniques/polarized-light/polarized-light-microscopy.

233. Chen, X., Nadiarynkh, O., Plotnikov, S. & Campagnola, P. J. Second harmonic generation microscopy for quantitative analysis of collagen fibrillar structure. *Nat. Protoc.* **7**, 654–669 (2012).

234. Wiens, R. *et al.* High spatial resolution (1.1 μm and 20 nm) FTIR polarization contrast imaging reveals pre-rupture disorder in damaged tendon. *Faraday Discuss.* **187**, 555–573 (2016).

235. Lin, C. P., Douglas, W. H. & Erlandsen, S. L. Scanning electron microscopy of type I collagen at the dentin-enamel junction of human teeth. *J. Histochem. Cytochem.* **41**, 381–388 (1993).

236. Doyle, A. D., Carvajal, N., Jin, A., Matsumoto, K. & Yamada, K. M. Local 3D matrix microenvironment regulates cell migration through spatiotemporal dynamics of contractility-

dependent adhesions. *Nat. Commun.* **6**, (2015).

237. Baniasadi, M. & Minary-Jolandan, M. Alginate-collagen fibril composite hydrogel. *Materials (Basel).* **8**, 799–814 (2015).

238. Moxon, S. R. *et al.* Blended alginate/collagen hydrogels promote neurogenesis and neuronal maturation. *Mater. Sci. Eng. C* **104**, 109904 (2019).

239. Visser, J. *et al.* Biofabrication of multi-material anatomically shaped tissue constructs. *Biofabrication* **5**, (2013).